Technical Report
TR-18-05
January 2019

The imprint of hemispheric-scale climate transitions on the European climate during the last deglaciation (15.5 ka to 9 ka BP)

Frederik Schenk
Barbara Wohlfarth

SVENSK KÄRNBRÄNSLEHANTERING AB

SWEDISH NUCLEAR FUEL
AND WASTE MANAGEMENT CO

Box 3091, SE-169 03 Solna
Phone +46 8 459 84 00
skb.se

SVENSK KÄRNBRÄNSLEHANTERING

ISSN 1404-0344
SKB TR-18-05
ID 1689116

January 2019

The imprint of hemispheric-scale climate transitions on the European climate during the last deglaciation (15.5 ka to 9 ka BP)

Frederik Schenk, Barbara Wohlfarth

Department of Geological Sciences and Bolin Centre for Climate Research, Stockholm University

Keywords: Rapid climate shifts, Climate transitions, Deglaciation, Younger Dryas, Bølling, Allerød, Climate proxy data, Climate modelling, Palaeoclimate, Atlantic Meridional Overturning Circulation, Ice sheets, Hydroclimate, Summer temperatures.

Preface

The following report constitutes a final report of a comprehensive paleoclimate study with the aim of reconstructing and analysing rapid large-scale climate transitions and their imprint on the regional to local climate over Europe and southern Sweden during the last deglaciation. The study makes use of various geological climate proxy records as well as climate modelling to gain a detailed spatiotemporal understanding of the underlying causes of these climate shifts. The study was initiated and administrated by Jens-Ove Näslund (SKB), Jenny Brandefelt (SKB) and Barbara Wohlfarth (Stockholm University). Barbara Wohlfarth coordinated the scientific work and conducted the research on the Swedish climate proxy records. Frederik Schenk (Stockholm University and KTH Mechanics) conducted the work on setting up and performing high-resolution climate model simulations and led the model-proxy comparison and evaluation of atmospheric and oceanic drivers behind rapid climate shifts.

The results will be used, together with other published scientific information, for constructing future climate scenarios in SKB's work on assessing the long-term safety of nuclear waste repositories in Sweden. The safety assessments performed for the planned repository for spent nuclear fuel in Forsmark, Sweden, focus on a time period of 100 000 years, and cover a total time span of one million years. Since this covers the timescale upon which Quaternary climate and ice-sheet cycles have operated, the effect of future glacial-interglacial conditions upon repository safety needs to be analysed. In this context, the present study provides important results on the highly varying climate and environmental conditions in Fennoscandia and Europe during the transition from glacial to interglacial conditions during the last deglaciation. Special focus is put on the warm Bølling-Allerød interstadial and cold Yonger Dryas stadial since this is the latest as well as one of the most extreme rapid climate shifts of the last deglaciation.

The report manuscript was scientifically reviewed by Prof. Dr. Hans Renssen (University College of Southeast Norway, Norway) and Prof. Dr. Antje Schwalb (Technische Universität Braunschweig, Germany). Input to an earlier version of the manuscript was provided by Christina Truedsson (Tintra konsult) and Jens-Ove Näslund (SKB).

Stockholm, January 2019

Jens-Ove Näslund
Coordinator Climate Research Programme SKB

Abstract

The end of the last ice age, the “Last Termination”, is characterised by a sequence of several rapid shifts between very cold (stadial) and warm (interstadial) periods. These rapid shifts point towards important climate instabilities which occured during the overall warming trend of the deglaciation. The abruptness of these changes stands in contrast to the gradual increase in orbital summer insolation at high northern latitudes and the global increase in greenhouse gases and indicates a non-linear response of the climate system to rapid warming. The climate instabilities have been linked to strong and partly abrupt variations in the strength of the Atlantic Meridional Overturning Circulation (AMOC) in response to ocean salinity disturbances by fresh water fluxes from melting ice sheets. The drivers and mechanisms behind these rapid shifts, their different regional climatic feedbacks and their global impacts via teleconnections, are, however, not well known.

To gain a more detailed knowledge and understanding of climate evolution and variability in Scandinavia and Europe during the transition from a glacial into an interglacial climate state, we conducted a comprehensive multi-proxy climate study and combine these results with data from new high-resolution global climate model simulations. We specifically focussed the study on the climate transitions of the last deglaciation and on the climate state and driving mechanisms that characterised the warm Bølling-Allerød interstadial and the cold Younger Dryas stadial.

To achieve the overall aim of the project, we compiled published quantitative paleo proxy records, compiled and quantified published pollen and plant macrofossil data sets across Europe and quantified the abrupt climatic and environmental shifts that have occurred in southern Sweden during the last glacial/interglacial transition based on a detailed analysis of two lake sediment records. The detailed multi-proxy approach provides an optimal testbed to compare the climate impacts behind the rapid shifts connecting the local to regional scale captured by the lake records with large-scale continental to hemispheric changes simulated by our full complexity high-resolution global climate model.

Multi-proxy data sets obtained for the two lake sediment records, Atteköpsmosse and Hässeldala Port in southern Sweden provide information on the response of the terrestrial environment to rapid shifts in hydroclimate and allow quantifying minimum mean July temperatures and mean July surface water temperatures for the pre-Bølling, Bølling, Allerød, Younger Dryas and early Holocene. Based on several Swedish lake records, we find clear evidence from plant macrofossils that remarkably high summer temperatures of at least ~ 16 °C prevailed throughout the deglaciation. Based on the oldest Swedish records, the high summer temperatures existed already directly after the ice sheet had retreated over southern Sweden during the pre-Bølling (15.5 ka BP) and remained high until the lakes became peatlands during the early Holocene (~ 10 ka BP).

In contrast to the warm summer air temperatures captured by plant macrofossils, lake water temperatures reconstructed from chironomids indicate distinct shifts between cold stadials and warm interstadials. These shifts co-vary with proxy-evidence from lipid biomarkes for dry conditions and a fresh moisture source during stadials and wetter conditions and a saltier moisture source during interstadials. The compilation and quantification of minimum mean July temperatures based on climate indicator plant species from over 120 European sites suggests that the warm summers seen in southern Swedish lake records were also present during the Bølling-Allerød and Younger Dryas.

Based on our new high-resolution climate model simulations, which take the presence of continental ice sheets, glacio-isostic vertical land movement and low sea-level into account, we find that summer temperatures during the Younger Dryas stadial remained at least as high as during the preceeding Allerød – consistent with the proxy evidence from southern Sweden and 120 European records. The persistence of high summer temperatures seen in both, proxy records and our climate simulation, results from atmospheric blocking of westerly winds over the Fennoscandian Ice Sheet during summer. The atmospheric blocking linked to the presence of the ice sheet is intensified by the cold North Atlantic sea-surface-temperatures during the Younger Dryas stadial and explains why thermophillous plants still thrived during the stadial. The blocking is, however, only stable during a short summer period, and severe cooling dominates during the Younger Dryas in spring, autumn and winter. The simulation hence supports previous studies which suggest that the abrupt climate shifts are dominated by a shift in seasonality with increased continentality during stadials.

In addition, the climate model simulation supports the proxy evidence of drier stadial conditions which according to the model might have been extreme owing to much lower humidity in response to a very cold ocean state and a more southerly position of the sea-ice front. During summer, the intensified blocking further reduces the advection of precipitation from the North Atlantic. Based on our comprehensive multi-proxy study and climate modelling results, we find a high agreement between proxy data and climate simulations that the shifts between cold stadials and warm inter-stadials during the deglaciation are dominated by shifts in seasonality/continentality where cold ocean states during a weak AMOC leads to severe winter-spring cooling and aridity and warm ocean states during a strong AMOC leads to milder winters and increased precipitation.

Sammanfattning

Slutet av den senaste glacialen karakteriserades av en sekvens av flera snabba skiften mellan mycket kalla och mycket varma perioder (stadialer respektive interstadialer). Dessa snabba skiften visar på en kraftig instabilitet hos klimatet under den generella trenden av uppvärmning under deglaciationen. Det snabba förloppet hos dessa förändringar står i tydlig kontrast till den gradvisa ökningen av solinstrålningen under sommaren på höga latituder och till den globala ökningen av växthusgaser i slutet av glacialen, vilket indikerar att klimatsystemet responderar icke-linjärt på en relativt långsam uppvärmning. Denna instabilitet hos klimatet har kopplats till stora och delvis abrupta variationer i styrkan hos transporten av värme norrut med havsströmmar i Nordatlanten. Drivkrafterna och mekanismerna bakom dessa snabba skiften i klimat, deras olika regionala klimatologiska återkopplingar och deras globala påverkan är dock dåligt kända.

För att få mer detaljerad kunskap och förståelse om klimatutveckling och variation i Skandinavien och Europa under övergången från ett glacialt istidsklimat till ett varmt interglacialt klimat, så utfördes en omfattande multi-proxy studie på historiska klimatarkiv som kombinerades med nya högupplösta, globala klimatmodellsimuleringar. Studien fokuserade på klimatövergångarna under den senaste deglaciationen, i synnerhet den varma interstadialen Bølling-Allerød och den kalla stadialen Yngre Dryas. I studien sammanställdes publicerade kvantitativa historiska klimatdata inklusive publicerade data från pollen och växtmakrofossil från hela Europa. Dessutom kvantifierades abrupta klimatologiska och miljömässiga förändringar i södra Sverige under övergången från glaciala till interglaciala förhållanden genom en detaljerad analys av två sjösedimentkärnor från Attemosse och Hässeldala Port.

De multi-proxydata som erhölls från de två sjösedimentkärnorna gav information om den terrestra miljöns respons på snabba skiften i hydroklimat och möjliggjorde en kvantifiering av luftens minimum-medeltemperatur under juli månad och ytvattnets medeltemperatur under juli för perioderna pre-Bölling, Bølling-Allerød, Yngre Dryas samt för tidig Holocen. Baserat på uppgifter från flera svenska sjöar konstaterades från analysen av växtmakrofossil att anmärkningsvärt höga sommartemperaturer, på åtminstone +16 °C, rådde genom hela deglaciationen, från tidpunkten för deglaciationen till tidig Holocen (för ungefär 10 000 år sedan). I kontrast till den varma lufttemperaturen under sommarperioderna som erhölls från växtmakrofossil, visade sjövattentemperaturen som rekonstruerades genom chironomider distinkta skiften mellan kalla stadialer och varma interstadialer. Dessa skiften samvarierar med proxy-data från andra biomarkörer vilka indikerar torra betingelser och nederbörd från en sötare källa under stadialer och fuktigare betingelser och en saltare källa till nederbörden under interstadialer.

Den nya högupplösta klimatsimuleringen, vilken tog hänsyn till närvaron av inlandsisar, isostatiska vertikala rörelser hos jordskorpan och låg havsnivå under glaciala förhållanden, indikerade överraskande att sommartemperaturerna under Yngre Dryas stadialen, som traditionellt ses som en kall period, förblev minst lika hög som under den föregående varma Allerød interstadialen. Detta resultat stämde vid en jämförelse väl överens med de historiska klimatdata från södra Sverige och från de övriga 120 platserna i Europa för vilka data sammanställdes. De ihållande höga sommartemperaturerna under deglaciationens alla faser är ett resultat av en atmosfärisk blockering av västliga vindar över den Fennoskandiska inlandsisen under sommarperioderna. Den atmosfäriska blockeringen, som är kopplad till inlandsisens närvaro, intensifierades av de kalla Nord-Atlantiska havsytetemperaturerna under Yngre Dryas stadialen och förklarar varför värmekrävande växter fortsatt kunde frodas i Skandinavien under Yngre Dryas. Situationen med den atmosfäriska blockeringen, och de associerade höga temperaturerna, rådde emellertid bara under korta sommarperioder, då sträng kyla dominerade under vår-, höst- och vinterperioderna under Yngre Dryas. Resultaten från klimatsimuleringen stödjer därför tidigare studier vilka har indikerat att abrupta skiften i klimatet på höga latituder domineras av förändringar i säsongsvariationen, med en ökad kontinentalitet hos klimatet under de stadiala perioderna.

Contents

1 Introduction and background

The overall aim of this project was to enhance knowledge on climate evolution and variability in Scandinavia during a global climate transition from a glacial into an interglacial climate state.

The best studied and chronologically best resolved time interval for addressing these questions is the "Last Termination" or the "Last Deglaciation" – the transition period from the Last Glacial Maximum (LGM) into the present interglacial (The Holocene), which occurred between 19 and 11 thousand years (ka) before present (BP) (Denton et al. 2010, Clark et al. 2012). This transition, which is often also termed the "late glacial", was characterised by a series of abrupt climate shifts between colder (stadial) and warmer (interstadial) states, which are prominently expressed in many geological archives and in their respective climate and environmental proxies (e.g. Clark et al. 2012, Rasmussen et al. 2014a). The sequence of stadials and interstadials during the Last Termination are often termed "Oldest Dryas" (> 14.7 ka BP), "Bølling" (14.7–14.1 ka BP), "Older Dryas" (14.1–13.9 ka BP), "Allerød" (14.1–12.9 ka BP) and "Younger Dryas" (12.9–11.7 ka BP) in reference to earlier pollen-stratigraphic work in Scandinavia (see for example Mangerud et al. 1974, Wohlfarth 1996, Rasmussen et al. 2014a).

A wealth of paleo-records exists, especially around the North Atlantic region that document these dramatic climate shifts and their impact on the environment in great detail: lake and marine sediments, peat deposits, speleothems, tree rings and ice cores (e.g. Björck et al. 1996, Lowe et al. 2008, Steffensen et al. 2008, Hoek et al. 2008, Rasmussen et al. 2014b). By employing a variety of physical, chemical and biological proxies it has been possible to determine the timing of these climate shifts and their regional impact as well as the response of various ecosystems to rapid warming and cooling. The Greenland ice core records suggest for example that a reorganisation of the atmospheric circulation in mid- to high northern latitudes, i.e. the source regions of the precipitation over Greenland, occurred within 1–3 years at the transition from a cold stadial to a warm interstadial, such as at the onset of the early Holocene (Steffensen et al. 2008).

Futhermore, ice core data sets from Greenland and Antarctica show that warm and cold phases were asynchronous between the northern and southern hemispheres (e.g. EPICA Community Members 2006). These findings, in conjunction with marine and terrestrial proxy data, have led to the hypothesis that large amounts of freshwater from the melting ice sheets caused disturbances of the Atlantic Meridional Overturning Circulation (AMOC) (e.g. Stocker and Wright 1991, Rahmstorf 1995, Björck et al. 1996, Broecker 1998, McManus et al. 2004, Stouffer et al. 2006). The asynchronous timing of warming/cooling over the two hemispheres is typically understood as a spatiotemporal imprint of strong AMOC changes and denoted as the "bipolar seesaw mechanism". However, the origin, timing and amount of freshwater discharged into the Atlantic Ocean are still open for debate (e.g. Weaver et al. 2003, Carlson and Clark 2012, Deschamps et al. 2012, Morill et al. 2012).

Climate models of varying complexity, ranging from Earth System Models of Intermediate Complexity (EMIC's) (e.g. Weaver et al. 2003, Menviel et al. 2011, Renssen et al. 2015) to fully coupled Atmosphere Ocean General Circulation Models (AOGCM's) (e.g. Liu et al. 2009, 2012, Cheng et al. 2011, Zhang et al. 2014, Zhu et al. 2014, Schenk et al. 2018) have been used to study the impact and propagation of these rapid climate transitions. These involved complex interactions between the ocean, cryosphere, atmosphere and biosphere, but the type and phasing of the different feedback mechanisms, as well as the spatial and temporal impact/responses to these shifts are still not fully understood. Although large progress has been made in understanding the (bi-)stability of the AMOC (e.g. Rahmstorf 1995, Stouffer et al. 2006) from a theoretical as well as a modeling perspective, a realistic climate model simulation of rapid climate shifts is still challenging.

Overall, at least three major problems persist for climate modeling approaches for the deglaciation. First, the largely unknown quantification, localisation and timing of fresh water fluxes into the oceans makes it necessary to explore several hosing simulations using different fresh water forcing options (He 2011) to potentially match proxy evidence for an AMOC slow-down (McManus et al. 2004) or its climatic impact as reflected for example in the Greenland ice cores. Second, even if the fresh water forcing would be better known, the climate models' sensitivity to these fluxes in terms

of an AMOC slowdown and/or related atmosphere-ocean-sea-ice feedbacks are model dependent and difficult to fully understand owing to the complexity of interacting feedbacks on different time scales. Related to these difficulties, a third problem has been the inability of Earth System Models of Intermediate Complexity (EMIC) as well as full complexity Atmosphere-Ocean-General-Circulation-Models (AOGCM) to simulate cold European summers for the Younger Dryas stadial, even though the AMOC is drastically reduced or even shut down in these simulations (e.g. Renssen et al. 2000, 2015). As a consequence, several studies suggest that other and/or additional forcing mechanisms might have led to the Younger Dryas cooling (Renssen et al. 2000, 2015, Wunsch 2006, Zhang et al. 2014).

To better understand the important linkages between atmosphere, ocean and land from a paleo-proxy perspective, the INTIMATE (INTegration of Ice core, Marine and Terrestrial records) Community attempts to integrate and compare ice core-, marine- and terrestrial paleo-records and paleo-proxies on a common time scale (Rasmussen et al. 2014b). Although much progress has been made (Moreno et al. 2014, Rasmussen et al. 2014b) since the first concerted effort within the framework of the North Atlantic Seaboard Project – a precursor of INTIMATE (Lowe et al. 1994), it is obvious that multi-proxy paleo-records that provide quantified temperature and precipitation estimates and/or other environmental parameters on a high temporal resolution are still scarce, both on a global scale and on regional scales (Moreno et al. 2014). Moreover, the few records that fulfil the requirements of high-temporal multi-proxy climate and environmental reconstructions and of a high-resolution chronology have shown that the impact of and response to the dramatic climate shifts of the Last Termination were spatially different in the North Atlantic region (Moreno et al. 2014, Rach et al. 2014, Muschitiello and Wohlfarth 2015). Apart from these few high-resolution records, a wealth of terrestrial paleo-data sets with limited age control has been published for Europe. The various proxies that have been analysed (e.g. pollen, plant macrofossil remains, chironomids, oxygen isotopes) allow climate and environmental reconstructions, albeit on a coarse resolution time scale.

For this project, we set out to analyse the climate transitions during the last deglaciation and their impact on terrestrial ecosystems in southern Sweden and to understand the climate state and driving mechanisms within the warm Bølling-Allerød interstadial in contrast to the cold Younger Dryas stadial to further our knowledge on high spatiotemporal climate variability over Europe and Sweden. Focus was on the following specific questions:

(1) Were the onsets of warm/cold intervals homogeneous in time and space or were they time transgressive?

(2) How did different components of the terrestrial environment respond to rapid climate transitions?

(3) Do changes in temperature co-vary with changes in hydroclimate?

(4) What is the atmospheric response over the Euro-Atlantic region to the strong oceanic cooling during the Younger Dryas based on a very high-resolution climate model simulation?

(5) What is the impact of simulated seasonality changes on biotic proxies?

(6) Is the simulated climatic response to the strong oceanic cooling during the Younger Dryas consistent with regional proxy evidence?

(7) Is the Younger Dryas climate consistent with a scenario where only the AMOC slow-down is the dominant driver or are other forcing mechanisms required?

To achieve the overall aim of the project, the work was organised in two sub-projects (A) quantifying climate transitions between 20 and 10 ka BP from geological records, and (B) high resolution global climate modelling and comparison with climate proxy-data. The two sub-projects had the following specific aims:

(1) Compilation and evaluation of published quantitative paleo proxy records from Europe.

(2) Compilation and quantification of published pollen and plant macrofossil data sets from Europe using the method developed by Väliranta et al. (2015).

(3) Quantification of the abrupt climatic and environmental shifts that have occurred in southern Sweden during the last glacial/interglacial transition based on the analysis of two lake sediment records.

(4) Analysis of global climate model results and set up, running and analysis of results from the global atmospheric model.

(5) Comparison of the obtained quantitative climatic and environmental data sets to climate model output data.

The project has so far resulted in the following published articles and was to a large part co-financed through various other grants to B. Wohlfarth, M. Steinthorsdottir and R. Smittenberg. The analytical work on the two lake sediment records was mainly conducted at the Stable Isotope Laboratory (SIL), Department of Geological Sciences and at the Delta Facility at Stockholm University. The development of a late-glacial climate model setup was done at the Linné FLOW Centre, Department of Mechanics, Royal Institute of Technology (KTH), Stockholm and model simulations and analysis were continued at the Bolin Centre for Climate Research and Department of Geological Sciences at Stockholm University.

1. **Schenk F, Väliranta M, Muschitiello F, Tarasov L, Heikkilä M, Björck S, Brandefelt J, Johannson A, Näslund J-O, Wohlfarth B, 2018.** Warm summers during the Younger Dryas cold reversal. Nature Communications 9, 1634. https://doi.org/10.1038/s41467-018-04071-5.
2. **Ahmed E, Parducchi L, Unneberg P, Ågren R, Schenk F, Rattray J E, Han L, Muschitiello F, Pedersen M W, Smittenberg R H, Yamoah K A, Slotte T, Wohlfarth B, 2018.** Archaeal community successions in Late glacial lake sediments: evidence from ancient DNA. Quaternary Science Reviews 181, 19–29. https://doi.org/10.1016/j.quascirev.2017.11.037.
3. **Wohlfarth B, Luoto T, Muschitiello F, Väliranta M, Björck S, Davies S M, Kylander M, Ljung K, Reimer P J, Smittenberg R H 2018.** Climate and environment in southwest Sweden 15.5–11.3 cal. ka BP. Boreas 47, 687–710. https://doi.org/10.1111/bor.12310.
4. **Muschitiello F, Pausata F S R, Lea J M, Mair D W F, Wohlfarth B, 2017.** Enhanced ice sheet melting driven by volcanic eruptions during the last deglaciation. Nature Communication 8, 1020. https://doi.org/10.1038/s41467-017-01273-1.
5. **Muschitiello F, 2016.** Deglacial impact of the Scandinavian Ice Sheet on the North Atlantic climate system. PhD thesis. Department of Geological Sciences, Stockholm University.
6. **Wohlfarth B, Muschitiello F, Greenwood S L, Andersson A, Kylander M, Smittenberg R H, Steinthorsdottir M, Watson J, Whitehouse N J, 2017.** Hässeldala – a key site for Last Termination climate events in northern Europe. Boreas 46, 143–161. http://dx.doi.org/10.1111/bor.12207.
7. **Muschitiello F, Lea J, Greenwood S L, Nick F M, Brunnberg L, MacLeod A, Wohlfarth B, 2016.** Precise timing of the first drainage of the Baltic Ice Lake from Swedish glacial-varve chronologies. Boreas 45, 322–334. http://dx.doi.org/10.1111/bor.12155.
8. **Muschitiello F, Pausata F S R, Smittenberg R H, Salih A A M, Watson J E, Brooks S J, Whitehouse N J, Karlatou-Charalampopoulou A, Wohlfarth B, 2015.** Fennoscandian freshwater control on Greenland hydrological shifts at the onset of the Younger Dryas. Nature Communications 6, 8939. https://doi.org/10.1038/ncomms9939.
9. **Muschitiello F, Andersson A, Wohlfarth B, Smittenberg R H, 2015.** The C20 highly branched isoprenoid biomarker – A new diatom–sourced proxy for summer trophic conditions? Organic Geochemistry 81, 27–33. https://doi.org/10.1016/j.orggeochem.2015.01.007.
10. **Muschitiello F, Wohlfarth B, 2015.** ime-transgressive environmental shifts across Northern Europe at the onset of the Younger Dryas. Quaternary Science Reviews 109, 49–56. http://dx.doi.org/10.1016/j.quascirev.2014.11.015.
11. **Ampel L, Kylander M E, Steinthorsdottir M, Wohlfarth B, 2014.** Abrupt climate change and early lake development – the Lateglacial diatom flora at Hässeldala Port, southeastern Sweden. Boreas 44, 94–102. https://doi.org/10.1111/bor.12081.

12. **Steinthorsdottir M, de Boer A, Oliver K I C, Muschitiello F, Blaauw M, Wohlfarth B, 2015.** Response to: Comment on “Synchronous records of pCO2 and D14C suggest rapid, ocean-derived pCO2 fluctuations at the onset of Younger Dryas” (Steinthorsdottir et al. 2014, Quaternary Science Reviews 99, 84–96). Quaternary Science Reviews 107, 270–273. http://dx.doi.org/10.1016/j.quascirev.2014.10.020.
13. **Steinthorsdottir M, de Boer A M, Oliver K I C, Muschitiello F, Blaauw M, Reimer P J, Wohlfarth B, 2014.** Synchronous records of pCO2 and Δ14C suggest rapid, ocean-derived pCO2 fluctuations at the onset of Younger Dryas. Quaternary Science Reviews 99, 84–96. https://doi.org/10.1016/j.quascirev.2014.06.021.
14. **Muschitiello F, Schwark L, Wohlfarth B, Sturm C, Hammarlund D, 2013.** New evidence of Holocene atmospheric circulation dynamics based on lake sediments from southern Sweden: a link to the Siberian High. Quaternary Science Reviews 77, 113–124. https://doi.org/10.1016/j.quascirev.2013.07.026.
15. **Steinthorsdottir M, Wohlfarth B, Kylander M, Blaauw M, Reimer,P J, 2013.** Stomatal proxy record of CO2 concentrations from the last termination suggests an important role for CO2 at climate change transitions. Quaternary Science Reviews 68, 43–58. https://doi.org/10.1016/j.quascirev.2013.02.003.
16. **Kylander M E, Klaminder J, Wohlfarth B, Löwemark L, 2013.** Geochemical responses to paleoclimatic changes in southern Sweden since the late glacial: the Hässeldala Port lake sediment record. Journal of Paleolimnology 50, 57–70. https://doi.org/10.1007/s10933-013-9704-z.

2 Data and Methods

We used three different types of data to analyse the regional to local Last Termination climate and its changes and the difference between a warm climate state (Bølling-Allerød (BA) interstadial) and a cold climate state (Younger Dryas (YD) stadial). First, high quality and well dated proxy records were used to study the transient climate evolution by means of continuous time series. For this we compiled published climate proxy data sets and created new high-resolution multi-proxy records. Second, because only a very low number of continuous, quantified paleo-proxy records exist in Europe, we additionally used discontinuous proxy data with poorer age control, but which are available for over 120 sites across Europe. These data allow us to study the magnitude and spatial pattern of temperature changes in the mean state of the summer climate between the distinct periods of BA versus YD. As a third data set we use output from high-resolution global climate simulations performed within this project to evaluate the mean climate states and their changes between the BA and YD. The different data sets and the methods related to the quantification and compilation of the data, as well as the setup and design of the climate model simulations are described below.

2.1 Proxy data compilation

In a first step, published quantified climate records from European terrestrial sites were searched for and evaluated in respect to sampling resolution and chronology. Specifically, we searched for climate proxy records that had been sampled continuously and in high temporal resolution and that were accompanied by an independent chronology allowing to obtain an uninterrupted climate record. However, it soon became clear that too few records classified in respect to these requirements exist, typically because the age assignments of most data sets were based on i) insufficient radiocarbon dates, ii) pollenstratigraphies only, iii) bio- and/or lithostratigraphic correlations to other sites or iV9 correlations to the Greenland ice core stratigraphy. Given these limitations, we decided to include all records with published quantified climate estimates in our data base, independent of a high-resolution chronology and leaned upon the stratigraphic assignment published by the respective authors. This group of climate proxy data sets includes chironomids, coleoptera, and cladocera and is here defined as Group 1 (Appendix 1).

In a second step, we searched for published pollen- and plant macrofossil stratigraphies and selected the plant taxa that constitute climate indicator plant species (Table 2-1). This data set, defined as Group 2, comprises local aquatic and telmatic pollen taxa, as well as plant macrofossil remains of aquatic, telmatic, and in some cases terrestrial species. The chronological/stratigraphic assignment of these data sets also follows that of the original publication. In many cases, however, the chronological framework for most of the data sets was poor and mainly based on pollenstratigraphy. Therefore, we grouped the available taxa and assemblages at each site into two time periods only, Bølling-Allerød (BA) and Younger Dryas (YD). This approach prevents the identification of site-specific temporal variability, but is the only possibility given the lack of good chronological constraints.

2.2 Proxy data quantification

2.2.1 Insect-based summer temperature quantification

Insect-based (chironomids, coleoptera) quantitative summer temperature reconstructions are made using two different methods. These methods have been extensively discussed in the literature (Atkinson et al. 1987, Juggins 2013). Chironomid-inferred reconstructions are based on mathematical transfer functions and established training sets that convert the fossil biological assemblage into a specific climate parameter (e.g. Birks and Birks 1998). Coleoptera-based reconstructions on the other hand are performed using the mutual climatic range (MCR) method (Atkinson et al. 1986), which has been extensively applied to beetle assemblages in Europe (Atkinson et al. 1987, Coope et al. 1998). This technique leans upon the assumption that today's climatic tolerance range of a species can be applied to fossil beetle assemblages (Coope 1986).

The insect data sets compiled here have been used in several previous studies (e.g. Björck et al. 1996, Coope et al. 1998, Heiri et al. 2014, Veski et al. 2015), including YD model-data comparisons (e.g. Heiri et al. 2014, Renssen et al. 2015). We therefore refer to the original studies for details on the specific transfer function or the MCR method used to transform proxy data into quantitative estimates (see also Sections 2.3.2 and 2.3.3 and Appendix 1). All insect-based temperature reconstructions in our proxy data compilation are reported according to the original publications.

2.2.2 Summer temperature quantification using climate indicator plant species

The second approach to reconstruct summer temperatures uses aquatic, telmatic and terrestrial climate indicator plant species (see also Section 2.3.3) and largely follows the method defined by Väliranta et al. (2015). It allows reconstructing quantitative minimum mean July temperatures and relies on a direct comparison of current plant species distribution data and measured meteorological data in Finland. A unique modern species-specific spatial plant distribution data set (http://www.luomus.fi/kasviatlas) covers the whole of Finland and long-term meteorological climate normals are readily available. The meteorological data are available from 10×10 km resolution grid cells. Thus, the plant distribution database, based on continuous botanical surveys, can be used to correlate modern species distributions with climate variables.

Unlike many European countries where human activities strongly influence plant distributions, Finland can be considered to be in a relatively natural state. The oceanity–continentality gradient is not particularly pronounced in Finland although continentality increases from the southwest (semi-oceanic) to the northeast (semi-continental) of the country. Likewise, the precipitation gradient is gradual with a difference of ca. 200 mm a^{-1} between southern and northern Finland. In contrast, Finland has a pronounced north–south temperature gradient as July temperatures range from ca. 17 °C in the south–southeast to ca. 7.5 °C in the mountains of western Lapland. As a result, Finland spans several bioclimatic zones from the boreo-nemoral to the boreal and to the subarctic vegetation belts. Therefore, many plant species reach their northern distribution limits within Finland. Only in the northernmost part of the country are plant distributions limited by elevation-related climatic conditions. These geographical facts provide an excellent setting to exploit observed modern plant species – temperature relationships for palaeo-temperature reconstructions.

To reconstruct minimum mean July temperatures from the compiled plant species in Group 2, we chose the species, which currently has the highest July temperature requirements. This allows us to reconstruct the minimum mean July temperature that is required for the growth of the specific plant species found in the compiled and analysed sedimentary records. We then compared this information with measured mean July temperatures for the years 1970–2000 at the present northern distribution limit of the respective species in Finland. For each species, we used an interpolated mean July temperature over a 10×10 km grid cell and analysed several grid cells containing species occurrences along the current distribution boundary. A median and mean July temperature range, i.e. the lowest and the highest value along the species-specific northernmost distribution boundary of these grid cells is given in Table 2-1. The median value integrates all July temperature values, i.e. also for those occurrences which may be located in unusually favourable microhabitats and exceptionally ideal microclimates. It should be kept in mind, however, that modern plant distribution maps typically show a pattern where the plant-specific minimum July requirement increases towards more continental areas, i.e., the distribution area shifts southwards. Conversely, in oceanic areas species distributions run northwards. This pattern may lead to underestimated July temperature reconstructions for continental areas and overestimations for highly oceanic areas (Valiränta et al. 2015).

Like macroscopic plant remains, pollen of aquatic and shoreline plant species are only locally dispersed (Birks and Birks 2000) and thus represent local rather than regional conditions. However, pollen of aquatic and riparian species are not always reported or published, and these species are therefore also always excluded from pollen-based temperature reconstructions. Aquatic and riparian pollen taxa are often scarcely present and are thus, similar to the plant macrofossil record, often not continuous. Therefore, we base the minimum mean July temperature reconstruction presented here on presence only and not on abundance of these species. Moreover, the absence of macroscopic plant remains or local pollen from fossil subsamples is not a solid proof of absence of the plant itself, whereas the presence of macroscopic species remains or local pollen can be taken as a strong evidence of actual presence *in situ*.

The discontinuous nature of the data set in Group 2, and the indicator species approach which only accounts for presence, prevents the estimation of a sample-specific error, which can be provided for instance by transfer function procedures. Moreover, it should be noted that our reconstruction is based on northernmost individual occurrences, while the main populations are always located further to the south. The derived temperature values are therefore minimum mean July temperatures. This implies that the July temperature of a given plant species represents only an inequality (at least as warm as, $T_{July} \geq$ the plant specific value in °C) and may result in colder temperatures than the actual July mean temperature. For the climate reconstruction, there is no possibility to define an uncertainty for the upper bound of the July temperature estimate leading to an underestimation of the true temperature (risk for cold bias). However, it is possible to define the uncertainty for even colder temperatures (risk for a warm bias) than given by the plant species. The amount of possible July temperature overestimations based on a given plant indicator species can be calculated from the differences between the "median observed" and the "lowest observed" July temperature for any plant species (Table 2-1). These median-to-lowest differences typically vary around 1 K (median 0.7 K) with a range of 0.1 to 3.3 K (Schenk et al. 2018).

A total of 38 plant taxa (fossil pollen and plant macrofossils) could be compiled from published sources (Appendix 1). These can be used as temperature indicators for the BA and YD intervals following the relationship between their current geographical distributions and corresponding July temperatures in Finland (Table 2-1).

Table 2-1: List of late-glacial (last deglaciation) plant species including plant macrofossil and pollen data with related minimum July temperature ranges determining the species' current northernmost distribution limit [in °C].

Taxon	Median of July mean	July mean range	Taxon	Median of July mean	July mean range
Alisma plantago-aquatica	14.3	14.1–14.9	*Myriophyllum spicatum group*	12.2	10.7–13.3
Calla palustris	13.6	13.3–14.0	*Myriophyllum verticillatum*	13.8	13.5–14.2
Callitriche cophocarpa	13.7	13.5–13.9	*Najas flexilis**	16.8*	16.7–16.8
Callitriche hermaphroditica	14	13–14.5	*Najas tenuissima*	16.6	16.1–16.7
Callitriche spp.	11.9	10.0–12.5	*Nuphar lutea*	13.1	12.5–14.0
Campanula latifolia	15.7	15.0–16.0	*Nymphaea alba*	13.5	13.2–14.0
Carex pseudocyperus	16.7	15.7–16.8	*Potamogeton berchtoldii*	12.2	10.0–13.6
Ceratophyllum	14.1	13.6–14.3	*Potamogeton crispus*	16.5	16.2–16.8
Cicuta virosa	13	12.1–14.1	*Potamogeton filiformis*	13.5	10.5–15.4
Cladium mariscus	16.0*	15.7–16.3	*Potamogeton lucens*	14.2	13.9–14.5
Elatine hydropiper	14.2	13–15	*Potamogeton natans*	12.9	12.2–13.8
Fragaria vesca	13.3	12.0–14.2	*Potamogeton obtusifolius*	13.9	13.6–14.3
Glyceria notata	16.7*	16.5316.8	*Potamogeton praelongus*	13.2	10.0–13.9
Isoëtes lacustris	12.7	10.9–13.0	*Potamogeton pusillus***	13.6	
Isoëtes echinospora	12.4	9.1–13.0	*Potamogeton spp.*	11.7	10.1–13.6
Lemna minor	13.6	12.3–14.3	*Subularia aquatica*	11.4	10.1–12.7
Littorella uniflora	16.1	14.3–16.8	*Trifolium repens*	12.5	10.4–12.9
Lythrum salicaria	14.3	14.2–14.9	*Typha latifolia*	15.7	15.1–16
*Menyanthes trifoliata***	8 (10)		*Zannichellia palustris****	14.4	

* Average value based on two occurrences only.

** Temperature value based on literature (Isarin and Bohncke 1999). However, 10 °C is a more realistic July value for this species because it does not grow beyond the tree line in Finland.

*** The species has a complicated current distribution pattern and lives mainly in brackish water environments in Finland, whereas it has an inland and temperate zone distribution on the European mainland; the temperature estimate remains therefore tentative.

2.2.3 Chronological assignment of the temperature-proxy data set

The paleo-proxy compilation contains a total of N = 122 records, which were sub-divided into two groups (Appendix 1). The first group with in total N = 34 records consists of insects with chironomids (N = 28), cladocera (N = 1) and coleoptera (N = 5) (Appendix 1). These records are mostly characterised by high temporal sampling resolution and provide relatively continuous time series. The age assignment of the Group 1 data set follows the published bio- and/or chronostratigraphic zonation of the respective authors. However, since we were only interested in comparing the general mean temperature difference between the BA and YD with the climate simulation, we ignored within-period temperature variations and calculated averages for the BA and YD intervals, respectively.

The second group, comprising plant climate indicator species, provided only discontinuous time series with low temporal resolution. Rather than using averages, temperature estimates in Group 2 are based on the presence of the species with the highest temperature requirements within a certain biostratigraphic zone. This second group consists of N = 88 records covering the BA and/or YD (Appendix 1) and is separated into aquatic (P, a) or emergent pollen (P, e), plant macrofossils from aquatic (M, a) or emergent (M, e) species, and tree macrofossil remains as the only terrestrial indicator (M, t). To define the boundaries for the BA and YD periods in each stratigraphic record, we generally adopted the pollenstratigraphic zonation presented in the original publications. Relying on the local pollenstratigraphy was the most conservative and suitable way to define transitions between the different time intervals and the transition into and out of the cold YD stadial.

2.3 Transient high-resolution multi-proxy lake sediment records from southern Sweden

The choice of the two lake sediment sites in southern Sweden, Atteköpsmosse and Hässeldala Port (Figure 2-1), was based on previous information and studies, which showed that both sites are promising for obtaining chronologically well-constrained multi-proxy records (Wohlfarth et al. 2006, 2018).

Atteköpsmosse (56° 23' N; 12° 51' E; at 180–175 m.a.s.l.), which today is a small wetland, is located on Hallandsåsen, a NW-SE trending horst in south-western Sweden (Figures 2-1 and 2-2). It has for a long time been known to contain a long Last Termination sediment record (Håkansson 1984, Wohlfarth et al. 2018). Multiple sediment cores and transects obtained in year 2000 had moreover allowed reconstructing the bottom topography and infilling of the ancient lake basin (Veres 2001, Wohlfarth et al. 2018). The first long sediment core, which had been obtained in 1981 (C-1981) and analysed for loss-on-ignition and pollen (Wohlfarth et al. 2018), suggested basal ages of around 13 ^{14}C ka BP (Håkansson 1984) and that the regional Oldest Dryas, Bølling, Older Dryas, Allerød, Younger Dryas and early Holocene pollen zones are well represented (Table 2-2). Later investigations on cores from the central part of the basin (C-2000/C6) (Wohlfarth et al. 2018) included loss-on-ignition, organic carbon, magnetic susceptibility, grain size analyses and ^{14}C dates and confirmed earlier basal ages of circa 13 ^{14}C ka BP (Veres 2001) (Table 2-2).

Hässeldala Port (56' 16°N; 15' 01°E; 63 m.a.s.l.) is a small peat bog (Figures 2-1 and 2-2) located in the province of Blekinge in southeastern Sweden and contains a distinct Lateglacial lake sedimentary record. Using multiple parallel cores and a set of biological (pollen, chironomids, coleoptera), physical and chemical proxies (sedimentology, tephra, radiocarbon chronology, major elements, loss-on-ignition, total organic carbon and nitrogen and their isotopes), climatic and environmental conditions could be reconstructed (Andersson 2004, Davies et al. 2004, Wohlfarth et al. 2006, Watson 2008, Kylander et al. 2013), see Table 2-3. These studies showed that the ancient lake at Hässeldala Port started to form some time before 14 ka BP, that the regional Older Dryas, Allerød, Younger Dryas and early Holocene pollen zones are clearly represented and that the sediments have the potential for high-resolution climate end environmental reconstructions.

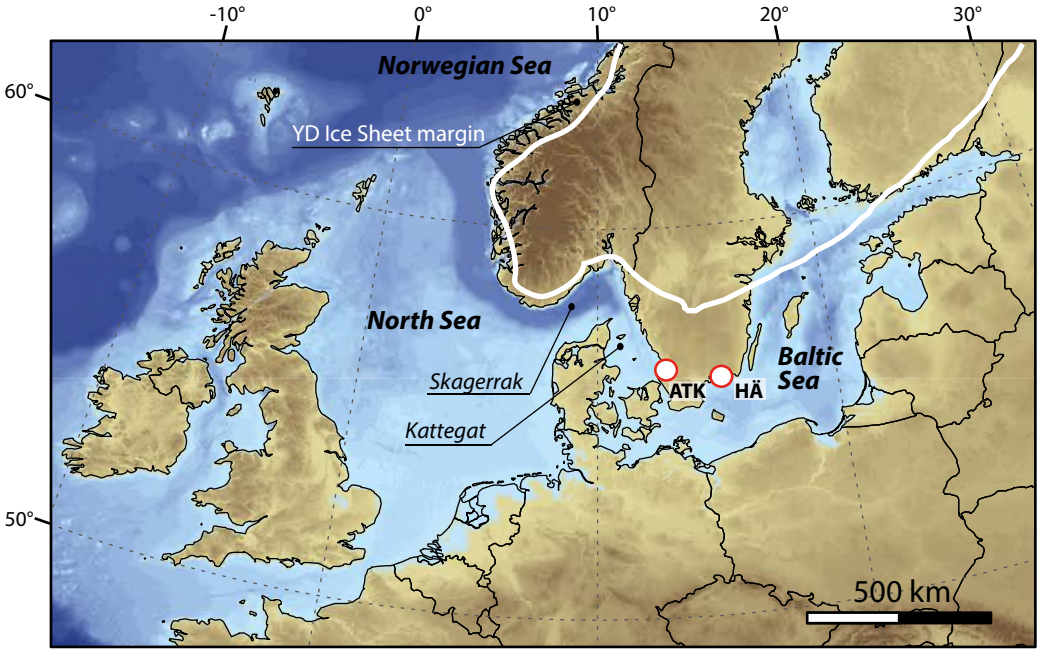

Figure 2-1. *Location of the studied lake sedimentary records in southern Sweden, Atteköpsmosse (ATK) and Hässeldala Port (HÄ). Redrawn after Muschitiello (2016).*

Table 2-2. Atteköpsmosse sediment cores and analysed proxies. LOI = loss-on-ignition, TOC = total organic carbon; C/N = carbon:nitrogen ratio, XRF = major elements. Core C-2011 was analysed within the frame of the present SKB project.

Core #	Proxy	Reference
C-1981	Pollen stratigraphy, LOI, ^{14}C	Wohlfarth et al. 2018, Håkansson 1984
C-2000/C6	LOI, TOC, magnetic susceptibility, grain-size, ^{14}C	Veres 2001, Wohlfarth et al. 2018
C-2011	XRF, LOI, tephra, C/N, $\delta^{13}C_{bulk}$, $\delta^{15}N_{bulk}$, ^{14}C chronology, age-depth model, plant macro remains, chironomids, biomarkers, hydrogen isotopes	Muschitiello 2016, Wohlfarth et al. 2018

Table 2-3. Summary of sediment cores and proxies analysed at Hässeldala Port during the past 15 years. LOI = loss-on-ignition; TOC = total organic carbon, C/N = carbon:nitrogen ratio, XRF = major elements. Cores #5 and 6 were analysed within the frame of the present SKB project.

Core #	Proxy	Reference
1	LOI, TOC, tephra	Davies et al. 2003
2	TOC, tephra, ^{14}C	Davies et al. 2004
3	TOC, tephra, pollen stratigraphy	Davies et al. 2004, Andersson 2004, Wohlfarth et al. 2006
4	TOC, C/N, $\delta^{13}C_{bulk}$, $\delta^{15}N_{bulk}$, XRF	Kylander et al. 2013
HP4	LOI, tephra, chironomids	Watson 2008, Muschitiello et al. 2015b
HP6	LOI	Watson 2008
HP9	LOI, tephra	Watson 2008
HP12	LOI	Watson 2008
5	LOI, ^{14}C chronology, leaf stomata	Steinthorsdottir et al. 2013, 2014
	diatoms	Ampel et al. 2014
	XRF	Unpublished
	biomarkers, age-depth model	Muschitiello et al. 2015a, b, Muschitiello 2016
	δD_{wax}, $\delta^{13}C$	Muschitiello et al. 2015b
6	LOI, pollen stratigraphy	Muschitiello et al. 2015b, Karlatou-Charalampopoulou 2016
1–6		Wohlfarth et al. 2017

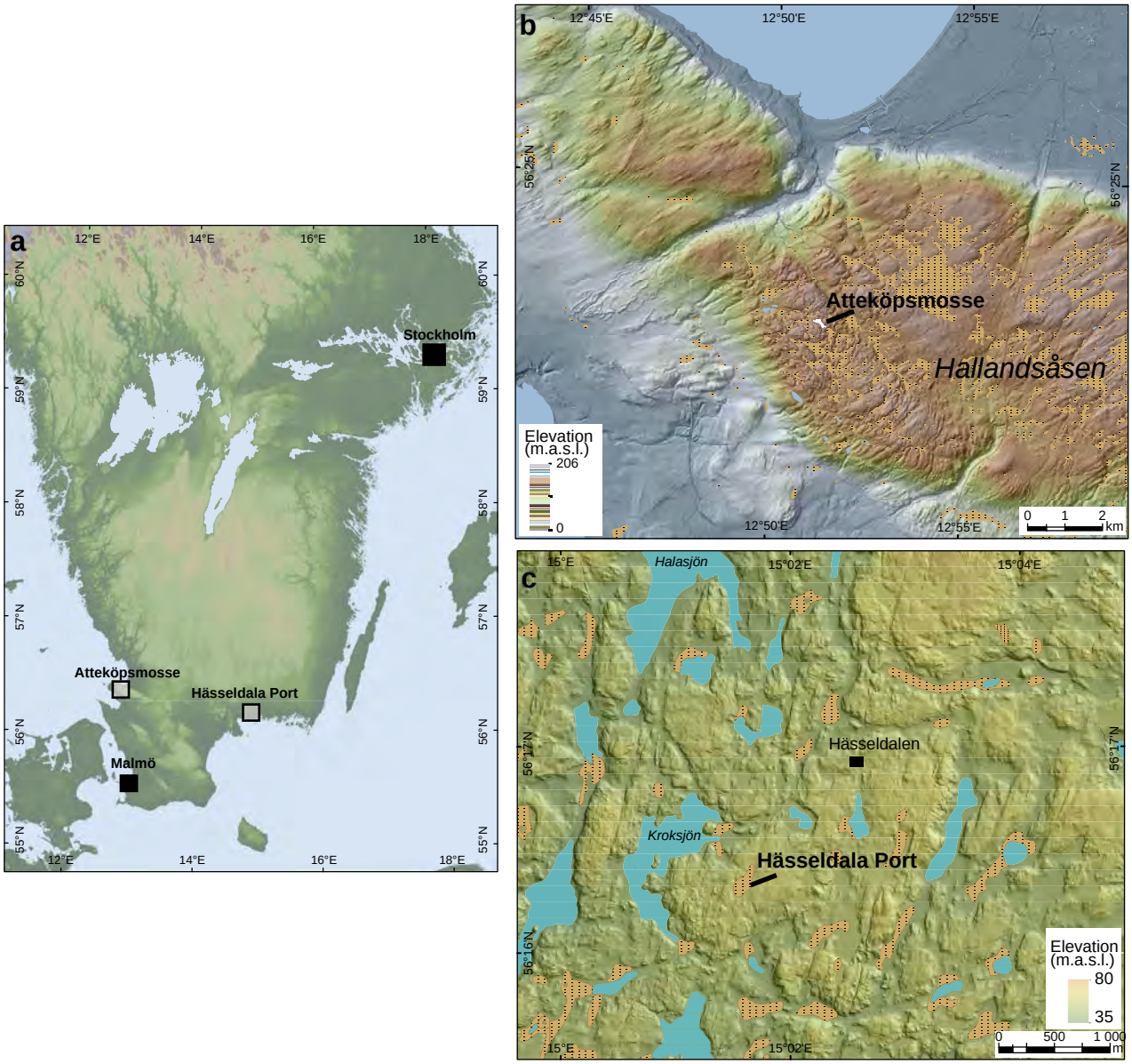

Figure 2-2. *A) Map over southernmost Sweden showing the location of the two study sites Atteköpsmosse and Hässeldala Port. Map provided by Sarah Greenwood. B) Topography around Atteköpsmosse on Hallandsåsen in south-west Sweden. Modified after Wohlfarth et al. (2018). C) Topography of Hässeldala Port in Blekinge, southeast Sweden. Modified after Wohlfarth et al. (2017).*

In autumn 2011, a new series of sediment cores were recovered from the deepest parts of the Hässeldala Port and Atteköpsmosse basins using a Russian corer (7.5 and 10 cm diameter, 1 m length). The sediment cores were wrapped in plastic foil, placed in PVC tubes and transported to the Department of Geological Sciences, Stockholm University, where they were stored at 4 °C until further analysis.

Analyses of the new Atteköpsmosse cores (C-2011) (Table 2-2) focussed on lithostratigraphy, geochemistry, tephra, biomarkers and hydrogen isotopes, pollen stratigraphy, plant macrofossils, chironomids, quantified summer temperatures, a high-resolution ^{14}C chronology and age-depth modelling and are described in detail in Muschitiello (2016) and in Wohlfarth et al. (2018). This new data set allowed a reconstruction of climatic and environmental changes in southwest Sweden between 15.5 and 10 ka BP.

Multi-proxy analyses of the new cores (cores #5 and 6) from Hässeldala Port (Table 2-3) focussed on diatom stratigraphy (Ampel et al. 2014), carbon dioxide reconstructions based on fossil leaf stomata and a new radiocarbon chronology (Steinthorsdottir et al. 2013, 2014), pollen stratigraphy (Karlatou-Charalampopoulou 2016), biomarkers, hydrogen isotopes, a revised chronology and detailed age-depth

modelling (Muschitiello et al. 2015a, b, Muschitiello 2016). The methodology and laboratory analyses are detailed in each respective publication and also in Wohlfarth et al. (2017), who presented an environmental and climatic summary for Hässeldala Port and for Blekinge in general, including quantitative summer temperatures, for the Last Termination (14.3–9.5 ka BP).

Several of the analytical methods mentioned above are well established techniques, which are routinely employed for the analysis of lake sediments (e.g. the analysis of major elements, loss-on-ignition, total carbon and nitrogen, diatoms, pollen, plant macrofossils and chironomids). Others, such as summer temperature reconstructions based on climate-indicator plant species (Väliranta et al. 2015) (see Section 2.2.2), carbon-dioxide reconstructions using fossil leaf stomata (Steinthorsdottir et al. 2013, 2014) and the application of biomarkers and of hydrogen isotopes to reconstruct past moisture sources and past hydrological conditions (Sachse et al. 2012) are methods that have been further developed and refined during the past years. Therefore, their application in the study of the two south Swedish lake sediment records has to be regarded as a novel approach. Moreover, the two studied sites are the first lake sediment records in southern Sweden for which a high-resolution chronology could be established, including state-of-the-art age-depth modelling. For the carbon-dioxide reconstructions using fossil leaf stomata we here refer to Steinthorsdottir et al. (2013, 2014), because this study was not directly related to or financed by the SKB project. For the approach to derive minimum mean July temperatures using climate-indicator plant species (Väliranta et al. 2015) we refer to Section 2.2.2. In Section 2.3.1 we provide a background on the analysis of biomarkers and hydrogen isotopes, since these were the major topic of the PhD project financed by SKB (Muschitiello 2016) and in Section 2.3.2 we shortly present the different proxies that have been studied at Atteköpsmosse and Hässeldala Port. For more details, we refer to the respective publications (Tables 2-2 and 2-3).

2.3.1 Hydrogen isotopes of lipid biomarkers as a paleo-hydrological tool

The membranes of algae and aquatic plants and the cuticular waxes of higher terrestrial plant leaves are composed of lipid biomarkers, which include n-alkanes (e.g. Ficken et al. 2000). N-alkane hydrocarbons are well preserved in sedimentary archives (Eglinton and Hamilton 1967, Eglinton and Eglinton 2008) and allow separating aquatic and terrestrial components in lake sediments, based on chain length. Given that water is the main source of hydrogen for photosynthesizing organisms, the hydrogen-isotopic composition (δD) of sedimentary lipids has emerged as a powerful tool to reconstruct past climate and environmental conditions (Sachse et al. 2012).

Following hydrogen-transfer reactions, the δD composition of these aquatic and terrestrial n-alkanes is generally highly correlated with the δD values of the source water used by the precursor organisms: intracellular water for aquatic plants and leaf water for terrestrial plants (Figure 2-3) (Sachse et al. 2004, 2012). This is the result of a series of environmental parameters (e.g. precipitation amount and source, temperature, relative humidity) and physiological processes involving intracellular water (e.g. leaf physiology, salinity, light intensity, biosynthetic pathway) that drive the source-water-to-lipids isotopic fractionation (i.e. net or apparent fractionation) (Sachse et al. 2012).

Although some of these processes are still not fully understood, the δD composition of lipid biomarkers from lake sediments has rapidly become an established proxy to reconstruct paleo-hydrological conditions and δD of precipitation (e.g. Aichner et al. 2010, Rach et al. 2014, Muschitiello et al. 2015b). Indeed, δD values of short-chain n-alkanes (n-$C_{17–23}$) from submerged and terrestrial plants collected from lake-surface sediments along climatic gradients appear to be highly correlated with lake-water δD values and precipitation δD values, respectively (Huang et al. 2004, Sachse et al. 2004, 2006, Garcin et al. 2012). These studies suggest a good preservation of the source water δD signal and damped variability associated with individual biological sources and specific processes owing to temporal and spatial (within the catchment) integration. Nonetheless, even though both aquatic and terrestrial plants undergo isotopic fractionation, which depends on the specific biosynthetic pathway, the net or apparent fractionation of the δD values of terrestrial n-alkanes is strongly affected by two additional fractionation steps: soil-water evaporation and leaf-water transpiration processes (Figure 2-3) (e.g. Sachse et al. 2006, 2012). Soil-water and leaf-water evapotranspiration are controlled by plant anatomy conditions, relative humidity and soil moisture availability. However, these parameters are poorly understood owing to the large number of biological unknowns and integration steps that are associated with the net or apparent fractionation, and due to the lack of experimental culture-based studies.

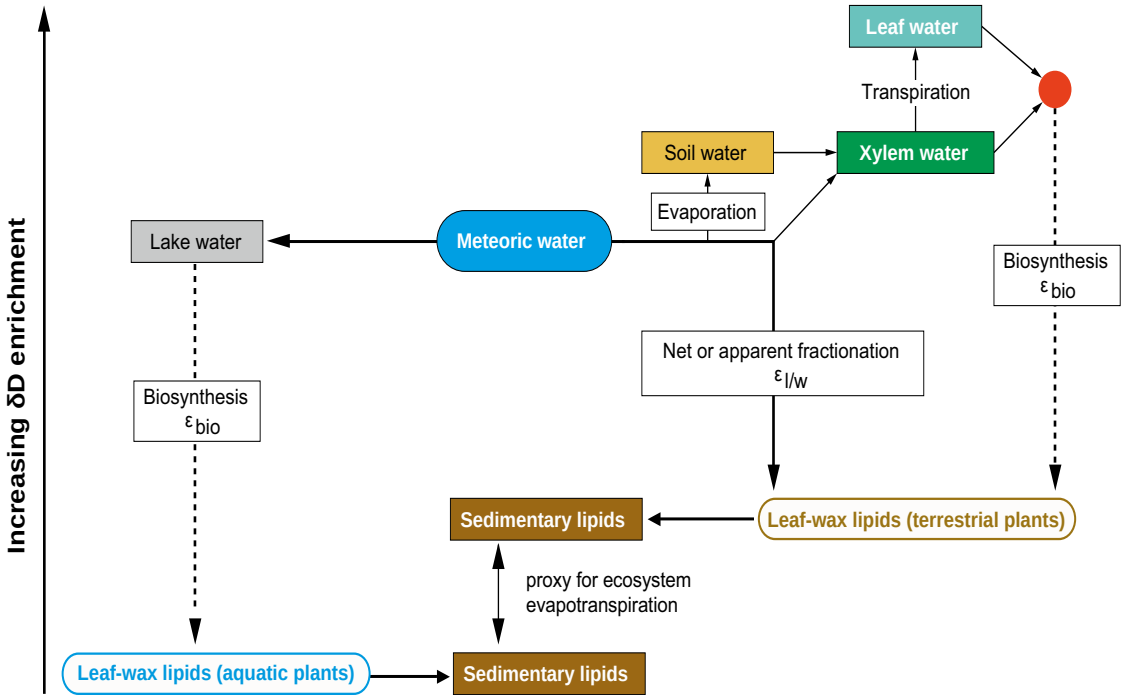

Figure 2-3. *Conceptual relationship between the hydrogen-isotopic composition of source water and sedimentary n-alkanes of aquatic and terrestrial plants (not to scale). The red dot illustrates a hypothetical mixture of water pools within the leaf, constituting the ultimate hydrogen source for lipid biosynthesis. εbio, biosynthetic hydrogen-isotopic fractionation; εl/w, isotopic fractionation between lipids and source water. Modified from Sachse et al. (2012).*

Although an empirical understanding of all the processes behind the net or apparent fractionation in higher plants may help to frame paleo-hydrological reconstructions in a quantitative fashion, at present, the isotopic difference between terrestrial and aquatic n-alkanes can only be used as a qualitative proxy for reconstructing changes in catchment evapotranspiration (Figure 2-3). It should also be born in mind that, before using lipid biomarker δD values for paleo-hydrological interpretations, it is important to characterise the paleo-environment using a multi-proxy approach. Specifically, pollen and plant macrofossil analyses can help to factor out or account for possible vegetation shifts, thereby allowing disentangling climatic versus physiological effects on leaf-water δD. Another reason to apply a multi-proxy approach consists in the simultaneous dependency of hydroclimatic variables on temperature and humidity.

2.3.2 Laboratory methods

Since sampling procedures and the employed laboratory methods for Atteköpsmosse and Hässeldala Port have already been described in detail in each respective publication (see Tables 2-2 and 2-3), we only shortly summarise the methods here.

The lithology of the individual cores was described and overlapping cores were correlated with each other using specific marker horizons. This, combined with XRF scanning (Kylander et al. 2013, Wohlfarth et al. 2018), allowed creating a composite stratigraphy for Atteköpsmosse and Hässeldala Port, respectively and formed the basis for further sub-sampling. All sub-samples were taken in contiguous 1 cm increments, freeze-dried and then split to accommodate for the analysis of various proxies. Samples for plant macrofossil analysis and radiocarbon dating, however, comprised contiguous 1 to 5 cm intervals.

Loss-on-ignition (LOI), bulk carbon and nitrogen and carbon and nitrogen isotope analyses were made to estimate the organic matter and carbon content respectively and to assess the contribution of aquatic and terrestrial plants at each level. In addition, individual LOI curves were used to correlate previously analysed sediment cores with the new cores from Atteköpsmosse and Hässeldala Port, respectively (Muschitiello et al. 2015a, b, Muschitiello 2016, Wohlfarth et al. 2018).

Lipid extraction was performed on freeze-dried samples with variable volume (2–8 cm^3) after sonication with dichloromethane: methanol (9:1) for 20 minutes and subsequent centrifugation. The process was repeated three times and supernatants were combined. Aliphatic hydrocarbon fractions were isolated from the total lipid extract using silica gel columns (5 % deactivated) that were eluted with pure hexane. Subsequently, a saturated hydrocarbon fraction was obtained by elution through 10 % $AgNO_3$-SiO_2 silica gel using pure hexane as eluent. The saturated hydrocarbon fractions were analysed by gas chromatography – mass spectrometry for identification and quantification, using a Shimadzu GCMS-QP2010 Ultra. C_{21} to C_{33} *n*-alkanes were identified based on mass spectra from the literature and retention times. The concentration of individual compounds was based on the comparison of peak areas relative to that of an internal standard (squalane) that was added to the samples before total lipid extraction. Hydrogen isotope ratios were determined using a Thermo Finnigan Delta XL mass spectrometer and all analyses were performed in triplicate. A standard mixture of *n*-alkanes with known δD composition (mix A4, provided by A. Schimmelmann, Indiana University, USA) was run several times daily to calibrate the measured δD values (‰) to VSMOW. For data interpretation, we only used sample values that were characterised in the isotope-ratio mass spectrometer chromatograms by baseline separated peaks, and also were of high enough peak size to fall within the linearity range of the instrument.

Among the samples analysed for plant macrofossils, those with abundant terrestrial plant remains were identified. Leaves, buds, flowers, seeds, and catkin scales were picked out with tweezers, rinsed multiple times in deionised water, placed in pre-cleaned glass vials and dried overnight at 105 °C. The dried samples were then submitted to the 14Chrono Centre, Queen's University Belfast for radiocarbon dating. Sample pretreatment and measurement followed the methodology described in Steinthorsdottir et al. (2014) and in Muschitiello et al. (2015b). The chronologies for the two sites were constructed using a Bayesian age-depth model and the calibrated ^{14}C dates (Reimer et al. 2013). The Bayesian age-depth relationship was established using OxCal4.2 (Bronk Ramsey 2010). The sequence of ^{14}C dates was modeled multiple times prescribing different prior information parameters until the optimal set up was achieved, i.e. an ideal trade-off between coherent prior information parameters and stability of the Monte Carlo Markov Chain simulation (Muschitiello 2016).

Pollen samples for Atteköpsmosse (core C-1981) (Wohlfarth et al. 2018) and Hässeldala Port (core #6) (Muschitiello et al. 2015b, Karlatou-Charalampopoulou 2016) were prepared in accordance with the method described in Berglund and Ralska-Jasiewiczowa (1986). Local pollen assemblage zones were identified based on major changes in herb/grass shrub and tree pollen percentages and the pollen diagrams were constructed using the program C2 of Juggins (2007).

Sub-samples for plant macrofossil analysis (Atteköpsmosse) were sieved under running water using a 150-µm mesh and the residue was examined under a stereomicroscope (Wohlfarth et al. 2018). All remains were counted and identified to as low taxonomic levels as possible. Zonation of the plant macrofossil diagram was made visually.

Sub-samples for fossil chironomid analysis (Atteköpsmosse) (Wohlfarth et al. 2018) and Hässeldala Port (Watson 2008, Wohlfarth et al. 2017) were prepared applying standard methods (Brooks et al. 2007). The wet sediment was sieved through a 100-µm mesh and the residue was examined under a stereomicroscope. Larval head capsules were extracted with fine forceps and mounted permanently on microscope slides. Identification was performed under a light microscope. The minimum chironomid head capsule number per sample was set to 50 (Heiri and Lotter 2001). Constrained unweighted pair-group average (UPGMA) cluster analysis (chord distance) was used to group samples into four local faunal zones to indicate temporal changes in fossil assemblages.

Since not all proxies had been analysed on the same cores (see Table 2-2 and 2-3), we used the respective LOI curves to align cores C-1981 and C-2011 from Atteköpsmosse and cores #3, 4, HP4, 5 and 6 from Hässeldala Port, respectively (Wohlfarth et al. 2018). This was done following the approach presented in Muschitiello et al. (2015a, b) and in Muschitiello (2016), who used a Monte Carlo Markov Chain algorithm for core-to-core alignment. The technique provides a suite of possible alignments between stratigraphic series and the target series and estimates the optimal correlation between cores. Once the optimal correlation between the LOI curves was found, proxies could be projected on the chronology of the master core and allowed presenting the suite of different proxies on one common time scale for Atteköpsmosse and Hässeldala Port, respectively.

2.3.3 Quantification of biological proxies

The quantitative plant macrofossil-based July air temperature reconstruction followed the procedure introduced in Väliranta et al. (2015) (see Section 2.2.2 in the present report for a detailed description of the method) and its application for the BA-YD period is presented in Schenk et al. (2018). The chironomid-based mean July surface water temperature (deduced from air temperatures) reconstruction for Atteköpsmosse used the expanded Fennoscandian calibration model (weighted-averaging partial least squares, WA-PLS) combining several data sets (Luoto et al. 2016). The temperature gradient in the training set varies from 7.9 to 17.6 °C and includes subarctic, boreal and temperate lakes. The 2-component model currently includes 180 lakes and 129 taxa having an r^2_{jack} of 0.86, a root mean squared error of prediction (RMSEP) of 0.85 °C and a maximum bias of 0.75 °C. Sample-specific errors (eSEP) were estimated using bootstrapping cross-validation (999 iterations). Using the modern analogue technique (MAT), the cut-level of the 5th percentile of all chi^2-distances in the modern calibration data were determined. These distances were then compared to the distance between each fossil assemblage and its most similar assemblage in the modern dataset and used to define 'no close' analogues.

2.4 Climate model simulations

To study the transient climate evolution from the warm Bølling-Allerød (BA) interstadial to the Younger Dryas (YD) cold stadial, we make use of the TraCE21k data from the fully coupled Atmosphere-Ocean General Circulation Model (AOGCM) of CCSM3 run for the last 21 ka (He 2011, Liu et al. 2012, He et al. 2013). The simulation provides the so far best constrained transient run with a full complexity model for the whole last deglaciation reproducing the rapid climate shifts. Besides incorporating the relatively well-known gradual changes in orbital and Greenhouse Gas (GHG) forcing, the advantage of the simulation lays in the significant efforts undertaken to find the best solution for simulating rapid shifts in the paleo-ocean. These are mainly triggered by fresh water disturbances of the thermohaline ocean circulation from melting ice sheets (He 2011).

The disadvantage of the TraCE21k simulation is its coarse horizontal resolution of ~375 km (T31, $3.75° \times 3.75°$), which makes the analysis of local to regional climate over Europe and Sweden questionable. We therefore performed dedicated high-resolution global climate simulations for the key periods of interest in this project to characterise the spatially detailed response of the climate system to the strong changes in the forcing by the ocean together with changes in orbital and GHG forcing.

2.4.1 Model version CESM1.0.5

For the climate simulations, we used version 1.0.5 of the Community Earth System Model (CESM1.0.5) (Gent et al. 2011). The model is maintained by the National Center for Atmospheric Research (NCAR) in Boulder, Colorado, USA. A detailed documentation of the model, including the model code, is available online at http://www.cesm.ucar.edu/models/cesm1.0/. Details about modifications of the model setup, boundary conditions and model experiments are given below.

In the absence of any objective criteria for choosing a specific model, the rationale behind using the model version for this project was to maintain consistency with a previous SKB study that modelled climate and ice sheet configurations for peak glacial conditions of the penultimate Saalian glaciation (Colleoni et al. 2014). For the simulation of climates very different from today, a reliable model version with existing experience and validations for the historical and modern climate is important. This excludes using the newest version to rule out that large changes and/or potentially unexpected results are caused by changes to a new model version rather than climatic changes.

Based on these considerations, we used the latest CESM version which has undergone thorough technical and scientific validations against climate observations, i.e. version 1.0.5 with release date 1 February 2013. The model code family CESM1.0.z, which is built on and hence includes the last CCSM4.0 version, has been the code basis used for CMIP5/AR5 simulations (Braconnot et al. 2012) and provides one of the so far latest officially released "scientifically supported model configurations". Scientifically, the version used here is identical with the newer CESM1.0.6 (1 May 2014) and previous CESM1.0.4 where major bug fixes were applied relative to version 1.0.3. As of January 2019, no model bugs of any technical or scientific relevance for our simulations have been found by the climate modelling community.

Newer versions 1.1.z (i.e. with a new atmospheric model CAM5) and 1.2.z (i.e. with a new land model CLM4.5) have been developed partly in parallel to the latest 1.0.z versions and are meanwhile available including scientifically relevant new model physics for different components. The process of developing scientifically supported model configurations and validation is however still ongoing. Information about significant changes for the validity of the fully coupled new components relative to previous versions is not yet available. We therefore consider our model version to be state-of-the-art.

2.4.2 Model setup, paleo-topography and ice sheets in CESM1

For the spatially detailed proxy-model comparison, we focussed on two time periods, which allowed us to contrast the climatic impact over Europe and Sweden in response to the extreme changes in the North Atlantic Ocean during the Younger Dryas relative to the preceding BA interstadial. For high-resolution simulations of the selected time periods we therefore use the F1850 component set for CESM1, which is a pre-industrial setup (parameters incl. land use setup for ~1850 AD) that interactively couples models of the atmosphere (CAM4), land (CLM4) and sea-ice (CICE) with pre-scribed sea-surface-temperatures and sea-ice fraction (DOCN). For the atmosphere, we used a horizontal model resolution of $0.9° \times 1.25°$ with a finite volume grid of 26 vertical levels. CLM consists of a complex land model with 15 vertical soil levels down to 35 m soil depth. Although the sea-ice fraction is prescribed, CICE calculates all fluxes and surface conditions over ice consistent with the actively run atmosphere.

To simulate the Last Termination, we modified all horizontal global boundary condition files by including large continental ice sheets, adjustments of the paleo-topography for glacial-isostatic vertical movement and new coastlines consistent with low sea-level stands. We used a new interim (GLAC1-b) version of the GLAC1 ice sheet reconstruction by Lev Tarasov. GLAC1-b includes three published continental ice sheets, North America (Tarasov et al. 2012), Antarctica (Briggs et al. 2014) and Greenland (Tarasov and Peltier 2002), together with an ongoing reconstruction of the Eurasian component using a Bayesian calibration based on the DATED Fennoscandian ice sheet retreat chronology (Hughes et al. 2016). The ice sheet reconstruction is a state-of-the-art version and makes use of climate forcing retrieved from results of the 2nd and 3rd phase of the Paleoclimate Model Inter-comparison Project (PMIP-II and III) of the Last Glacial Maximum (LGM). The version GLAC1-b is very similar to the meanwhile completed official version of GLAC1-D which will be used for simulations within the recently started 4th phase of the PMIP4 project (Ivanovic et al. 2016).

The paleo-boundary condition files for BA and YD were created by interpolating the GLAC1-b ice sheets and changes in paleo-topography onto the pre-industrial boundary condition files of CESM1 following the technical steps described by Colleoni and Rosenbloom (2014). As no vegetation maps are available for the selected periods, we maintained constant pre-industrial values with urban areas set off. The surface types of new land areas due to 60–70 m lower sea-level stands were set with a next-neighbour interpolation. Grid points with new ice sheets are defined as glaciers using the ice-mask provided by GLAC1-b.

The use of pre-industrial instead of late-glacial vegetation cover adds to the uncertainties of our simulations because forests e.g. across Europe decreased during the YD relative to BA (e.g. Theuerkauf and Joosten 2012, Birks and Birks 2014). The disappearance of darker forests could lead to a negative forcing via higher albedo during summer and hence act as a potential cooling signal. In the same time, drier soil conditions during the YD without forests might enhance a positive evaporative feedback leading to warmer summer conditions (see Section 4.2.4 and Figure 4-4). The impact of vegetation changes on the regional climate is hence uncertain. Given the lack of complete paleo-vegetation maps for BA and YD, we do not study such potentially important regional climate impacts in this project.

Within this project, we include changes in paleo-topography and ice sheets based on GLAC1-b, which represent the periods 13 ka BP (AL) and 12 ka BP (YD). Although differences in coastlines, elevation and ice sheets are included in our simulations for AL vs. YD, they introduce only low-order changes at the given model resolution and are not studied explicitly here. The paleo-topography and ice sheets used for our simulations are shown in Figure 2-4.

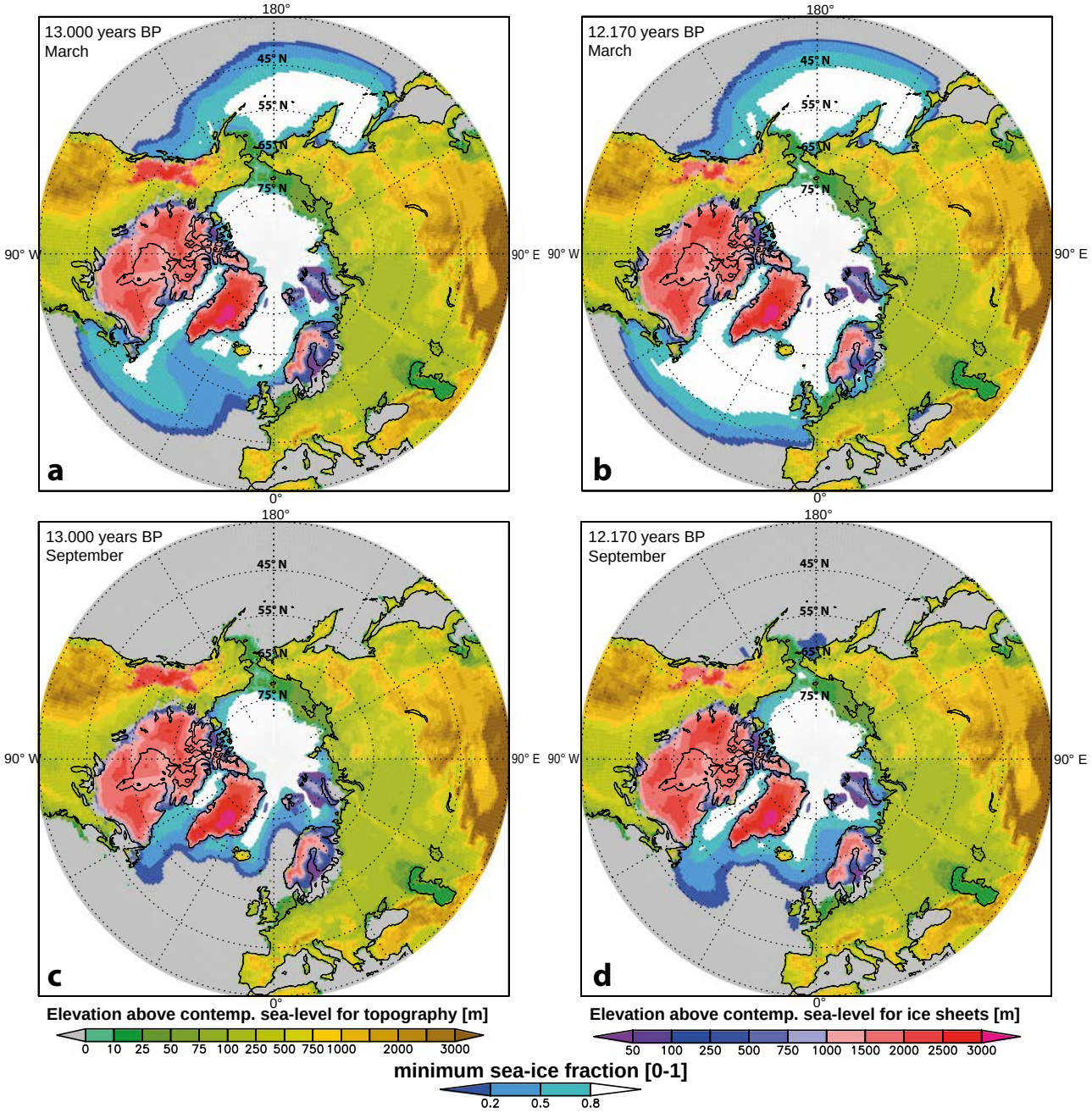

Figure 2-4. *Paleo-topography, ice sheets and sea-ice fraction used as horizontal boundary conditions for our CESM1 simulation for the Allerød at 13 ka BP (clim13k, AL) and Younger Dryas at 12.17 ka BP (clim12k, YD). The paleo-topography and ice sheets are according to GLAC1-b. The sea-ice fraction is according to the CCSM3 simulation (He 2011). The changes in maximum (March) and minimum (September) sea-ice fraction from the Allerød to the Younger Dryas represent a slowdown of the AMOC by ~36 % (~5.3 Sv) in the fully coupled CCSM3 simulation.*

2.4.3 Boundary conditions and radiative forcing for our CESM simulations

Horizontal boundary condition files for the prescribed paleo-ocean state were calculated from a previous *Simulation of Transient Climate Evolution over the last 21 000 years* with CCSM3 (TraCE-21ka (Liu et al. 2009, 2012, He 2011, He et al. 2013). Several sensitivity tests have been performed with CCSM3 for the YD using different hosing scenarios (He 2011). The scenario with the so far best- known fit with paleo-proxy data and an AMOC proxy used here (McManus et al. 2004) is from TraCE. Simulated YD air temperatures by CCSM3 have been found to be too warm compared to the δ^{18}O-based temperatures from Greenland ice cores. However, because δ^{18}O-based temperatures during the YD are as cold as during the Oldest Dryas, although the AMOC was

much weaker during the Oldest Dryas compared to the YD, a cold bias has been suggested for the $\delta^{18}O$-values during YD rather than a warm bias for the simulation (Liu et al. 2012). Recent proxy evidence for Dansgaard-Oeschger oscillations between 48 and 30 ka BP and multi-model hosing experiments generally question a uniform cooling over the whole North Atlantic and Greenland region (Wary et al. 2017) (see also discussion Chapter 4). However, the paleo-ocean state is still not well known from proxy data so that any simulated ocean state introduces large uncertainties for any type of analysis.

For the simulations in this project, we focussed on the warmest period directly before the onset of the YD and compared it to the coldest period during the mid-YD. The definition of these periods is based on the simulated surface temperature evolution over Denmark and southern Sweden from CCSM3. Based on this simulation, we calculated the sea-surface-temperatures (SST), sea-ice fraction and greenhouse gas (GHG) forcing as the average of ±50 years around 13 ka BP (model experiment = clim13k) for the warm AL interstadial period and ±50 years around 12.17 BP (model experiment = clim12k) for the cold YD stadial period, respectively. Because the land-sea distribution is very different in the coarse CCSM3 model as compared to the high resolution of CESM, we used surface temperatures (TS) from CCSM3 rather than SST's to calculate a climatology for monthly mean SST/TS and ice fraction for both periods. Some land points in CCSM3 constitute ocean grid cells when using the high-resolution land-sea mask in CESM1. For these CESM1 grid cells, surface temperatures below −1.8 °C were set to this value, which is the freezing point of salt water in the model.

GHG concentrations were calculated as an average of ±50 years around the orbital years of 13 ka BP (AL) and 12.17 ka BP (YD) using merged values derived from air bubbles in Greenland and Antarctic ice cores. Following the PMIP3/4 protocol, the merged GHG values were taken from (Joos and Spahni 2008) and are hence consistent with the TraCE simulation from which the SST's/TS are prescribed (He 2011). Based on the GHG values for the AL and YD periods, the change in radiative forcing due to GHG between AL and YD can be calculated using empirical equations derived from atmospheric radiative transfer models. Compound specific radiative forcing ΔF (W/m²) can be derived as (Ramaswamy et al. 2001, Table 6.2):

CO_2: $\Delta F = \alpha ln \frac{C}{C_0}$ (2-1a)

CH_4: $\Delta F = \beta\left(\sqrt{M} - \sqrt{M_0}\right) - [f(M, N_0) - f(M_0, N_0)]$ (2-1b)

N_2O: $\Delta F = \gamma\left(\sqrt{N} - \sqrt{N_0}\right) - [f(M_0, N) - f(M_0, N_0)]$ (2-1c)

with $f(M,N) = 0.47 ln[1 + 2.01\times10^{-5}(MN)^{0.75} + 5.31\times10^{-15}\, M(MN)^{1.52}]$ and $\alpha = 5.35$, $\beta = 0.036$, $\gamma = 0.12$, $C_0 = 278\ ppm$, $M_0 = 722\ ppb$, $N_0 = 270\ ppb$.

The Equations 2-1a to 2-1c use C_0, M_0, and N_0 values as pre-industrial reference values for GHG concentrations of 1750 AD. The user given values for C, M and N are the actual GHG concentrations for CO_2, CH_4 and N_2O either for AL or YD, respectively. As we are not interested in ΔF (W/m²) relative to 1750 AD but in ΔF (W/m²) between AL and YD, the differences of ΔF (YD) minus ΔF (AL) [W/m²] are given in Table 2-4. Hence, a total ΔF of −0.907 W/m² for AL and −1.086 W/m² for YD relative to the reference values of 1750 AD leads to a small negative radiative forcing (ΔF=−0.180 W/m²) for the YD relative to AL in terms of GHG. Using the sum of the compound specific derivations of ΔF for CO_2, CH_4 and N_2O of −0.180 W/m² according to Equations 2-1a–c, the negative radiative forcing in terms of CO_2 equivalent [ppm] can be derived by inverting Equation 2-1a (Myhre et al. 1998) to derive C with ΔF=−0.180 W/m² as input. Hence, the negative radiative forcing represents a total reduction in terms of CO_2 equivalent of only −7.75 ppm for the YD relative to AL.

Table 2-4. Greenhouse gas (GHG) concentrations for the Allerød interstadial (AL) and the Younger Dryas stadial (YD), as well as the resulting radiative forcing difference between the two periods (YD-AL) used in this simulation. AL corresponds to the simulation clim13k and YD to clim12k.

GHG forcing	AL (13 ka)	YD (12.17 ka)	ΔF for YD-AL
CO_2	237.8 ppm	238.4 ppm	+0.013 W/m²
CH_4	633.6 ppb	475.9 ppb	−0.107 W/m²
N_2O	265.2 ppb	241.3 ppb	−0.085 W/m²
Total change YD-AL	**−7.749 ppm CO_2-equivalent**		**−0.180 W/m²**

The orbital forcing was set to the exact years and calculated by CESM1. The prescribed SST and sea-ice fraction from CCSM3 reflects a weakening of the AMOC of ~36 % (−5.27 Sv) from 14.5 Sv in the simulation clim13k (AL) to 9.2 Sv during simulation clim12k (YD). The simulated oceanic response by CCSM3, which is used as horizontal boundary conditions for our CESM simulation, is hence consistent with the AMOC proxy, i.e. that the AMOC was significantly reduced during the YD, but still active relative to the Oldest Dryas (McManus et al. 2004). Although the clim12k simulation (YD) is the coldest period in CCSM3, a large increase in solar insolation of +5 W/m² takes place relative to clim13k (AL) owing to the rapidly increasing orbital forcing for summers at high northern latitudes (June, 60°N) during the later part of the Last Termination. We therefore ran an additional sensitivity experiment (model experiment = clim13kYD) where we used the radiative forcing (GHG + orbital) for clim13k (AL), but prescribed the cold ocean state of the YD as in clim12k. This sensitivity experiment is crucial to identify the competing effects of increasing summer radiation on the one hand and a strong oceanic cooling on the other hand.

While the orbital forcing is precisely known and GHG concentrations for the late-glacial are well constrained through various ice cores from Greenland and Antarctica, a potentially important uncertainty remains regarding the role of dust as a potential negative radiative forcing for summer temperatures. Although there is a clear increase in dust in the Greenland ice cores during the YD, it is unclear at this stage which dust sources, dust distribution and dust amount would be realistic to be added to our CESM1 simulations. Owing to the large general uncertainties regarding the radiative forcing of dust and the limited knowledge about dust during the BA-YD period, we do not take paleo-dust into account. For the Last Glacial Maximum, Lambert et al. (2013) suggested a quite strong radiative cooling by dust of around −3 to −6 W/m² over Greenland. Applied to the BA-YD period, such a negative forcing would be significant at the onset of the YD. However, already during the early part of the YD, an extreme dust scenario would be already compensated for by the strong increase in orbital summer insolation at high northern latitudes which yields +5 W/m² from the AL to the mid-YD. Combined with the potential negative forcing by vegetation changes, dust may provide an additional potential negative radiative forcing which may yield slightly colder YD summers than simulated here.

3 Results

The results from this study are presented in five sections. First, we present the transient climate evolution of the late deglaciation over southern Sweden as reconstructed from two high quality well-dated lake records (Section 3.1). In a second step, we focus our analysis on the wider spatial scale to identify the patterns of regional climatic changes in terms of reconstructed mean summer temperatures across Europe based on our multi-proxy data compilation (Section 3.2). In a third part, we briefly compare the model-resolution dependent climatic response of the YD relative to BA as simulated by CCSM3 and CESM1 (Section 3.3) before we present a detailed spatial analysis of climate change and atmospheric drivers for the CESM1 simulations (Section 3.4). Finally, we compare the reconstructed and simulated summer temperatures and analyse the impact of changes in seasonality (Section 3.5).

3.1 Transient changes in climate and environment in southern Sweden during the last deglaciation from proxy data

3.1.1 Chronological limitations

Both of the studied Swedish lake sediment records, Atteköpsmosse (Swedish west coast) and Hässeldala Port (Blekinge), have an excellent radiocarbon chronology, based on fairly dense and more or less continuous radiocarbon dates on selected terrestrial plant macrofossil remains. Moreover, the age-depth model was made using the latest Bayesian age-modelling techniques (Wohlfarth et al. 2018, Muschitiello et al. 2015b). Despite this, the precision of chronologies and age models has limitations, which are discussed below.

Depending on the availability of suitable terrestrial plant macrofossil remains in the lake sediments, radiocarbon samples comprised between one and four centimetres in thickness. In the case of Hässeldala Port most radiocarbon samples encompassed one to two centimetres of sediment, with rare exceptions amounting to 3.5 cm of sediment (Wohlfarth et al. 2017). For Atteköpsmosse, most radiocarbon samples comprised between 0.5 and 1 cm of sediments. However, material for dating was scarce in the bottom part of the sediments, where each sample encompassed between 3 and 4.5 cm. Moreover, parts of the stratigraphy between 542 and 518 cm depth were not possible to sample and dates are therefore lacking from this interval. Each radiocarbon date is reported with its specific error, and this error and a suite of other parameters were taken into consideration in the calibration of a radiocarbon age, i.e. its translation into calendar ages, and in age-depth modelling (Bronk Ramsey 2008, 2009, Muschitiello 2016) (Figure 3-1).

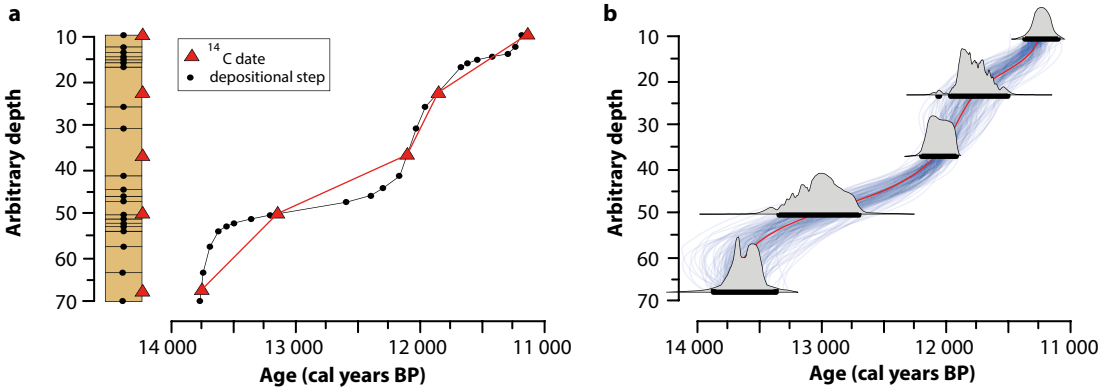

Figure 3-1. *Synthetic example of a radiocarbon-dated sequence and the resulting age model. From Muschitiello (2016). A) Example of a depositional process with sediment progressively accumulating over time. Black dots show changes in accumulation rate and the black line reflects the "true" age-depth history of the sedimentary record. The red triangles represent radiocarbon-dated samples and the red line reflects a tentative age-depth relation based on linear interpolation between the chronological constraints. B) Construction of a probabilistic age-depth model using the radiocarbon dates in (a). For details see Muschitiello (2016).*

The age-depth curve for Atteköpsmosse shows the uncertainties associated with each calibrated radiocarbon date, the error envelopes of the age-depth model, as well as the large uncertainties in the upper part of the stratigraphy (Figure 3-2) due to a lack of radiocarbon dates. These uncertainties are important information, but cannot be shown in, for example a pollen diagram or summary figure, and are also not included in a discussion of the climatic and environmental development, because they would make the text and figures impossible to read. Instead median ages are used throughout, with the implication that each of these median ages comes with a certain error, which is only shown by the age-depth model figure or in a table. Although median ages for successive samples generally do not overlap with each other, it has to be kept in mind that if their respective errors were included, possible age ranges could overlap.

In the case of one stratigraphic record only, this is of less importance, since interest is mainly placed on how the different proxies, analysed in the same sample and at the same level, relate to each other in relative time. However, when two separate stratigraphic data sets are compared with each other in time, the limitations of even an excellent age-depth model and its inherent errors become obvious.

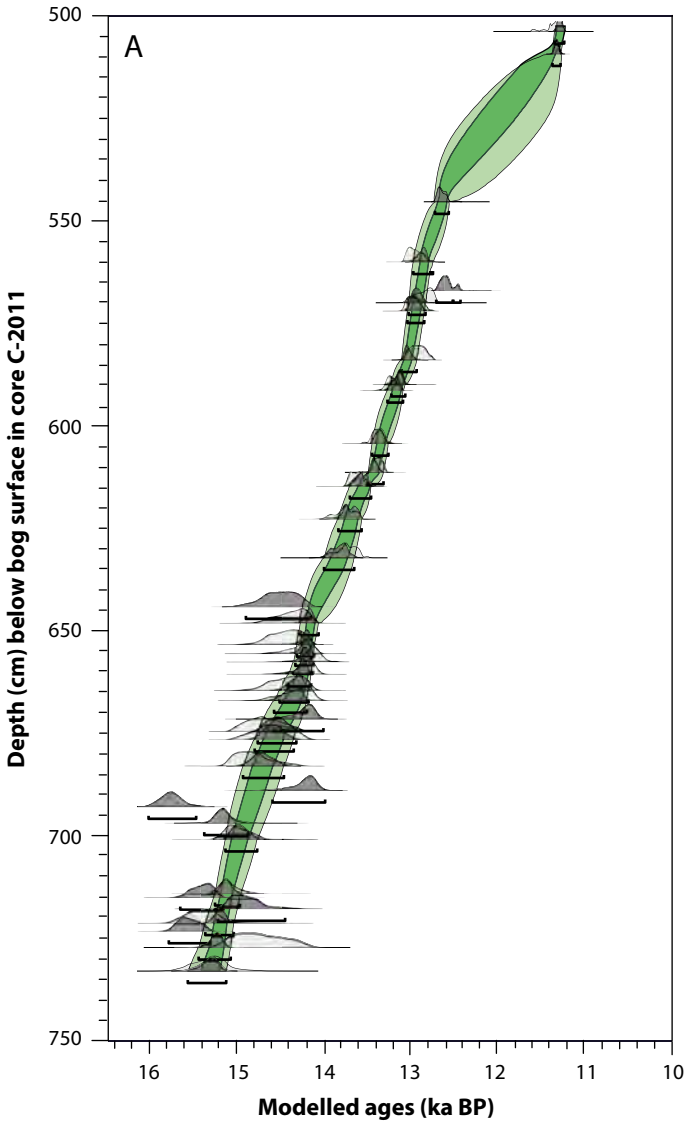

Figure 3-2. *Age-depth model for Atteköpsmosse based on 37 calibrated radiocarbon dates (Wohlfarth et al. 2018) including the 1-sigma (dark grey) and 2-sigma (light grey) standard deviation of each calibrated date. The inner and outer green envelopes indicate the 68 % and 95 % calendar age confidence intervals, respectively. Note that the upper part of the age-depth model, where the green envelopes are very wide, is very uncertain due to a lack of radiocarbon dates between 542 and 518 cm depth.*

As an example, a change in proxies (e.g. temperature) occurs in record A at 12.9 ka ± 200 years, but in record B at 12.6 ka BP ± 200 years. At first sight one can conclude that the temperature change seen in record B lags that in record A by 300 years. However, when the respective errors are included, it becomes obvious that the temperature changes in records A and B actually overlap with each other in time. Unless we have a distinct stratigraphic marker that occurs after event A, but prior to event B, we cannot draw the conclusion that the change in record A occurred before the change in record B. Based on the age-depth model only, we can also not exclude the possibility that there was a time lag between the temperature changes in A and B and that the two events may represent the same temperature change. Moreover, we cannot estimate the duration of a possible time lag between A and B.

Figure 3-3 shows the 2-sigma error of each modelled median age point for Atteköpsmosse and Hässeldala Port, respectively. This error, which is given by the model, shows large variations for Atteköpsmosses's age-depth model, ranging from less than 100 years to 230 years, and attaining as much as 500 years in the upper part. In contrast, much lower errors are evident for Hässeldala Port.

Although modelled errors for the two age-depth curves are fairly narrow, except for the upper part of Atteköpsmosse, they do not include sample thickness, the reported error of each radiocarbon date and the errors of each calibrated date. Instead, and since the age-depth model tries to find the best fit (through numerous iterations) between depth and radiocarbon dates (see Figure 3-1), only the modelled error, corresponding to the green envelopes in Figure 3-2, is given. This, however, underestimates the total error for each age point at a given depth. This error varies for each data point.

Despite these limitations, we first present the results for Atteköpsmosse and Hässeldala Port on their respective age-depth models and inferred time scales, i.e. we use median ages for each data point and do not include the modelled errors. We thus follow the same approach as that in the published data sets (Wohlfarth et al. 2017, 2018).

However, in the discussion chapter we revisit this problem and discuss whether the available age-depth models provide us with enough confidence to decipher spatial and temporal differences between the site on the Swedish west coast and the site in Blekinge, or whether apparent temporal differences in the response of the different proxies only are artefacts.

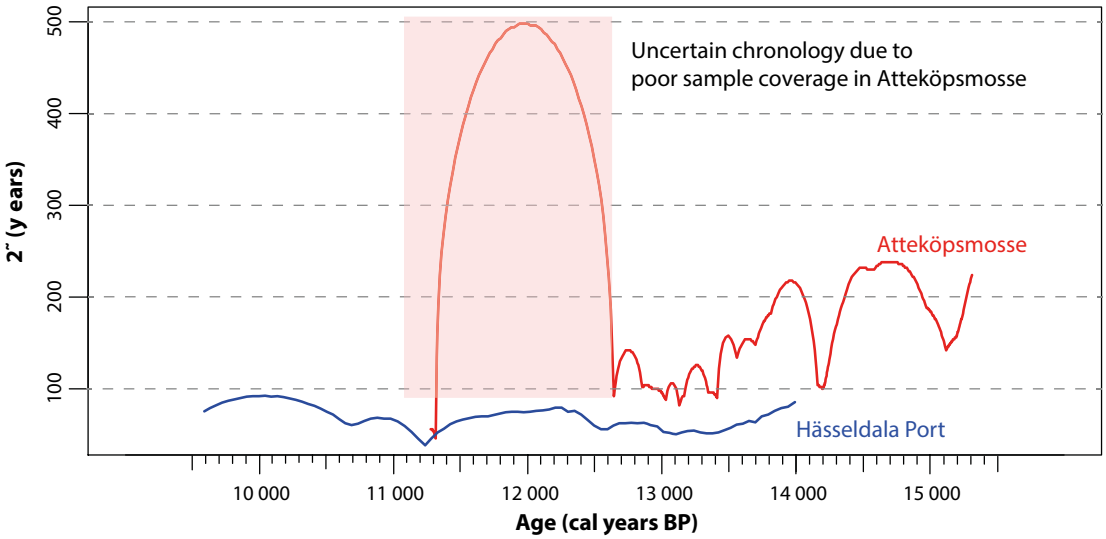

Figure 3-3. *2-sigma error for each point on the age-depth curve of Atteköpsmosse and Hässeldala Port given by the OxCal age model. Note that this error does not take into consideration sample size/thickness, the reported errors of each radiocarbon date and the resulting calibrated age errors (see Figures 3-1 and 3-2).*

3.1.2 Local and regional environmental and climatic development in south-western Sweden during the last deglaciation – the Atteköpsmosse data set

Multiple evidences suggest that parts of the Swedish southwest coast had become free of active ice already by around 17 ka BP (Sandgren and Snowball 2001, Hughes et al. 2016) (Figure 3-4). Since infilling of the Atteköpsmosse basin did not start until 15.3 ka BP, local stagnant ice probably remained in the region for around 2 000 years after the general deglaciation. The oldest phase of the ancient lake (15.3–14.7 ka BP) was characterised by oligotrophic, cold water and low aquatic productivity and compares in time to Greenland Stadial GS-2.1a (Wohlfarth et al. 2018). The unstable catchment slopes around the lake supported a fairly poor herb and shrub flora and contributed with easily erodible material (Figure 3-5). Reconstructed lake surface water July temperatures fluctuated around 6–9 °C (Figure 3-5), whereas minimum mean July air temperatures probably reached above 13 °C and possibly as much as ≥16 °C (Wohlfarth et al. 2018). This marked difference between chironomid-inferred and plant-inferred summer air temperatures could be explained by melting of stagnant ice, which kept lake water temperatures colder than ambient air temperatures (Luoto and Nevalainen 2013). The δD_{aq} record, which is a proxy for changes in the isotopic composition of the marine moisture source and/or condensation temperature (Rach et al. 2014, Muschitiello et al. 2015b) displays strongly fluctuating values between 15.3 and 14.7 ka BP (Figure 3-5). Lower values (15.2–15.1 ka BP; 14.95–14.75 ka BP) likely represent periods when the Nordic Seas were much fresher due to large amounts of glacial meltwater inflow and higher values between 15.1–15.0 ka BP depict a short interval with incursion of warm Atlantic waters and saltier Nordic Seas (Wohlfarth et al. 2018). The transport of colder/warmer air masses could in turn have led to colder/warmer conditions, respectively, around Atteköpsmosse.

A series of distinct changes is reflected in several of the analysed proxies between 14.7–14.5 ka BP. Lake surface water summer temperatures rise from 10 to 13 °C at 14.7 ka BP. This, together with the distinct peak in hydrogen isotope values at 14.65 ka BP, suggests inflow of warmer and moisture-rich air masses into the region (Wohlfarth et al. 2018). The change in circulation regime and temperature could have been the underlying trigger for the stabilisation of the catchment around Atteköpsmosse, for the rise in lake aquatic productivity and the subsequent higher abundance of aquatic plants.

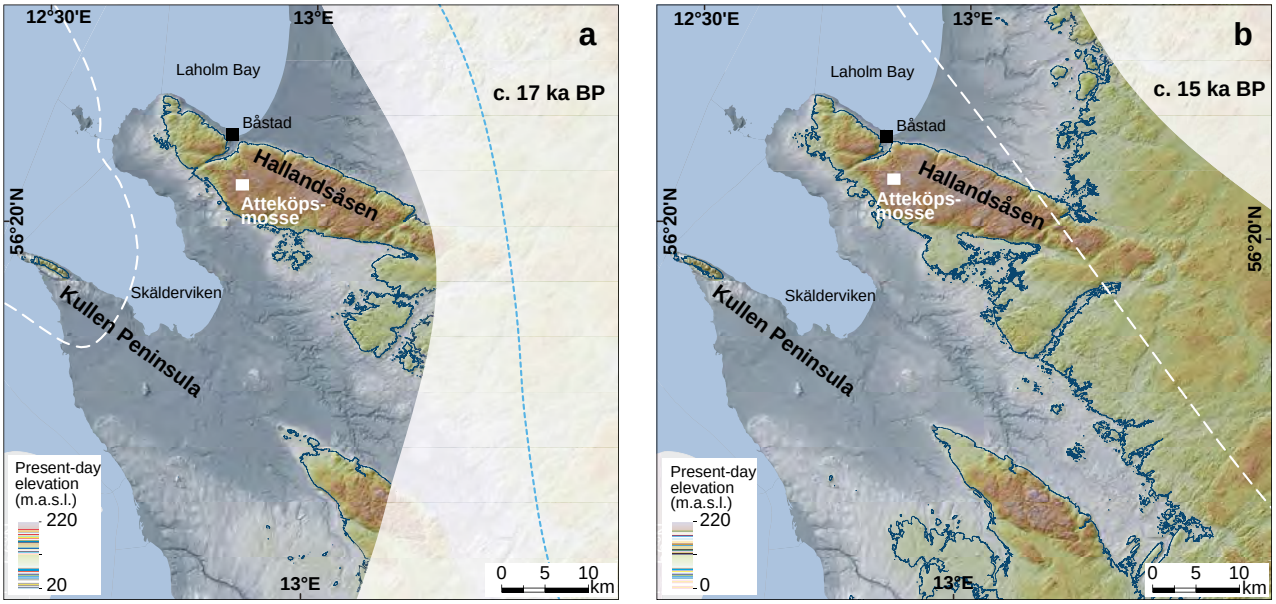

Figure 3-4. *A, b) Last deglaciation topography in south-western Sweden and around Atteköpsmosse, position of the Fennoscandian Ice Sheet and of the marine limit at c. 17 and c. 15 ka BP, modified after Wohlfarth et al. (2018). The possible maximum (white dashed line) and minimum (blue dashed line) extent of the ice sheet is according to Hughes et al. (2016). The marine limit has been estimated to 88 m above present-day sea level (17 ka BP) and to 77 m above present-day sea level (15 ka BP) and is according to Sandgren and Snowball (2011). The position of Atteköpsmosse on Hallandsåsen is shown by a white square.*

These latter changes, which are seen about 100 years after the changes in chironomid and hydrogen isotope proxies, coincide with the development of denser herb, shrub and dwarf shrub vegetation and with the establishment of tree birch (Betula pubescens) around the lake (Wohlfarth et al. 2018). The lake water July temperature inferred from chironomid assemblages also compares well with minimum mean July air temperatures of 12–13 °C suggested from plant indicator species (*Myriophyllum spicatum, Potamogeton berchtoldii/filiformis*; *Potamogeton alpinus*) and shows that the lake was no longer influenced by run-off from melting of stagnant ice. The response seen in the various proxies between 14.7 and 14.5 ka BP temporally coincides with the transition from Greenland Stadial (GS) 2.1a to Greenland Interstadial (GI) 1e (Rasmussen et al. 2014a) (Figure 3-5), which was characterised by a distinct temperature rise in the North Atlantic region (Steffensen et al. 2008). It therefore seems that the former lake and its catchment responded more or less directly to this large-scale hemispheric climate shift.

The time interval between 14.5 and ~12.8 ka BP (corresponding to the regional Bølling and Allerød pollen zones) can be regarded as a period of stability around Atteköpsmosse. Lake aquatic productivity further increased, chironomid assemblages typical for boreal forest lakes became established, and chironomid-inferred lake surface water summer temperatures rose to 14–15 °C at 14.3 ka BP and fluctuated thereafter between 11 and 15 °C (Wohlfarth et al. 2018). These temperature estimates compare well with those based on plant indicator species (*Callitriche hermaphroditica, Potamogeton compressus*), which suggest minimum mean July temperatures of around 14 °C. In addition to tree birch, pine (*Pinus sylvestris*) now also colonised the area around the lake (Figure 3-5). The inflow of warm and moisture-rich North Atlantic air masses continued as suggested by higher fraction of heavy hydrogen isotope However, at ~13.7 ka BP hydrogen isotope values start to decrease reflecting a shift towards a fresher moisture source, likely associated with an increase in freshwater discharge into the Nordic Seas from the decaying Fennoscandian ice sheet (Figure 3-5) (Wohlfarth et al. 2018). Hydrogen isotope values decline further between 13.1 and 13.0 ka BP, indicating a shift towards an even fresher moisture source and/or colder and drier conditions relative to the previous time interval (Figure 3-5). Charcoal – a proxy for forest fires - was earlier present in the sediments in very low numbers, but increases distinctly at 12.9 cal. ka BP and indicates the availability of fire sensitive woody plants and dry conditions.

The pollen stratigraphy places the transition between the regional Allerød and Younger Dryas pollen zones at 12.9–12.8 ka BP and coincident with the GI-1 to GS-1 transition in Greenland ice cores. This time marker therefore allows exploring the response of the various proxies before and close to the transition into the Younger Dryas. As described above, moisture production and transport to Northern Europe became less efficient around 13.1–13.0 ka BP. By 12.9 ka BP conditions around Atteköpsmosse had become drier, resulting in forest fires and a lake level lowering. Moreover, lake water surface summer temperatures decreased from around 14 °C to around 12 °C (Figure 3-5) (Wohlfarth et al. 2018). Despite these marked changes, the local plant communities, and thereof inferred minimum mean July air temperatures, display no major changes. Similarly, aquatic productivity declined gradually and low values were only reached by 12.5 ka BP, coincident with a slight change in chironomid assemblages. It may therefore be possible that the inferred dry conditions around the start of the Younger Dryas pollen zone did not affect the local plant communities until a time when climatic conditions also became progressively and distinctly colder and possibly also drier. This may indicate that significant local vegetation changes may lag the large-scale climate transition by several centuries.

Aquatic productivity as inferred from loss-on-ignition measurements remained low throughout the Younger Dryas pollen zone, while run-off and erosion increased (Figure 3-5). Chironomid-inferred mean lake surface water July temperatures fluctuated around 12 °C and only reached maximum temperatures of 10 °C by 12.3 ka BP. Sediments were void of plant macrofossils between 12.5 and 11.8 ka BP, i.e. for most of the Younger Dryas pollen zone. Only the samples younger than 11.8 ka BP provide some information about the local vegetation, which was composed of herbs and shrubs. Plant indicator species inferred minimum mean July temperatures are 12 °C, i.e. slightly higher than lake surface water July temperatures (Figure 3-5).

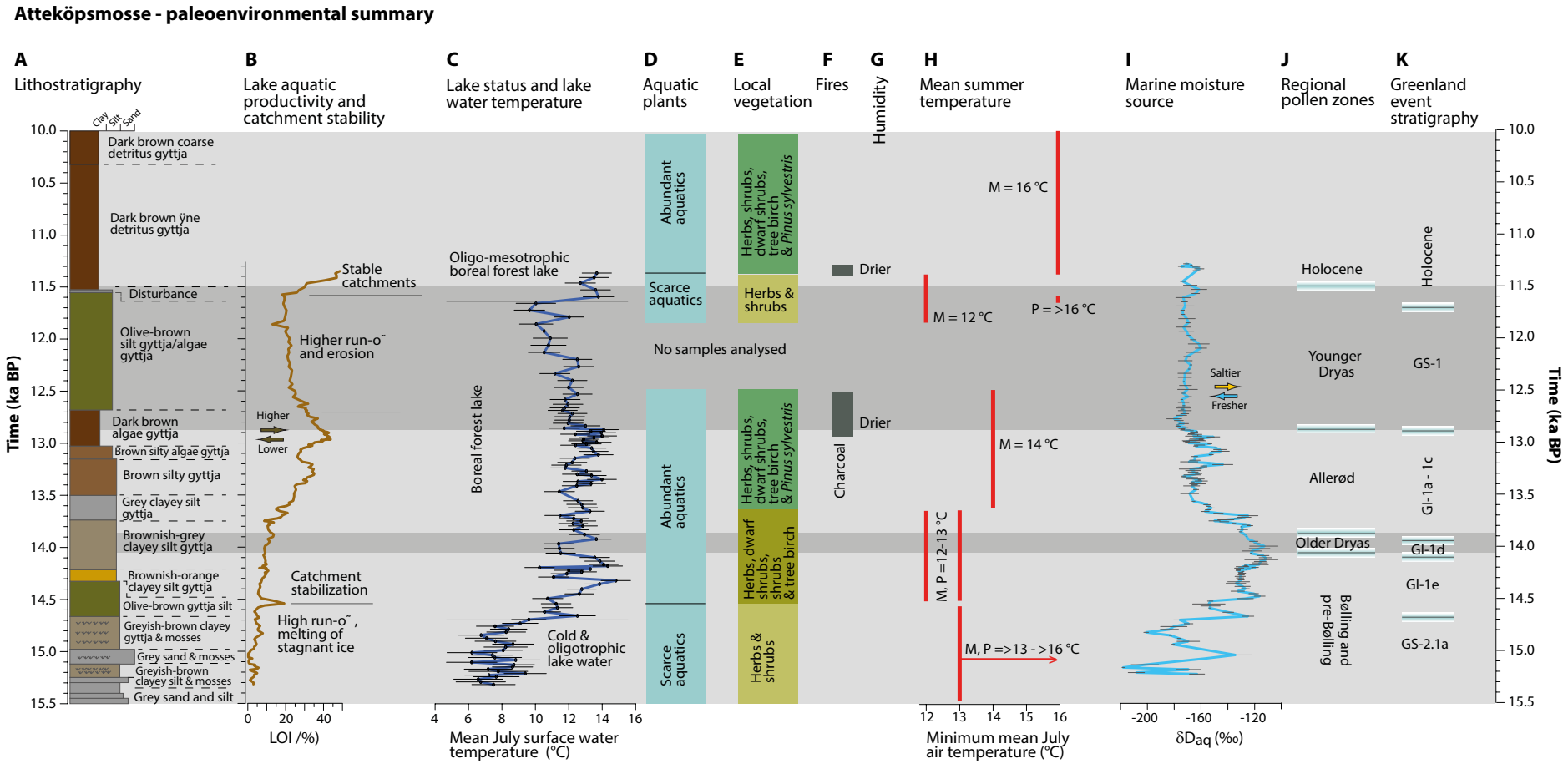

Figure 3-5. *Climatic and environmental development in and around Atteköpsmosse during the last deglaciation. After Wohlfarth et al. (2018). A) Lithostratigraphy; B) Loss-on-ignition (LOI) (organic matter content as a proxy for lake organic productivity); C) Chironomid-inferred mean July surface water temperature and lake status; D) Occurrence of aquatic plants; E) Local vegetation based on plant macrofossil finds; F) High amounts of charcoal indicate the occurrence of forest fires; G) Humidity inferred from presence of charcoal; H) Minimum mean summer temperatures derived from climate indicator plant species; I) Biomarker based inference of moisture source composition; J) Regional pollen zones; K) Greenland event stratigraphy (Rasmussen et al. 2014a).*

The transition into the Holocene (11.6–11.5 ka BP) is documented by a change in chironomid assemblages and a rapid increase in mean lake surface water July temperatures from 10 to 14 °C at 11.65 ka BP. Aquatic plants became abundant again by 11.4 ka BP and local vegetation now included tree birch and *Pinus sylvestris* (Figure 3-5). A chironomid fauna typical for oligo-mesotrophic boreal forest lakes suggests more stable catchments, higher aquatic productivity and presence of trees close to the ancient lake. Charcoal became abundant again at 11.4 ka BP and indicates dry conditions and availability of fire sensitive woody plants and perhaps also of litter.

A fresher moisture source and/or colder and drier conditions are indicated by changes in the ratio of hydrogen isotopes for the entire Younger Dryas time interval and also for the onset of the Holocene (Figure 3-5). This is surprising, given that significant changes in several proxies occurred at the transition from the Younger Dryas into the Holocene. The stable hydrogen isotope record could therefore reflect that the isotopic composition of precipitation, and by extension of the marine moisture source, remained substantially unchanged. It is likely that the Skagerrak-Kattegatt system and the North Sea remained largely fresh also after the onset of the Holocene due to enhanced melting of the Fennoscandian Ice Sheet in response to warming (Figure 3-5) (Wohlfarth et al. 2018).

3.1.3 Local and regional environmental and climatic development in south-eastern Sweden during the last deglaciation – the Hässeldala Port data set

Following the rapid decay of the Fennoscandian Ice Sheet margin in response to the temperature rise at the start of the Bølling at 14.7 ka BP, the area around Hässeldala Port gradually became free of active and stagnant ice (Wohlfarth et al. 2017). Sparse vegetation consisting of Arctic herbs and shrubs became established on unstable soils in ice free areas (Wohlfarth et al. 1994).

Gradual land uplift and emergence of new land areas during the regional Bølling and Older Dryas pollen zones (Björck 1981, 1984) (14.7–14.1 ka BP) changed Hässeldala Port's location from an archipelago setting to further inland (Wohlfarth et al. 2017) (Figure 3-6). The basal mineral-rich sediments in Hässeldala Port's ancient lake indicate deposition from stagnant ice or run-off from poorly vegetated slopes (Figure 3-7), and the herb, grass, shrub and dwarf-shrub dominated pollen assemblages (pollenzone HÄP-1) (Andersson 2004, Wohlfarth et al. 2006) assign these lowermost sediments to the regional Older Dryas pollen zone (Figure 3-8). Coleoptera assemblages suggest mild and cool summers during this early period with mean summer air temperatures of about 14 °C (Watson 2008) and the presence of *Nymphaea alba* in the aquatic pollen record of Hässeldala Port (Andersson 2004) (HÄP-1 in Figure 3-8) indicates minimum mean July air temperatures of $\geq$13.5 °C (Table 2-1). In contrast, mean July surface water temperatures reconstructed from chironomid assemblages are only around 7–8 °C (Figure 3-7) and may thus represent a lake water temperature that was strongly influenced by run-off from stagnant ice.

Hässeldala Port's pollen stratigraphy between 14.1 and 12.7 ka BP (HÄP-2 and HÄP-3 in Figure 3-7) (Andersson 2004) compares to the regional Allerød pollen zone (Berglund 1966, Björck and Möller 1987, Wohlfarth et al. 2017). Herbs, shrubs and dwarf shrubs still dominated the vegetation around Hässeldala Port (Figures 3-7 and 3-8). Other areas in Blekinge may, however, have supported more diverse vegetation, which also included tree birch (*Betula pubescens)* as indicated by a single macroscopic find (Berglund 1966, p 175). This is supported by the gradual increase in sediment organic matter and the distinct shift in diatom assemblages at 13.7 ka BP in Hässeldala Port that show that the catchment vegetation had become denser and the season of lake ice cover gradually shorter (Ampel et al. 2014, Wohlfarth et al. 2017). Chironomid-derived mean July surface water temperatures show a step-wise increase from 8 °C at 14.1 ka BP to maximum values of 12–13 °C at around 13.3–13.2 ka BP (Figure 3-7). Coleoptera assemblages now reconstruct summer temperatures > 14 °C (Watson 2008) and the presence of *Nymphaea alba* pollen (HÄP-2 and lower part of HÄP-3) (Andersson 2004) indicates minimum mean July temperatures of at least 13.5 °C (Table 2-1). Plant indicator species, such as *Typha latifolia* and *Jasione montana*, which are reported from pollen diagrams in Blekinge (Berglund 1966), moreover suggest that minimum mean July temperatures could locally have reached as much as $\geq$16.5 °C (Tables 2-1; 4-1). Leaf-wax derived hydrogen isotopes, $\delta D_{n\text{-}}C_{21}$ and $\Delta\delta D_{terr\text{-}aq}$, which reflect the isotopic composition of the source moisture and terrestrial evaporation, respectively, indicate a saline moisture source for Hässeldala Port's precipitation and minor shifts between drier and wetter conditions (Figure 3-7).

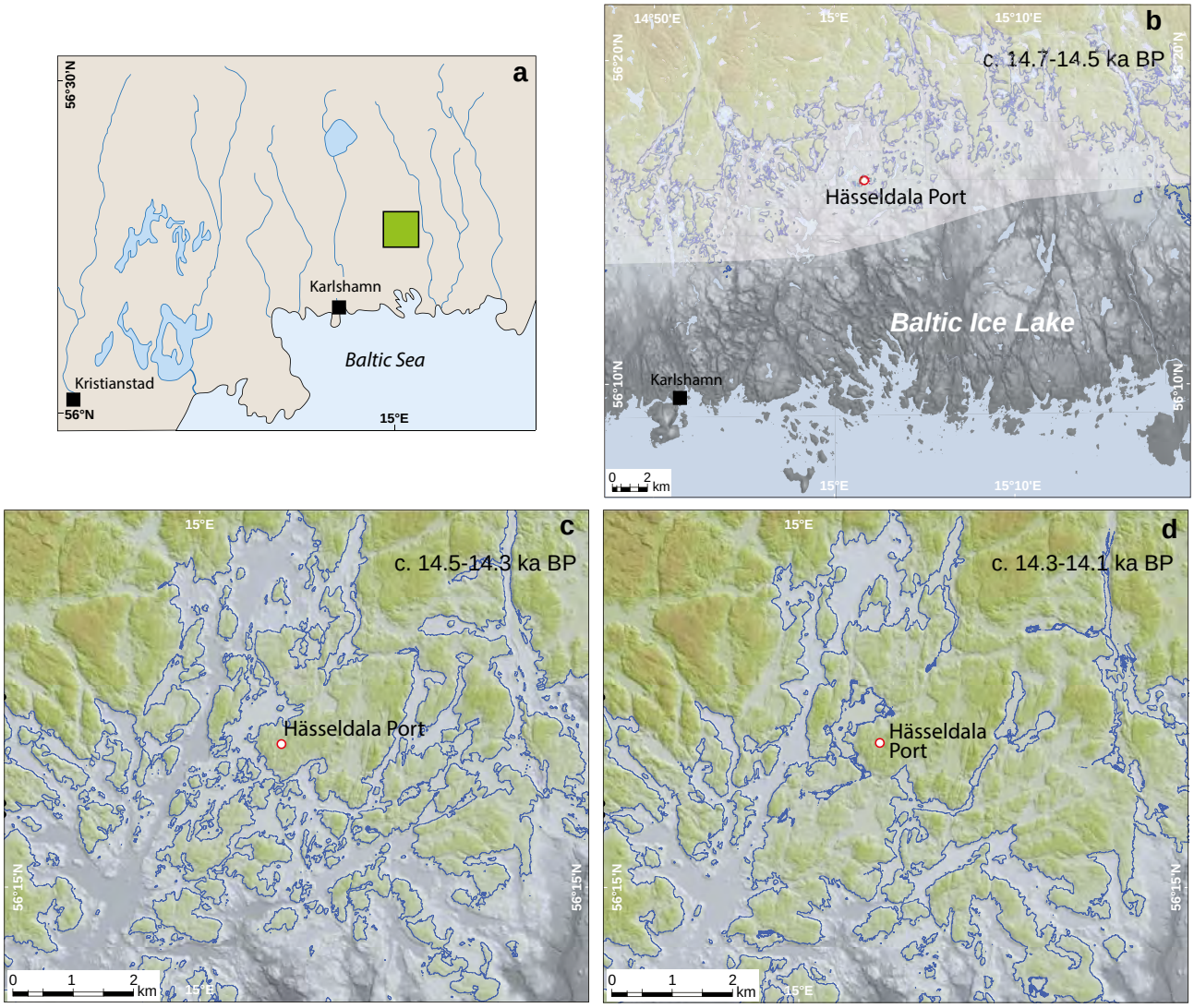

Figure 3-6. *A) Location of the study area (green filled square) in Blekinge, southernmost Sweden. B) Location of Hässeldala Port in relation to the receding ice sheet and the Baltic Ice Lake. Modified after Wohlfarth et al. (2017). The scenario shown on this map approximately corresponds to the start of the Bølling pollen zone around 14.7–14.5 ka BP. The white shaded area represents the extent of the Fennoscandian Ice Sheet, which at this time still covered Hässeldala Port. The highest coastline (blue line) was located about 65–57 m above present-day sea level at this time, resulting in that most parts of southern Blekinge, except for the easternmost part on this map were located below water level. Grey areas mark the present-day coastline. C–d) Close-in on the area around Hässeldala Port. Rapid land uplift during the Bølling pollen zone changed the landscape around Hässeldala Port so that the site was already situated within an archipelago in the Baltic Ice Lake by around 14.5–14.3 ka BP. At this time, the coastline (blue line) was located about 55–50 m above present-day sea level. The rapid ongoing uplift moved Hässeldala Port further inland and a few hundred years later, the coastline was situated at about 50–45 m above present-day sea level.*

However, the measurement errors in this part of the stratigraphy are too large to render these values significant. After 13.2 ka BP chironomid-inferred mean July surface water temperatures decreased and remained at 10–11 °C between 13.1 and 12.7 ka BP. This temperature decrease co-occurred with a distinct decline in $\delta D_{n\text{-}C_{21}}$ (δD_{aq}) values, which reach minimum values between 13.0–12.8 ka BP, coincident with higher $\Delta\delta D_{terr\text{-}aq}$ values (Figure 3-7). The shift in hydrogen isotope values suggests a freshening of the marine moisture source region and distinctly drier conditions at Hässeldala Port, likely caused by melting of the Fennoscandian Ice Sheet (Muschitiello et al. 2015b). The very detailed temperature evolution inferred from the chironomid data sets cannot be resolved by plant climate indicator species. However, one could speculate that the absence of *Nymphaea alba* pollen and the presence of pollen of the *Myriophyllum spicatum* group in the upper part of local pollen zone HÄP-3 (Andersson 2004) could indicate a decrease in minimum mean summer temperatures to around ≥12 °C (Figures 3-7 and 3-8).

The high-resolution sampling and analytical approach employed here allows describing the sequence of events that characterised the transition from the warmer Allerød into the colder Younger Dryas, occurring 12.8–12.5 ka BP at Hässeldala Port (Wohlfarth et al. 2017). Especially, the highly resolved pollenstratigraphy of core #6 (pollen zone Hä-2) shows that changes in vegetation (Karlatou-Charalampopoulou 2016) occurred synchronously with the changes reflected in several of the other proxies (Figure 3-7). Lake aquatic productivity started to decline and the ice-covered season became longer shortly after 12.8 ka BP. Coincident with these changes, lake surface water summer temperatures decreased and herb/shrub vegetation began to expand (Wohlfarth et al. 2017). The hydrogen isotope proxies initially show a brief return to wetter conditions due a more saline North Atlantic moisture source, but this short excursion was followed by progressively drier conditions and a fresher marine moisture source (Figure 3-7) (Muschitiello et al. 2015b, Wohlfarth et al. 2017).

During the regional Younger Dryas pollen zone (HÄP-4; 12.7–11.8 ka BP) shrubs, grasses and herbs dominated the catchment vegetation around Hässeldala Port's lake (Wohlfarth et al. 2017). Lake aquatic productivity remained low, the ice-covered season was comparably longer and mean July surface water temperatures fluctuated around 8–10 °C (Figure 3-7). Interestingly, *Nymphaea alba* pollen, which are present during the lower part of the Younger Dryas pollen zone (lower part of HÄP-4) (Andersson 2004) suggest minimum mean July temperatures of ≥13.5 °C (Tables 2-1, 4-1). These values are considerably higher than those reconstructed from chironomid assemblages (Figure 3-7), but find support from other plant climate indicator species present in Blekinge during the Younger Dryas pollen zone, such as *M. spicatum*, *M. verticillatum* and *Jasione montana* (Berglund 1966, Wohlfarth et al. 2017). These suggest that minimum mean summer temperatures could locally have reached ≥16.5 °C (Tables 2-1, 4-1). Hydrogen isotope values indicate progressively drier conditions and a progressively fresher moisture source for Hässeldala Port, which culminated at 11.85 ka BP (Muschitiello et al. 2015b).

The gradual transition out of the Younger Dryas and into the Preboreal pollen zone (11.9–11.6 ka BP) started at 11.9 ka BP and was accompanied by changes in several of the studied proxies. The first rise in lake organic productivity around 11.85 ka BP more or less coincided with the increase in mean July surface water temperatures, which rose from 9 °C to 12 °C between 11.9–11.85 ka and also with changes in vegetation composition (pollen zone Hä-5) (Karlatou-Charalampopoulou 2016). The start of a gradual shift in hydrogen isotope values may, however, have lagged these changes by a few decades (Figure 3-7), since a return to a more saline marine moisture source of precipitation and wetter conditions can only be observed around 11.8 cal. ka BP (Muschitiello et al. 2015b, Wohlfarth et al. 2017). Macroscopic charcoal appears in large quantities around 11.8 ka BP suggesting the availability of easily ignitable woody plants.

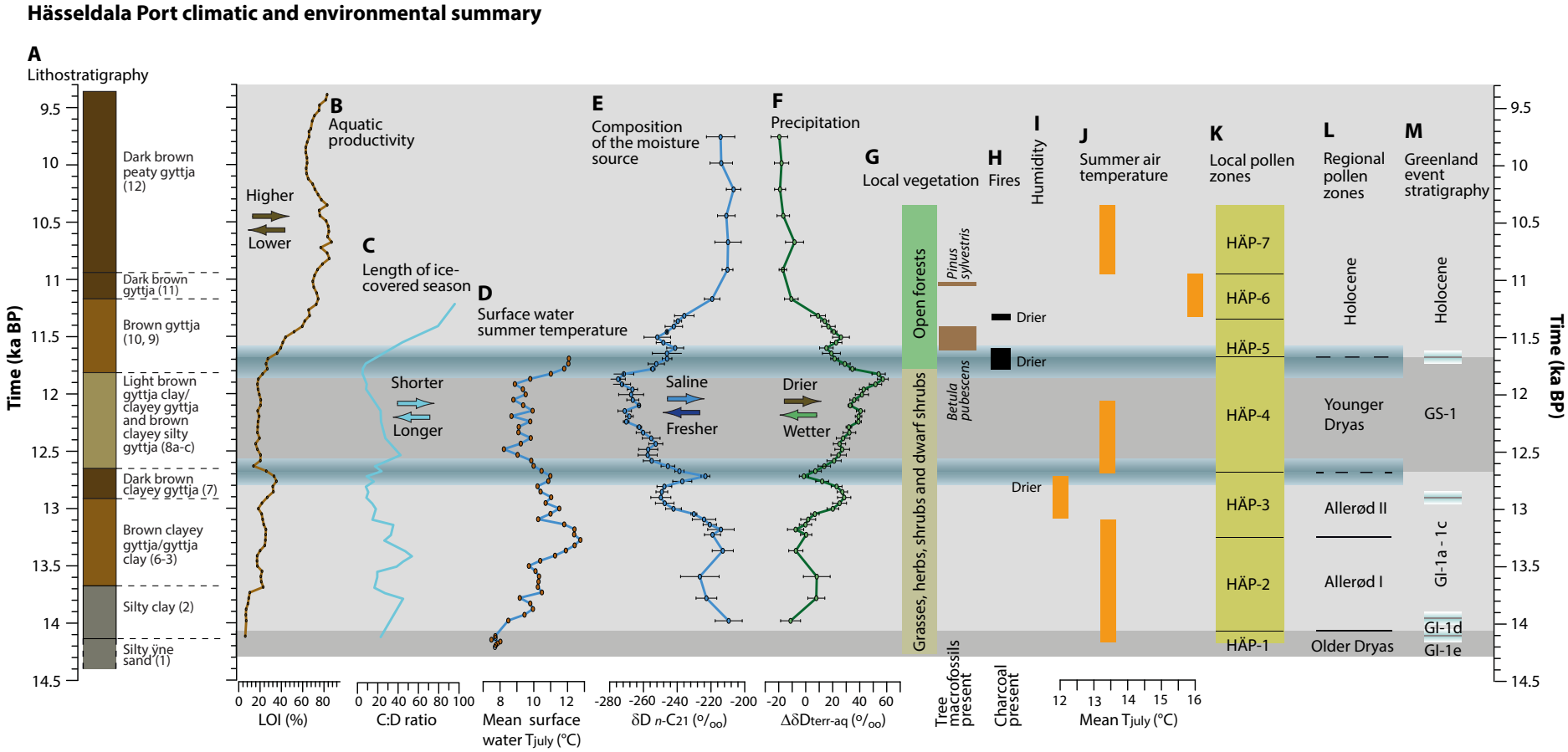

Figure 3-7. *Summary of the climatic and environmental development in and around the lake of Hässeldala Port during the last deglaciation modified after Wohlfarth et al. (2017). A) Lithostratiraphy; B) Loss-on-ignition (LOI) (organic matter content as a proxy for lake organic productivity); C) Crysophyte-diatom ratio, a proxy for lake ice cover (Ampel et al. 2014); D) Chironomid-inferred mean July surface water temperature (Watson 2008); E and F) Biomarker based inference of moisture source composition and precipitation (Muschitiello et al. 2015b); G) Local vegetation based on pollen stratigraphy and macroscopic finds of plant remains. H and I) High amounts of charcoal indicate the occurrence of forest fires and as such dry conditions; J) Minimum mean summer temperatures as derived from climate indicator plant species; K) Local pollen zones (Andersson 2004); L) Regional pollen zones; M) Greenland event stratigraphy (Rasmussen et al. 2014a).*

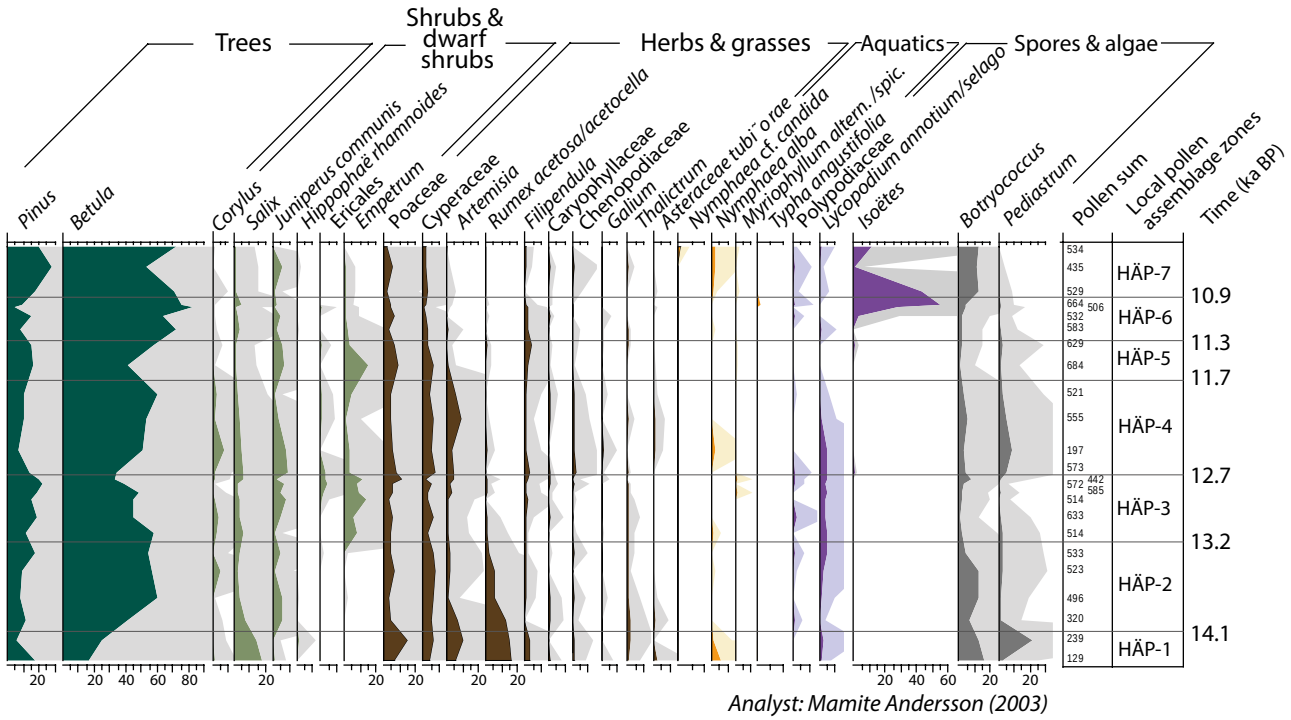

Figure 3-8. *Pollen stratigraphy of core #3 from Hässeldala Port. Modified after Andersson (2004).*

Lake aquatic productivity further increased during the early Holocene. Herb and shrub communities around the lake declined (Andersson 2004) and the presence of tree birch (*Betula pubescens)* and pine (*Pinus sylvestris*) at 11.6 and 11.0 ka BP, respectively is documented by macro fossil finds (Wohlfarth et al. 2006, 2017). The chironomid record for Hässeldala Port does not extend into the Holocene, but the presence of pollen of aquatic plants (*Typha angustifolia* and *Nymphaea alba* in HÄP-6) *(*Andersson 2004) suggests that minimum mean July temperatures had reached ≥16 °C by around 11.6 ka BP (Tables 2-1, 4-1). Overall wetter conditions and a saline marine moisture source of precipitation are indicated by the hydrogen isotope values.

3.2 Proxy-based European summer temperature compilation

The detailed analysis for southern Sweden in the previous section reveals not only large temporal variations during the deglaciation but also notable spatial differences already for two lake sites being located only some 100 km apart. While such a detailed spatio-temporal reconstruction of the local southern Swedish climate represents a very valuable insight into late glacial climate conditions and variability, the availability of such detailed reconstructions is quite unique and not available for other locations across Europe. In this section, we present summer temperature reconstructions on a larger spatial scale for Europe where we focus on the mean temperature patterns of the warm state of BA and cold state of YD. These can then be compared to steady state simulations of BA and YD temperatures from our climate model simulations.

The group 1 data set used to reconstruct summer or July temperatures comprises published temperature records derived from chironomids, coleoptera and cladocera, and includes sites in the UK, Ireland, The Netherlands, France, Italy, Spain, Norway, Sweden, Switzerland, Latvia, Estonia and Romania (Figure 3-9a–c). Reconstructed averaged temperatures for the BA period are 11–14 °C (UK, Ireland), 14–18 °C (Netherlands, France, Italy), 9–15 °C (Switzerland), 6–11 °C (Norway, Sweden), 12–13 °C (Estonia, Latvia) and 8 °C (Romania). Sites in the UK, Ireland and The Netherlands show the largest temperature differences between the BA and YD time periods with a cooling of −2.2 to −4.3 °C, while the YD minus BA temperature differences for other sites are between around 0 to −2 °C

(Figure 3-9c). The overall spatial pattern of chironomid-inferred summer temperature changes for YD minus BA thus shows a clear meridional gradient with strong cooling over northwest Europe and only slight cooling over continental parts of eastern Europe, consistent with previous chironomid-based temperature reconstructions (Heiri et al. 2014). A disadvantage of the group 1 data set is the poor data coverage in continental regions of central and eastern Europe. The strong cooling signal for the YD is therefore dominated by locations close to the North Atlantic while little to no information is available for continental areas. Another limiting factor of chironomid-based temperature reconstructions is that chironomid assemblages in lakes are affected by, for example, lake water temperature (Luoto and Nevalainen 2013), nutrient availability and water depth (Juggins 2013), all of which can influence transfer-function based temperature reconstructions.

The group 2 dataset is based on aquatic, telmatic and terrestrial climate indicator plant species that were extracted from published pollen- and plant macrofossil diagrams (Figure 3-9d–e, Table 2-1, Appendix 1). The compilation comprises sites in Belgium, Bulgaria, Czech Republic, Denmark, Estonia, Finland, France, Germany, Hungary, Ireland, Italy, Latvia, Lithuania, Netherlands, Norway, Poland, Portugal, Russia, Romania, Slovakia, Slovenia, Spain, Switzerland, Sweden and the UK and thus covers large parts of Europe, including different altitudes and climate regimes. Reconstructed BA minimum mean July temperatures using plant indicator species cover a range between ≥10 °C and ≥16 °C, and reconstructed minimum mean July temperatures for YD are between ≥ 8 °C and ≥16.5 °C. Clear temperature differences between the BA and the YD (both in terms of colder and warmer temperatures) can only be observed for a few sites in the UK, Poland, Latvia, Switzerland, Spain, Romania, and Russia (Appendix 1). Overall, however, the plant indicator species suggest that similar minimum summer temperatures prevailed during the BA and the YD (Figure 3-9d–e). To better understand why reconstructed minimum mean summer temperatures were colder or warmer at certain sites across Europe, a more detailed assessment of each record would be necessary. This was, however, outside of the scope of the present study and would require comparably detailed proxy information as presented for southern Sweden in Section 3.1, something that is lacking for most sites.

Although both proxy-groups are traditionally interpreted as July or summer temperatures, the comparison in Figure 3-10 clearly shows systematic differences between the two groups across large spatial scales. As shown in Section 3.1 for the transient temperature evolution over Southern Sweden in Figure 3-5 and 3-7, July temperature estimates based on chironomids and plant indicator species do not always co-vary in the same way over time since insect and plant assemblages are influenced by different environmental factors. During comparably warm periods, both proxies show a similar temperature evolution, but diverge during cold periods, when chironomids display colder temperatures than plant indicator species. The results of the data compilation (groups 1 and 2) (Figures 3-9 and 3-10) point in the same direction and suggest similarities/divergences between these two types of summer temperature proxies also on a subcontinental-scale across Europe. This indicates that the differences are not merely caused by local changes.

Noteworthy is that minimum mean July temperatures were ≥15 °C during both BA and YD (Figure 3-9d–e). This is the case even for the western region of The Netherlands, where plant indicator-based summer temperatures appear to be significantly warmer than indicated by chironomid-based temperatures. The comparison of the two proxy groups moreover indicates that the elevation-adjusted regional median (see caption to Figure 3-10) of mean July temperatures derived from plant indicator species is systematically higher than that based on chironomid assemblages for both the BA and the YD (Figure 3-10).

A detailed spatial comparison of the temperature reconstructions is not possible because the different sites in groups 1 and 2 partly cover different regions. However, the finding that plant indicator species generally reconstruct warmer summer temperatures than chironomid assemblages is important since it rules out the possibility that reconstructed warm YD temperatures are an artefact (e.g. caused by inter-mixing of plant macro remains from a warm time interval). These differences are further explored in Section 3.5, where we analyse the proxy-type differences in respect to summer temperatures using detailed seasonal climate information from our climate model simulations.

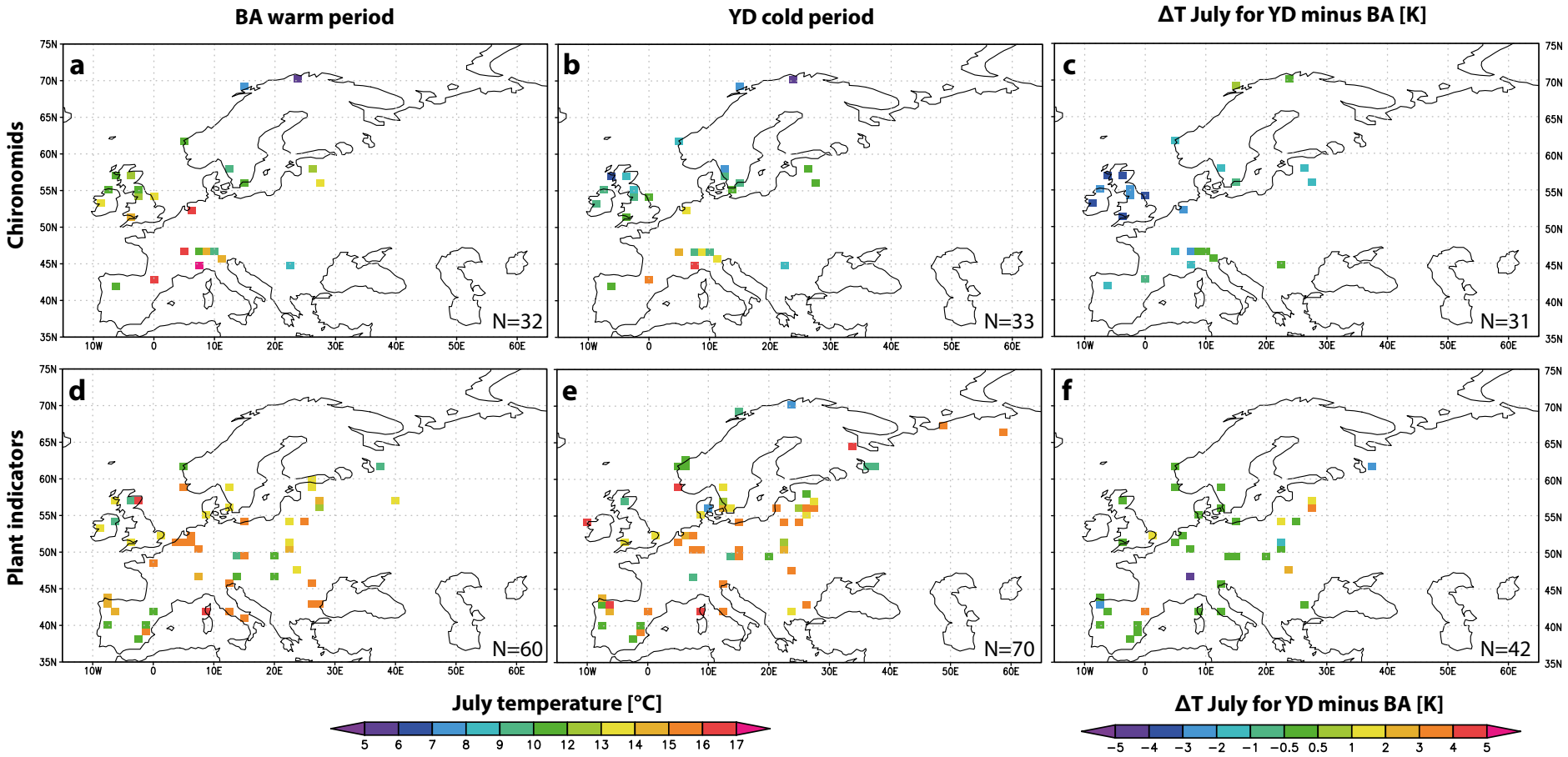

Figure 3-9. *Spatial distribution of mean July temperatures [°C] based on insects (group 1) and of minimum mean July temperatures [°C] based on plant indicator species (group 2) for BA and YD and the related temperature difference between BA and YD (YD minus BA) [K].*

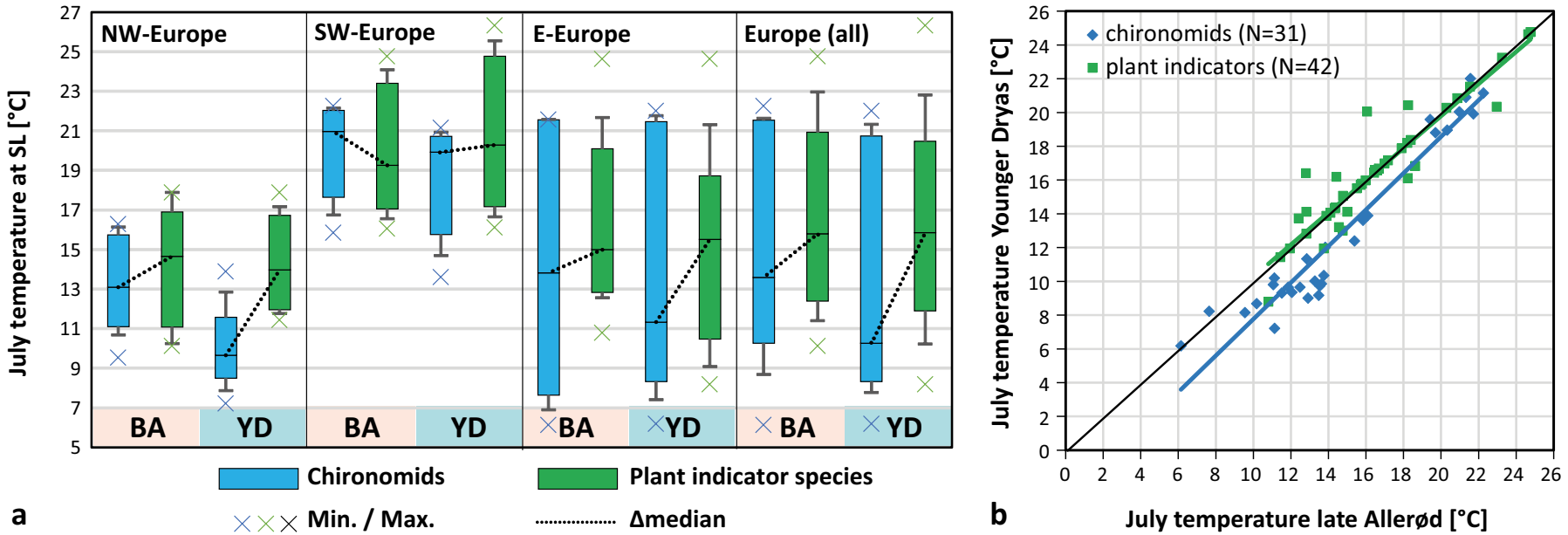

Figure 3-10. *Comparison of elevation-adjusted (minimum) mean July temperature ranges for Bølling-Allerød (BA) and Younger Dryas (YD) for different regions in Europe as reconstructed from both proxies. The coloured boxes represent 80 % of regional July temperatures around the median, whiskers the 90 % spread and X minimum/ maximum temperatures of the coldest/warmest site in northwestern Europe, southwestern Europe and eastern Europe, as well as all sites together (Europe, all). The scatter plot for YD minus BA temperatures for both proxy types for Europe (all) clearly shows the systematically colder YD temperatures for group 1 (chironomids) with no overall change for group 2 (plant indicator species). For better comparison, elevations are here adjusted to modern sea-level based on the present-day altitude of each sites (Appendix 1) assuming a lapse rate of 0.65 K per 100 m in altitude.*

3.3 Climate modelling – large-scale differences between coarse and high-resolution simulations

Results from the (Paleo-) Climate Model Inter-comparison Project (PMIP/CMIP) (Braconnot et al. 2012) revealed in most cases a good skill of models to simulate large-scale patterns and trends, but a clear underestimation in simulating the magnitude of regional-scale changes in comparison with proxy data. The latter is, however, important for describing and understanding regional to local climatic changes and the driving mechanisms, which influence multi-proxy records and/or ice sheets. Here, we briefly compare the key differences between our high-resolution climate simulations with CESM1 and the coarse resolution CCSM3 simulation of TraCE21k for the climate states of AL and YD. Since surface temperatures over the ocean, ice fraction, GHG concentrations and orbital forcing are exactly the same in CCSM3 and CESM1 for the time slices compared here, the major difference between both models is related to their resolution of the atmosphere with ~375×375 km for CCSM3 and ~100×100 km for CESM1.

3.3.1 Opposite Eurasian summer temperature response in CCSM3 and CESM1

Before the regional temperature changes during the YD relative to AL are analysed in more detail for the Euro-Atlantic region (Section 3.4), we first present here a brief global comparison of simulated seasonal mean temperature changes between YD and AL (YD minus AL) for CCSM3 and CESM1 for winter (DJF; December, January, February) and summer (JJA; June, July, August). As shown in Figure 3-11, the changes in surface temperatures over ocean areas are generally similar because SST's from CCSM3 are identical to the prescribed SST's in CESM1. Although the sea-ice fraction is identical in both simulations, temperatures over sea-ice are actively calculated by CICE in CESM1, consistent with the high-resolution climate model. Hence, surface temperatures over ocean areas with a sea-ice fraction of >0 differ between CCSM3 and CESM1.

For the winter season (DJF), CESM1 simulates at least 5 K colder temperatures over Arctic sea-ice areas and the Eurasian continent down to around latitude 40°N compared to CCSM3 (Figure 3-11). Over Europe, the winter cooling during the YD is more severe based on CESM1 with up to 10 K on average, whereas a less strong cooling is simulated by CCSM3. For the British Isles, today's North Sea and southern Baltic Sea region, CESM1 suggests at least 10 K and up to 20 K colder winters relative to AL and up to 30 K colder mean winter temperatures over the central North Atlantic. This is considerably colder than simulated by CCSM3 with only up to 5 K cooling over Europe and less than 20 K over the central North Atlantic. Both simulations simulate warming of 1–3 K over North America.

The YD warming in CCSM3 over the Bering Strait and over parts of the Barents and Kara Sea is, however, not entirely due to climate, but is also related to changes in topography. For simulating the period from the LGM to 12.9 ka BP, CCSM3 uses the low sea-level stand of the LGM, while a sea-level adjusted for the deglaciation is used for the YD simulation (He 2011). As a result, temperature changes for YD minus AL over shallow shelf areas in CCSM3 are related to changes in land-sea mask, rather than to climate. This spatially large inconsistency does not exist in CESM1 and climate-related winter warming is only found over Northern America in the AL and YD simulations. Although some fraction of the warming may be attributed to changes in the elevation of the Laurentide Ice Sheet between AL and YD, the simulated temperature changes are real as the changes in ice sheets in CCSM3 and CESM1 are supposed to reflect consistent elevation changes between both climate states. A detailed assessment of the isolated impact of ice sheet changes on the local climate is, however, beyond the scope of this study.

Simulated changes in (northern) summer (JJA) temperatures in both simulations clearly show the strong oceanic cooling (prescribed in CESM1) of up to 6 K along the European coasts and in the subpolar central North Atlantic, which is related to an AMOC slowdown during the YD. A striking difference is simulated directly downstream of the strongest ocean cooling. In CCSM3, the oceanic cooling extends onto the European continent with a drop of summer temperatures of up to 4 K, while warming of 0.5 to 1.5 K is simulated by CESM1 for continental areas of central to eastern Europe. This implies that despite the same ocean state, GHG and orbital forcing, CESM1 simulates fundamentally different summer temperatures over the Eurasian continent in response to the YD ocean state than CCSM3. As shown below, the different temperature response in both models can be linked to the different resolution of the atmosphere in the presence of large continental ice sheets.

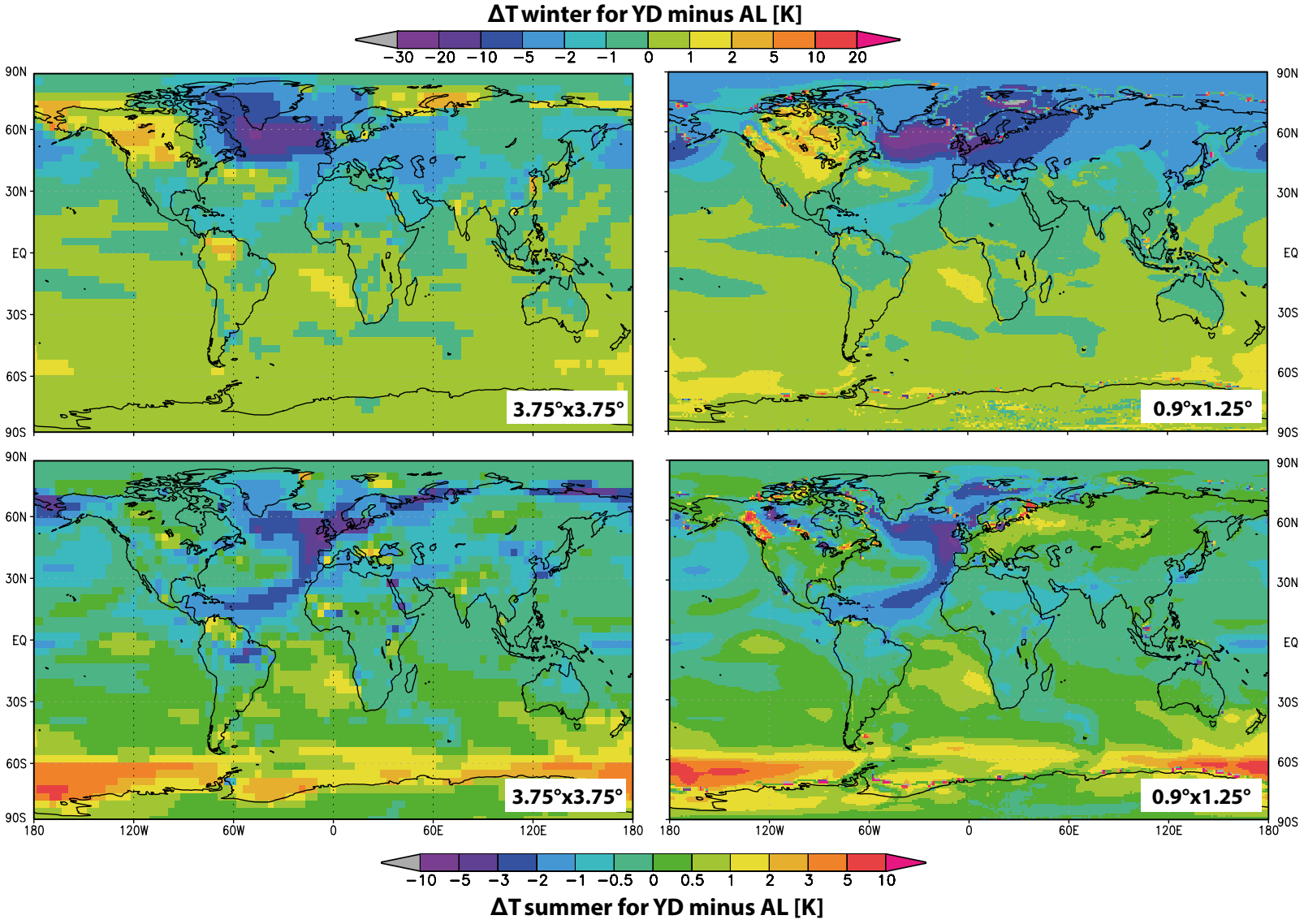

Figure 3-11. *Comparison of seasonal temperature differences [K] for Younger Dryas (YD) minus Allerød (AL) for winter (top) and summer (bottom) between the coarse- (CCSM3, left) and high-resolution (CESM1, right) model simulations.*

3.3.2 Model resolution dependency for large-scale atmospheric circulation

While notable local to regional differences in the simulated near-surface climate are typical for high-resolution simulations relative to a coarse-resolution model, and usually provide added-value relative to a coarse-resolution simulation, significant continental-scale differences in large-scale atmospheric circulation and wind patterns like for summer over Eurasia (Figure 3-12) are usually not expected.

A comparison of large-scale atmospheric flow for the near-surface wind fields between CCSM3 and CESM1, yields fundamentally different patterns of large-scale atmospheric flow over the Northern Hemisphere. As shown for the monthly mean wind fields during the YD in July (Figure 3-12), strong westerly flow dominates in CCSM3 also in summer reaching from the North Atlantic Ocean over Europe and across whole Eurasia. This is opposite to the flow pattern in the high-resolution simulation with CESM1, where the flow from the North Atlantic is split with one branch being deflected northward over the NE Atlantic towards the Arctic and the other branch southwards towards the Mediterranean Sea.

An additional difference over Europe is the very low wind speeds in CESM1 with on average weak winds from the North, while relatively strong westerly winds dominate in CCSM3. The fundamentally different mean atmospheric flow in summer in CESM1 relative to CCSM3 explains why an opposite sign in temperature changes is simulated by CCSM3 and CESM1 in Section 3.3.1, although the same radiative forcing and the same horizontal boundary conditions for the ocean are applied. In case of CCSM3, the westerly flow directly advects very cold air from the North Atlantic across Europe, while the cold air in CESM1 is blocked by the Fennoscandian Ice Sheet and does not lead to any cooling over continental Europe in summer. More details about the importance of atmospheric circulation and European summer temperatures in CESM1 are presented in Section 4.2.

3.4 Proxy data – climate model output comparison of European summer temperatures

As described in Sections 2.1 and 3.2, the proxy data compilation and quantification were made using data sets attributed to the Bølling, Allerød and Younger Dryas. In many cases, it was not possible to distinguish between Bølling and Allerød, and in some cases only Allerød data sets were available (see Section 2.1). Therefore, we decided to group the proxy data into a general Bølling – Allerød (BA) interval, which is separated from the Younger Dryas (YD) interval. For the model simulations, however, we only focus on a specific time within the Allerød (AL) and the Younger Dryas (YD), respectively, i.e. we chose 13 ka BP (AL) and 12.17 ka BP (YD) for our simulations (see Sections 2.4 and 3.3). In the following comparison between proxy-inferred summer temperatures and simulated summer temperatures, we use BA to denote the Bølling-Allerød time period, as well as the simulated 13 ka BP time slice.

The proxy-data comparison (Section 3.2) and the CCSM3-CESM1 model comparison (Section 3.3) yielded no consensus regarding the magnitude and spatial pattern of European summer temperature changes during the YD relative to BA. In Figure 3-13 we directly compare simulated summer (JJA) temperature changes from CESM1 with the temperature changes derived from the two proxy groups.

In more spatial detail, CESM1 suggests little temperature change for western Europe and a non-significant cooling directly at the coast lines (Figure 3-13a–b). Significant warming of 0.5 K over central Europe east of ~10°E further increases to up to 1–1.5 K over continental regions east of ~30°E and north of ~55°N over eastern Europe. Grid points close to the ice sheets and in or around the contemporary Baltic Ice Lake are difficult to compare due to changes in paleo-topography between both time slice simulations. The Baltic Ice Lake during YD is here represented by the prescribed SST's from CCSM3 and does not reflect real lake temperatures. However, even if the Baltic Ice Lake would have been set as a lake in CESM1, the resulting temperatures would be unrealistic owing to the absence of runoff from the melting ice sheet in the climate model and the fact that the ice sheet calved into the Baltic Ice Lake, also absent in the simulations.

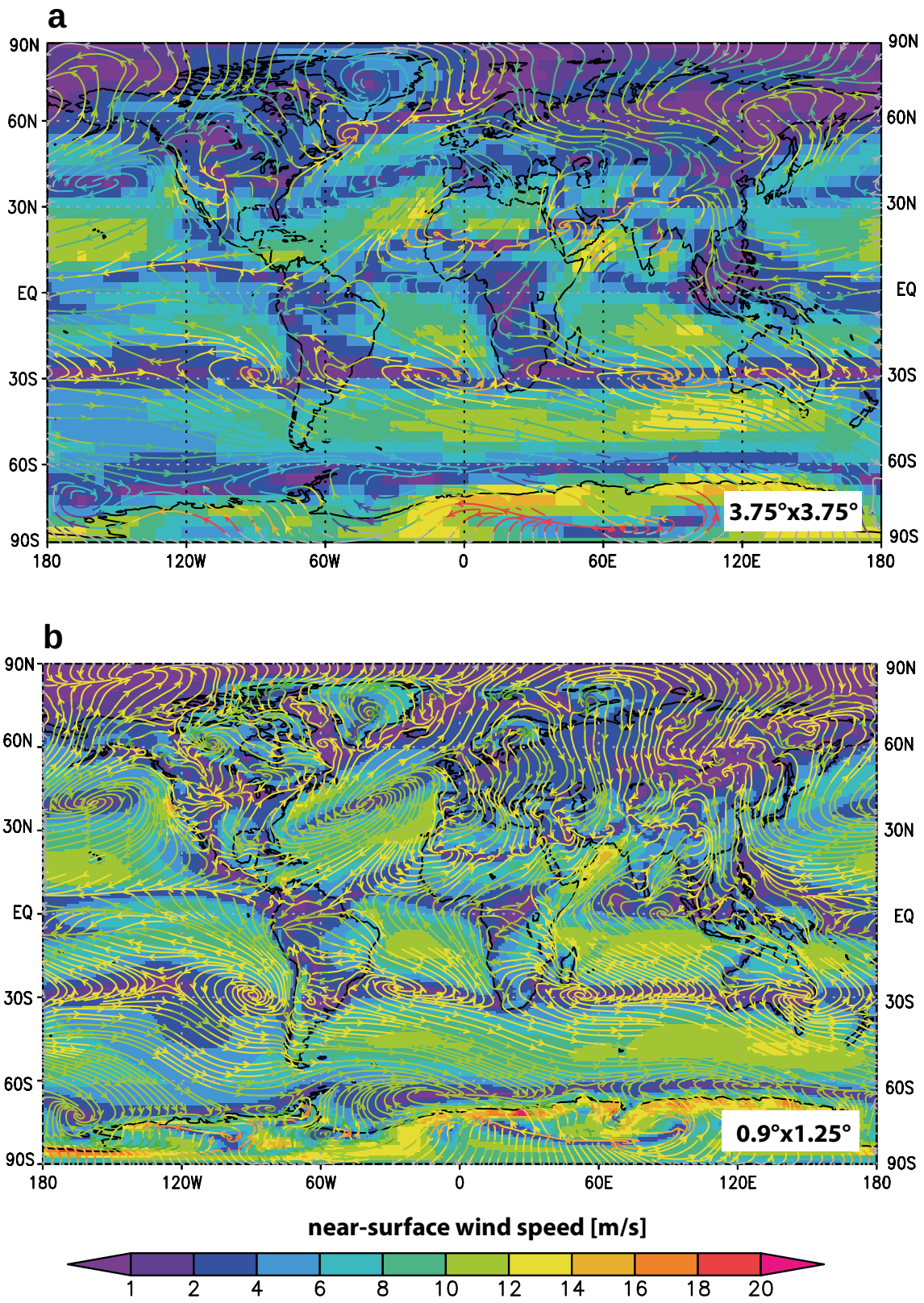

Figure 3-12. *Comparison of near-surface monthly mean wind speeds (shaded colours) and atmospheric flow (streamlines) during the YD in July as simulated at coarse (CCSM3, top) and high resolution (CESM1, bottom). Note the fundamentally different large-scale flow pattern over Eurasia.*

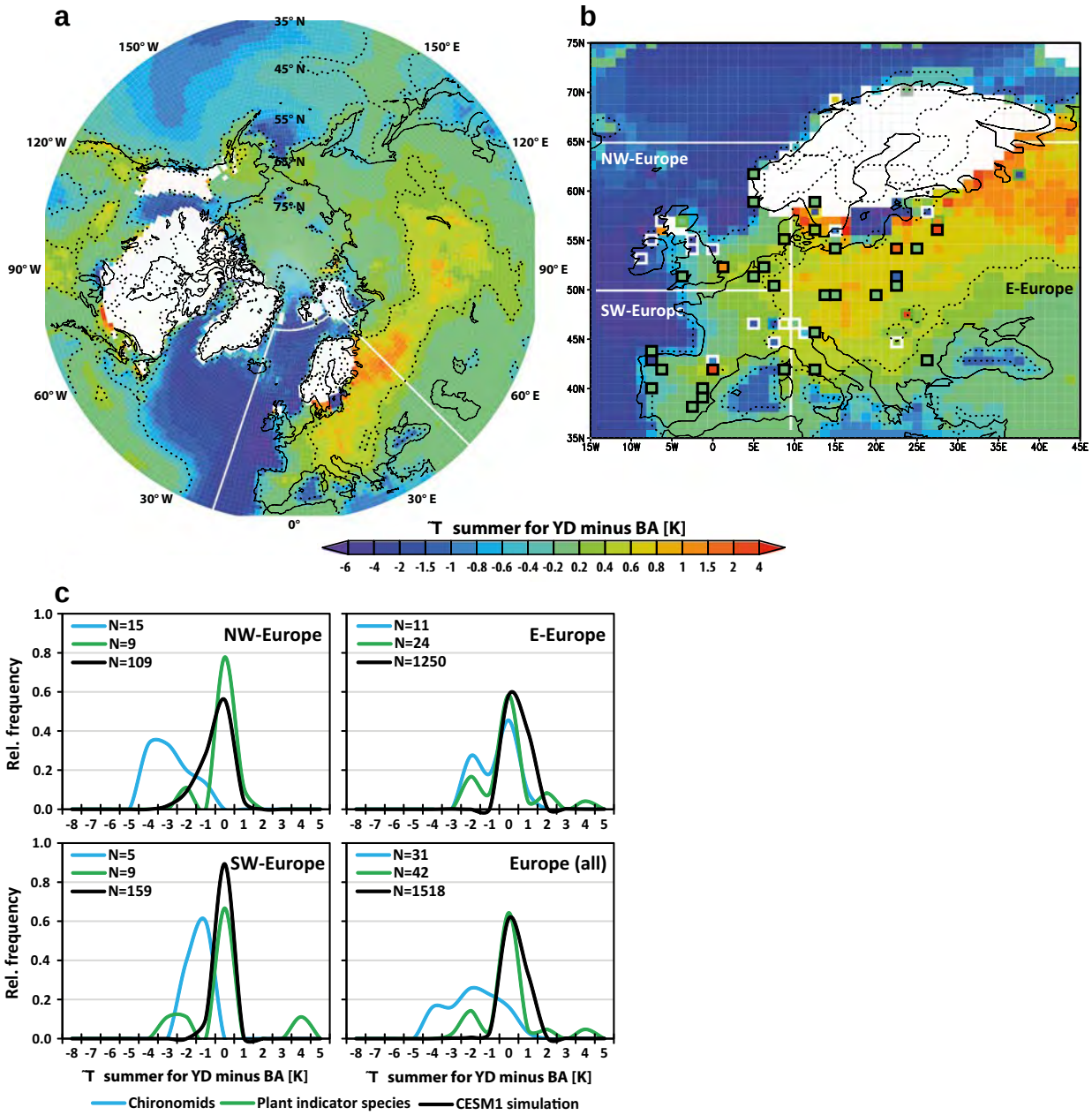

Figure 3-13. *Comparison of mean summer (JJA) temperature differences [K] for YD minus BA as simulated at high-resolution (CESM1) and as reconstructed from proxy data. A) Simulated JJA YD-BA differences for the Northern Hemisphere by CESM1. B) Close-up of proxy-model temperature differences over Europe using the same colour-scale as in (a). C) Relative frequency distribution of regional temperature changes according to proxy data in comparison to the climate model simulation. The warmest temperature change is shown for grid points in (b) when several sites were within the same grid (within ~100×100 km²). In (b) chironomid records are marked by a white frame, tree macro remains by a green frame and other plant indicator species by a black frame. The number of local values per region in (c) is given by N samples for proxy type and/or model grid points. The relative frequency distributions of certain temperature changes within a region are based on the regions indicated in (b).*

For a direct comparison with climate proxy data, the close-up of the simulated European YD-BA summer temperature changes (Figure 3-13b) includes proxy-based July temperature differences where grid boxes of the proxy site are marked with white frames (group1 proxies), black frames (plant indicator species) and green frames (tree macro remains) showing July temperature differences from the available proxy records (see Section 3.2), which display a rather heterogeneous picture. A good agreement exists for western Europe between temperatures simulated with CESM1 and temperatures from plant indicator species as both show only small temperature changes. The very strong cooling over northwestern Europe

reflected by chironomid-inferred temperatures (grid cells with white rectangles, Figure 3-13b) is, however, not supported by the CESM1 results. Furthermore, the 0.5 to 1.5 K warming simulated by CESM1 over central and eastern Europe is only supported by two proxy records, while the majority of proxy records does not indicate any YD-BA summer temperature change.

The relative frequency of regional temperature changes for northwest, southwest and eastern Europe (Figure 3-13c) clearly reflects the (dis-)agreement between both the chironomid and plant indicator species inferred summer temperatures and the climate model simulations. The clear meridional cooling gradient, with strong cooling over northwest and southwest Europe and less cooling over eastern Europe, suggested by chironomids, is neither supported by plant species nor by our CESM1 simulations. The median of regional temperature changes based on plant indicator species is zero for all regions, while chironomids suggest a median cooling of −3 K over northwest Europe and a median cooling of −0.4 K for eastern Europe. CESM1 simulates a median cooling of −0.4 K for northwest Europe, 0 K for southwest Europe and +0.4 K for eastern Europe. Over the whole region, there is a very high agreement between plant indicator species (N = 42) with a median ΔT of 0 K (0 K Δmean) and CESM1 (N = 1 518 grid points) with ΔT of 0.3 K (0.3 K Δmean). The CESM1 grid points used for these statistics are only based on those which have a land fraction of 100 % and 0 % glacier in both periods, BA and YD, to avoid comparisons across grid points subject to land use change.

3.5 Analysis of simulated changes in European summer climate

The comparison of European summer temperature changes (YD minus BA) in Section 3.4 suggests two different possible interpreations for the Younger Dryas depending on the proxy-type and the climate model employed. The coarse resolution CCSM3 simulation, which has been used in previous studies, tends to support chironomid-inferred temperature changes (Group 1) (Heiri et al. 2014, Renssen et al. 2015) and shows a clear meridional gradient with strong summer cooling over northwestern Europe and moderate cooling of ~1K towards eastern Europe. In contrast, little to no summer temperature change (YD minus BA) and absence of a meridional temperature gradient is suggested by the climate indicator plant species (Group 2). These findings are more in line with our high-resolution climate simulation with CESM1.

In this section, we analyse the atmospheric drivers, which lead to the suggested warm summer climate during the YD in CESM1 and evaluate to which extent simulated changes in seasonality may explain differences between the two types of proxies.

3.5.1 Atmospheric circulation and the role of atmospheric blocking during summer

The high agreement regarding summer temperature changes for YD minus BA between plant indicator species (median ΔT = 0 K) and the CESM1 simulation (median ΔT = 0.3 K) presented in Section 3.4 clearly suggests that YD summers had temperatures comparable to BA summers. The median of ΔT based on N = 42 plant indicator sites, which have a relatively wide spatial spread across Europe, provides a robust measure for the overall temperature change because local outliers have little impact on the median. To explain why YD summer temperatures remained relatively stable despite the strong oceanic cooling and a southward extension of sea-ice, we here analyse key features of atmospheric circulation over the Euro-Atlantic region, which dominate the mean summer climate state and potential changes.

Based on the analysis of the mean state and changes in atmospheric circulation during summer for BA and YD, we can identify four important mechanisms explaining the persistence of warm European summers during the YD. The first dominant aspect is the mean sea-level-pressure (SLP) pattern during summer. As shown in Figure 3-14a, the SLP-pattern is characterised by a stable high-pressure ridge which connects the dynamical Azores High with the thermal high over the Fennoscandian Ice Sheet. In a modern synoptic classification, such a ridge would be classified as atmospheric blocking. Today, such a pattern occurs only in some years and persists for about 5–10 days. For BA and YD, the ridge, or atmospheric blocking, is, however, simulated as a mean state. This means that cold westerly winds from the North Atlantic are mostly deflected away from central and continental Europe during summer creating a stable warm summer climate, partly independent from the current ocean state.

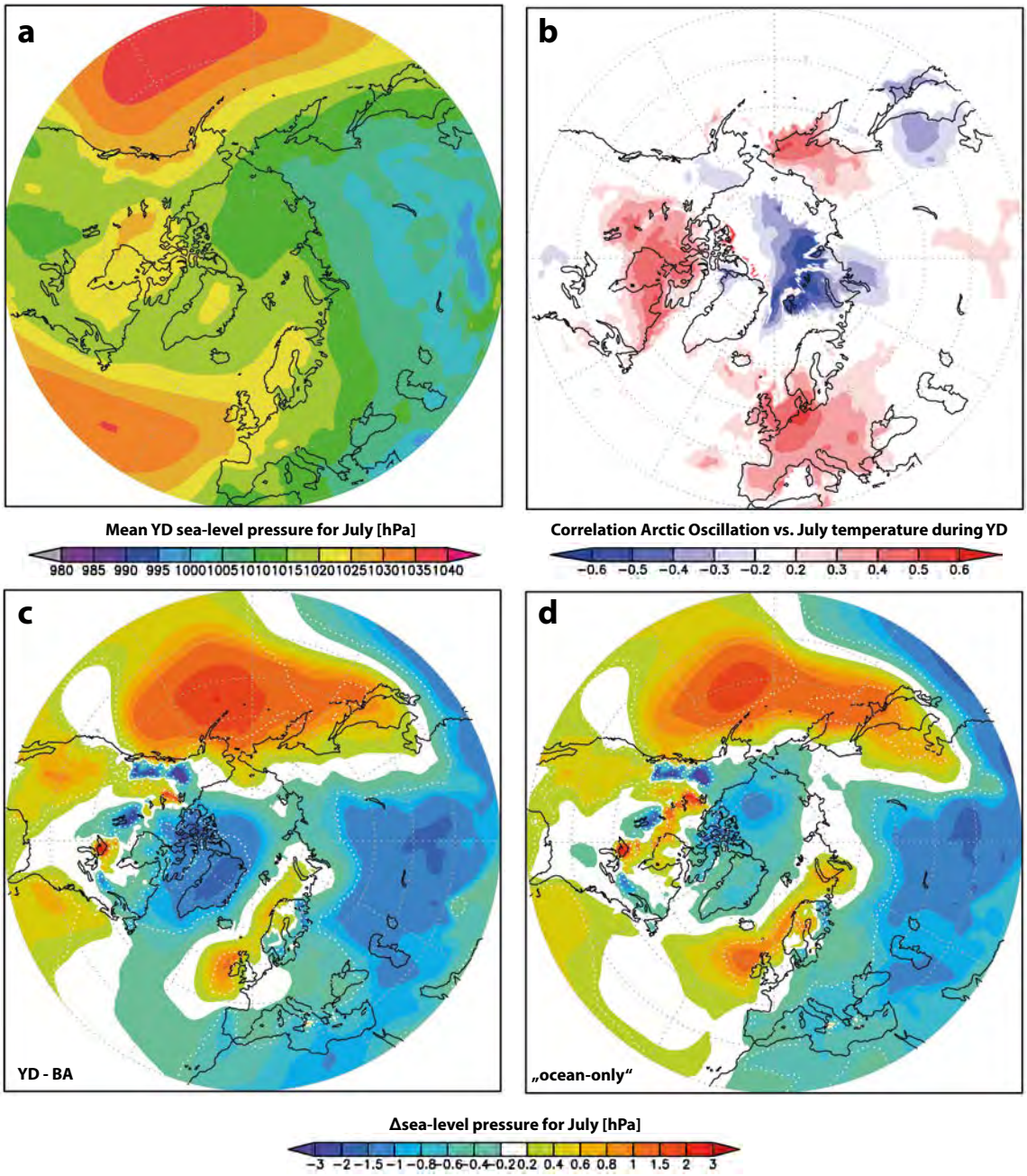

Figure 3-14. *Main atmospheric drivers behind European summer temperatures during the YD. A) Mean SLP pattern during the YD with a high-pressure ridge connecting the Azores High with the Fennoscandian Ice Sheet. B) Correlation pattern of mean July temperatures with the Arctic Oscillation (AO) Index. C) Changes in mean SLP for YD minus BA including full changes in orbital forcing and GHG and (d) the same changes excluding changes in radiative forcing. The dipole of SLP changes in (c) and (d) corresponds to a positive mode of the AO, which is positively correlated with temperatures and implies warming over Europe during the YD due to AO+.*

A second mechanism, which also supported the persistence of warm summer conditions during the YD lays in a strengthening of the blocking ridge i.e. over the northeast Atlantic, but also along the Norwegian coastline (Figure 3-14c–d). The enhanced blocking is related to a thermodynamically induced strengthening of high pressure and hence blocking of cold westerly winds in response to the strong oceanic cooling. Such a link has recently been observed for major European heat waves since the 1980's (Duchez et al. 2016) or droughts like in 2015 (Ionita et al. 2017), which occurred in response to unusually cold North Atlantic SST's and persistent atmospheric blocking. Interestingly, the competing effects of increased summer insolation during the YD and oceanic cooling have a

compensating effect on changes in atmospheric blocking. The full realistic forcing for the simulated mid-YD period implies a somewhat weaker intensification of atmospheric blocking (Figure 3-14c) than a cold-ocean-only experiment without changes in radiative forcing (Figure 3-14d). This indicates that the cold ocean alone would lead to stronger atmospheric blocking at the beginning of the YD, while the rapid increase in summer insolation towards the middle and end of the YD would weaken this blocking.

A third mechanism supporting warm European YD summers is related to the teleconnection pattern of the Arctic Oscillation (AO). The AO is here defined as the first leading mode of the pressure field variability north of latitude 20°N (1st Empirical Orthogonal Function of the latitude weighted anomaly field of SLP, EOF1) and links changes in the zonal pressure gradient relative to the Arctic with variations in Northern Hemispheric climate. In case of Europe, the simulated dipole of SLP changes during the YD, with a decrease in SLP over the Greenland-Arctic region and an increase in SLP over the NE-Atlantic, implies a shift to a stronger zonal pressure gradient over the North Atlantic relative to BA. A stronger zonal pressure gradient implies a positive deviation of the AO-Index (AO+). As shown in Figure 3-14b, the 1-point-correlation-map of the AO-Index with the summer temperature field yields a clear positive correlation over Europe. As the shift in the SLP pattern from BA to YD means a shift towards AO+, the positive correlation over Europe implies warmer summer temperatures during YD in response to the AO+. A fourth driver for warm summers during the YD is the high and also increasing orbital forcing at high northern latitudes during summer, discussed in the following section.

3.5.2 The role of increased orbital forcing during the Younger Dryas

As mentioned above, a fourth driver for warm summers during the YD is the high and increasing orbital forcing at high northern latitudes during summer. Summer insolation during YD increased by +5 W/m² (mid-July at 60°N) relative to BA with only −0.18 W/m² in terms of ΔF related to GHG changes (see Section 2.4.3). To disentangle the cold-ocean-effect during the YD from the changes in radiative forcing during the YD relative to BA, we conducted a sensitivity experiment where we simulated the YD without changes in orbital forcing, GHG concentrations and ice sheets relative to BA. Technically, this means that the clim13k simulation for BA is repeated by replacing the BA ocean state with the YD ocean state (denoted as clim13kYD). As shown in Figure 3-15, the cold-ocean-only impact (clim13kYD) yields already warmer European summers during July and August over central to eastern Europe, consistent with recent observations that link unusually cold North Atlantic SST's to European heat waves and droughts since the 1980's (Duchez et al. 2016, Ionita et al. 2017). The increase in orbital summer insolation is hence not the main reason for warm summers during the YD over central Europe, but contributes to further warming over very continental regions in Eurasia and has a slight warming effect also on western Europe ("radiation-only-effect" ~ residual of clim12k minus clim13kYD).

3.5.3 Simulated changes in seasonality as a key feature of the Younger Dryas

The simulated four dominant atmospheric drivers behind stable and warm summer conditions during the YD support the proxy evidence for warm summers based on our plant indicator species and further increases the confidence in the simulated warm summer conditions. However, this poses however the question why chironomids (and other proxies, such as terrestrial pollen) suggest cold summers during the YD and a clear meridional W-E cooling gradient which is neither captured by plant indicator species nor by our CESM1 simulation. To evaluate which temperature patterns and atmospheric drivers may be reflected by chironomid-inferred temperatures, we extent our analysis of simulated temperature changes beyond the summer season, June, July and August (JJA).

As shown in Figure 3-16, the stable warm summer conditions during YD are very short. Monthly mean temperatures during May and September were much colder during the YD compared to BA. The warm months are hence restricted to July and August over northwest Europe and to June, July and August over eastern Europe, whereas spring/autumn were very cold and winters were extremely cold. As a result of much colder conditions lasting until May, considerably larger snow depths are still present during May over northwest and partly central Europe. The strong cooling and large snow depths during May lead to a considerably shorter Growing Season Length (GSL). The GSL of a year is here defined as the number of days (duration) which are counted after the first 6 consecutive days with air temperatures ≥5.5 °C until the last time of the year with 6 consecutive days with temperatures ≥5.5 °C. The changes in GSL suggest that growing season length in coastal regions decreases by more than one month. Over western Europe, the growing season decreases by 10–25 days and also becomes significantly shorter (by at least 1–2 weeks) south of around latitude 50°N. Only the region directly east of the ice sheet shows a slight but mostly non-significant increase in GSL, while no changes in GSL are evident in most parts of eastern Europe.

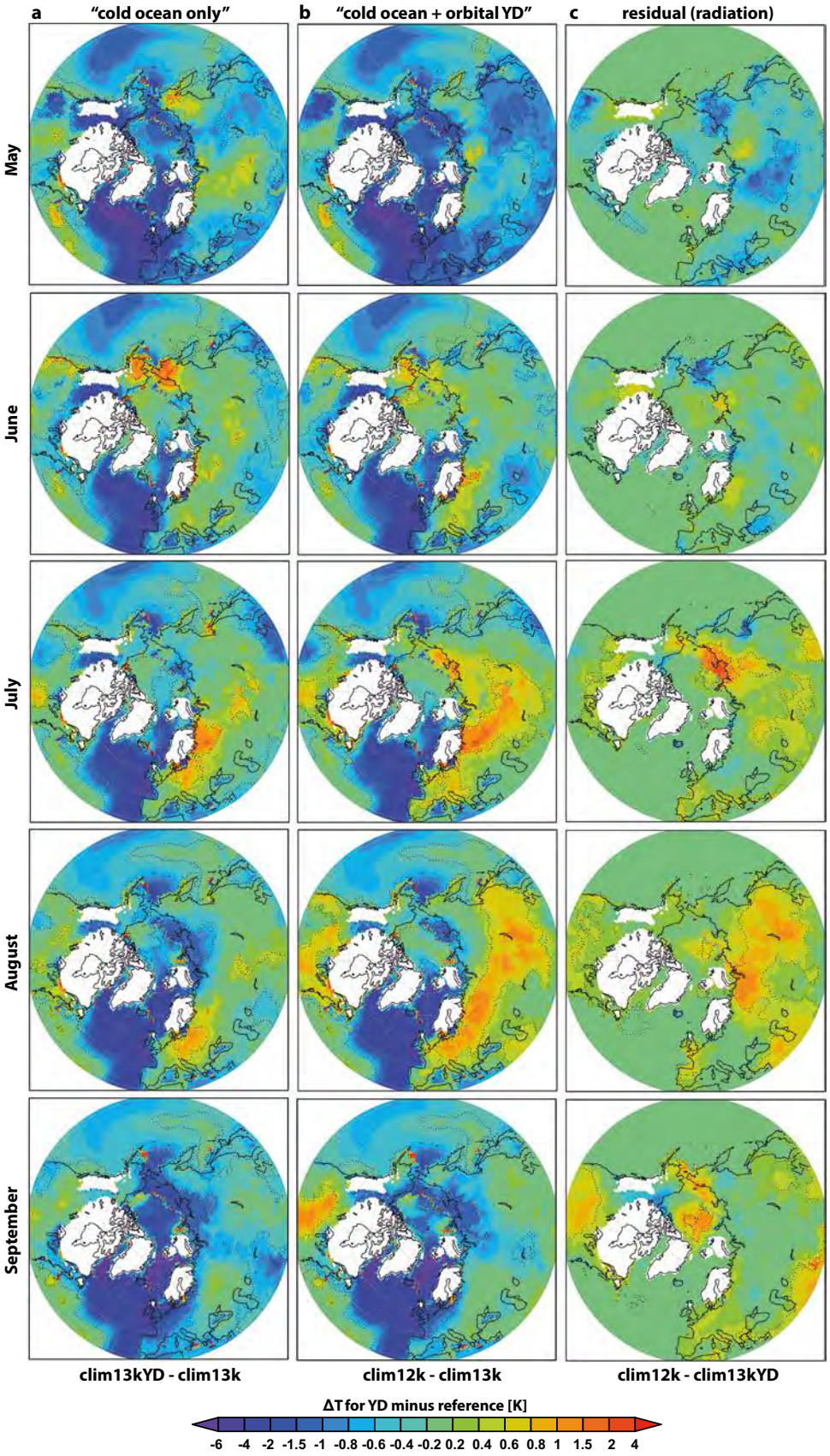

Figure 3-15. *Sensitivity study for changes in monthly mean temperatures [K] between BA and YD in response to oceanic cooling with and without changes in radiative forcing. Clim13k and clim12k represent the standard simulation with realistic forcing for BA and YD, while clim13kYD represents a sensitivity simulation where the ocean state of BA is replaced by the ocean state of YD (=cold-ocean-only experiment clim13kYD). The difference between clim12k and clim13kYD reflects the residuals, which are dominated by changes in radiation, but may include also noise/unaccounted feedbacks.*

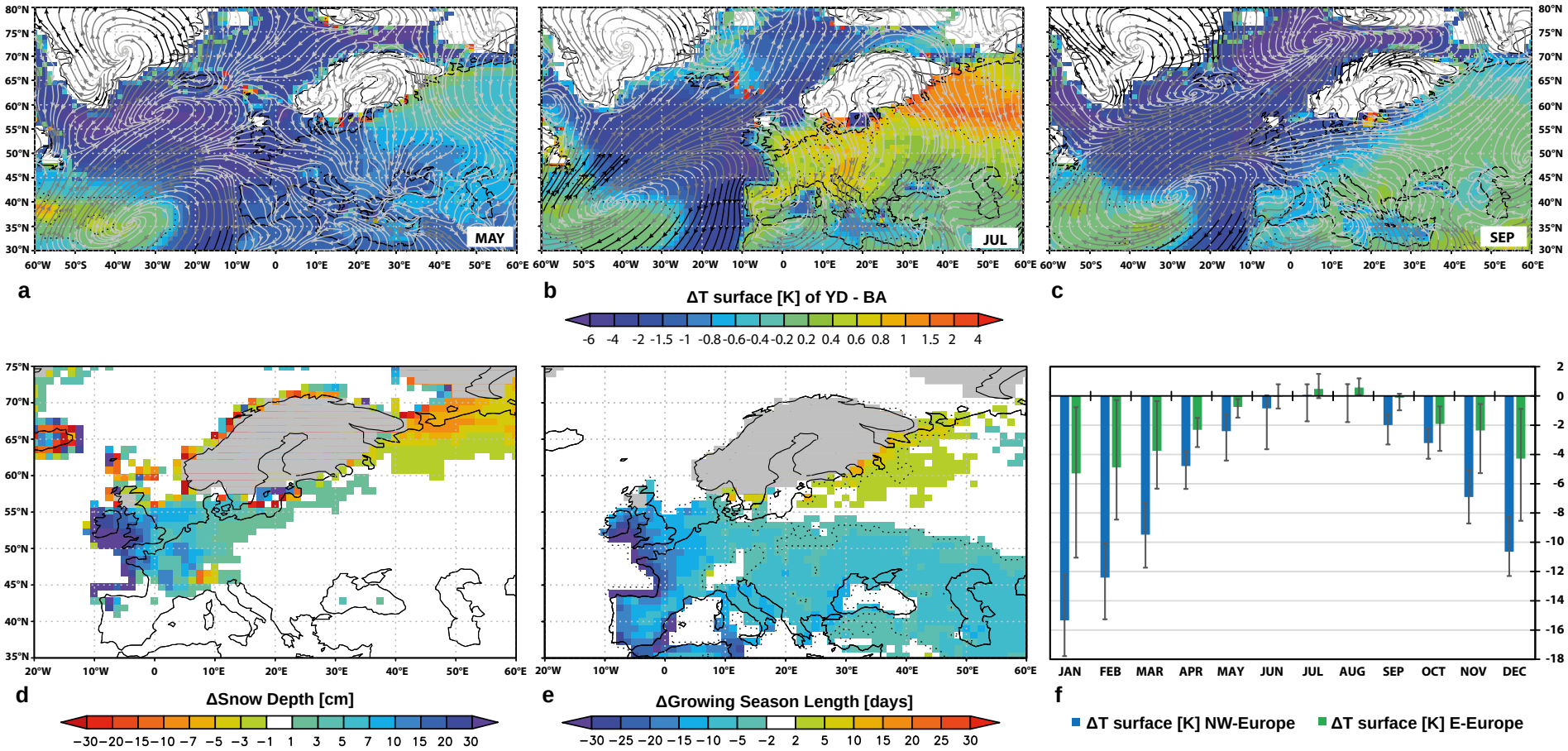

Figure 3-16. *Simulated changes in seasonality of surface air temperatures and related changes of the growing season length for YD minus BA. Simulated changes in monthly mean temperatures (shaded) for (a) May, (b) July and (c) September together with the related mean wind flow patterns during the YD (contour lines). d) Simulated changes in May snow depth [cm] and (e) changes in Growing Season Length (N days ≥5.5 °C). f) Simulated monthly mean temperature changes averaged over northwest Europe (blue) and eastern Europe (green). For the latter, error bars represent the 90 % spread around the mean of temperature changes within each region.*

Based on Figure 3-16, the short warm summers during July and August or June, July and August appear to be of minor relevance in the context of the extreme changes in seasonality during the rest of the year. Interestingly, the clear meridional cooling gradient with strong summer cooling over northwest Europe and less so over eastern Europe as reflected by chironomid-inferred temperatures closely matches the W-E gradient simulated by CESM1 for the cooling in May, greater snow depths in May and also the decrease in GSL. Although chironomids are typically used to infer July or summer air temperatures, they actually live in close dependency of the actual lake water temperature. It is hence very likely that a shorter GSL and a strong YD-BA cooling in May led to a longer lake-ice coverage, a considerably later ice-out, cooler early summer temperatures and to an overall shorter YD warm season in terms of lake water temperatures (Ahmed et al. 2018). In contrast, our plant indicator species (aquatic and telmatic) grow in very shallow lake water or along the lake shore and may thus more directly reflect the actual air temperature. A detailed evaluation of the effect of such extreme seasonality changes on lakes and their implications for various lake-sediment proxies is, however, beyond the scope of this study.

Recent results from reconstructing July temperatures of the Eemian at Sokli, northern Finland (Plikk 2018) based on chironomids suggest that July temperatures were up to three degrees warmer if a continental training dataset is used rather than an oceanic training set. Our model simulations with CESM1 and also previous proxy-based studies (Denton et al. 2005) clearly point towards a shift to more continental climate conditions during the YD. It is hence plausible to assume that a re-calculation of chironomid-based July temperatures with a more appropriate continental dataset might lead to warmer July estimates for the YD than inferred from more oceanic training sets. This could significantly reduce the gap relative to warmer July estimates from plant macrofossils and our climate simulation with CESM1.

3.5.4 Simulated changes in seasonal precipitation during the Younger Dryas

In the previous section we focused on simulated changes in thermal parameters with respect to summer/spring climate as these parameters have a significant impact on all aspects of the ecosystem and hence on geo(bio-)chemical proxies. The detailed analysis of transient proxy-based changes over southern Sweden (Section 3.1) has, however, also shown that large changes must have occurred with respect to hydroclimate conditions during the last deglaciation. Earlier studies have also highlighted the importance of hydroclimatic changes (Lowe et al. 1994, Björck 2007, Rach et al. 2014), which are confirmed by the two Swedish multi-proxy records studied by Muschitiello (2016). Together these studies demonstrate that cold periods (stadials), including the Younger Dryas, were accompanied by a shift to generally drier conditions downwind of the cold North Atlantic as shown in Figure 3-17.

A general difficulty of proxy-based humidity estimates is that they can only account for qualitative and relative changes between drier and wetter conditions. This makes it difficult to directly compare these changes with simulated changes in precipitation and/or humidity. Here, we show simulated relative changes in seasonal precipitation during the YD relative to BA [%] to estimate the tendency to wetter or drier conditions and the spatial pattern of these changes.

Figure 3-17 shows that the strong oceanic cooling and southward extension of sea-ice cover generally leads to a very strong reduction in total precipitation (which is the total sum of large-scale advective precipitation, convective precipitation and snowfall/hail) over the North Atlantic Ocean in all seasons, albeit somewhat less for summer. The reduction of regionally more than > 30 % to 50 % in total precipitation over the ocean is due to the direct impact from the extension of sea-ice cover. The strong reduction in precipitation (including snow in winter) continues downstream, towards the east, and northwards over the North Atlantic following large-scale wind patterns. Over Europe, the strongest reduction in seasonal precipitation occurs during winter and spring. In autumn, drier conditions are mostly concentrated over western Europe, while drier conditions in summer are spatially more homogenous over Europe with a reduction of ~ 10–20 % over most regions.

The simulated reduction in precipitation is extreme, both in relative magnitude and spatial extent. Important for the analysis of past ecosystems, and hence for most climate proxies, is, however, that summer precipitation was only reduced by ~ 10–20 %, because very cold YD winter conditions lasted until May and winter cooling began already in September (Figure 3-17). The simulation thus confirms proxy-inferred changes in humidity both in southern Sweden (Muschitiello et al. 2015, Wohlfarth et al. 2016, 2018) and in other regions (Lowe et al. 1994, Björck 2007, Rach et al. 2014, Muschitiello 2016) and suggests that YD was characterised by a shift to significantly drier conditions

in response to a strong oceanic cooling and a southward extension of sea ice. The southward shift of sea ice and partly, or fully, frozen oceans also imply that moisture transport to Europe needed to travel a considerably longer distance. The hydrogen isotope signal during the YD in southern Sweden (Sections 3.1.2 and 3.1.3) (Muschitiello 2016, Wohlfarth et al. 2016, 2018), and e.g. central Germany (Rach et al. 2014) could thus not only indicate drier conditions, but also a fresher moisture source either due to sea-ice cover or a fresher surface ocean due to meltwater discharge from Scandinavia. The good correspondence between a simulated reduction in precipitation and various proxy evidence (Lowe et al. 1994, Björck 2007) (see also Sections 3.1.2; 3.1.3), as well as hydrogen isotope evidence for a fresher moisture source (Rach et al. 2014, Muschitiello 2016), is a robust confirmation that the boundary conditions of a largely ice-covered northern North Atlantic during the YD are adequate in our CESM1 simulation.

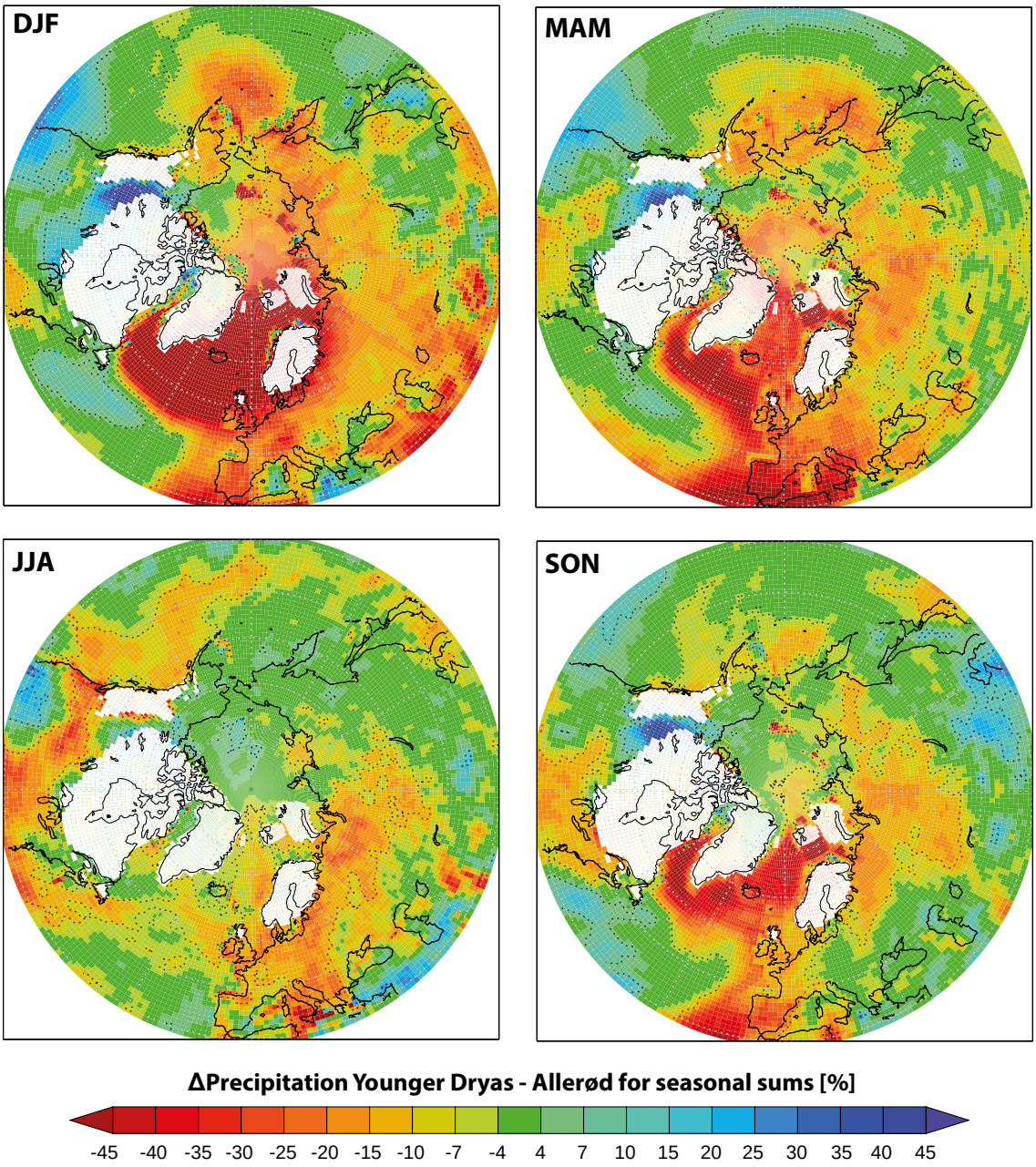

Figure 3-17. *Relative difference in seasonal precipitation sums during the Younger Dryas relative to the Allerød [%] based on simulations with CESM1 (clim12k minus clim13k). Changes over Europe reflect the strong ocean cooling and extended sea-ice while changes in GHG and orbital forcing alone have no significant influence (residual of sensitivity run, clim12k minus clim13kYD, not shown). DJF = December, January, February; MAM = March, April, May; JJA = June, July, August; SON = September, October, December.*

4 Discussion

4.1 Synthesis of climatic and environmental development in southern Sweden during the Last glacial/interglacial transition

The precision of chronologies and of age-depth models for each respective multi-proxy record is an important issue when comparing paleo-data sets along transects (see Section 3.1.1). In Sections 3.1.2 and 3.1.3 we presented the data sets for the two multi-proxy records, Atteköpsmosse and Hässeldala Port, on their respective age-depth model (Wohlfarth et al. 2017, 2018), but noted that large age uncertainties exist for the upper part of Atteköpsmosse's chronology due to a lack of radiocarbon dates. Here, we compare the two data sets with each other to better understand whether spatial and temporal differences existed in respect to the climatic and environmental development in southern Sweden during the last deglaciation.

In a first step, we compare selected proxies for Atteköpsmosse and Hässeldala Port (chironomid-inferred summer surface water temperature; local vegetation; changes in the composition of the moisture source) on their original chronology (Figure 4-1a–c) and as presented in Sections 3.1.2 and 3.1.3. This comparison suggests that the response of certain proxies in Atteköpsmosse lagged that in Hässeldala Port. The marked decline in summer lake surface water temperature, which is registered at around 13.1–13.0 ka BP in Hässeldala Port seems to have occurred 200–300 years later, i.e. around 12.9–12.8 ka BP in Atteköpsmosse (Figure 4-1a). Also, the rise in summer lake surface water temperature seems to have been delayed by a few hundred years in Atteköpsmosse as compared to Hässeldala Port. Similarly, the change in local vegetation from herb and grass dominated to open forests occurred at 11.7 ka BP in Hässeldala Port, but only at 11.4 ka BP in Atteköpsmosse (Figure 4-1b). These temporal differences could be due to various local conditions around the sites, such as soil conditions, nutrient supply, micro-climate, changes in lake level, etc., but could also be an expression of the chronological uncertainties for Atteköpsmosse between 12.6 and 11.3 ka BP (see Section 3.1.1). To further evaluate these discrepancies, we compare reconstructed changes in moisture source composition with each other (Figure 4-1c). The two hydrogen isotope curves (δD_{aq}) for Atteköpsmosse and Hässeldala Port not only display different values, but also show opposing trends between the sites. Transitions from a more saline moisture source to a fresher moisture source are for example registered at 13.7 ka BP and 12.9 ka BP in Atteköpsmosse, but at 13.1 ka BP and 12.6–12.5 ka BP in Hässeldala Port (Figure 4-1c).

In a second step, we test whether these temporal differences are 'real' and not an artefact of chronological uncertainties by aligning the rise in summer surface lake water temperatures at the two sites with each other using the assumption that the rapid hemispheric temperature rise across the Younger Dryas – Holocene transition was synchronously registered in southernmost Sweden (Björck et al. 1996) (Figure 4-1c–f). Following this alignment, the time lags between the two sites become negligible also in respect to vegetation changes (Figure 4-1e) and changes in moisture source composition, such as the transition from a saltier to a fresher moisture source at 13.1 ka BP (Figure 4-1f) seem more compatible with each other. Given these observations, we conclude that temporal differences in the response of the various proxies likely relate to uncertainties in Atteköpsmosse's chronology and that they are not an expression of time lags.

In a third step, we compare the age and timing of the regional pollen zones using the adjusted age model of Atteköpsmosse (Figure 4-2). This comparison suggests that the pollen zone transition between the Older Dryas and Allerød regional pollen zones and between the Younger Dryas and the early Holocene pollen zones occurred approximately at the same time. The only temporal difference in terms of regional pollen zone transitions is at the Allerød/Younger Dryas boundary (Figure 4-2). The pollen diagram for Atteköpsmosse, on which the local pollen zone boundaries are based, was originally established on an older core (C-1981; Table 2-2). Samples for pollen analysis had been analysed in varying temporal resolution and, except for a few radiocarbon dates, no age-depth model existed for this core (Wohlfarth et al. 2018). However, by aligning the loss-on-ignition curves of core C-1981 and the new core C-2011 the age-depth model for C-2011 could be transferred to C-1981 and provided approximate ages for the pollen zone boundaries (Wohlfarth et al. 2018). The low temporal resolution of the analysed pollen samples especially across the Allerød-Younger Dryas pollen zone boundary (25 cm difference between the samples above and below the pollen zone transition) (Wohlfarth et al. 2018) can easily explain the noted difference of up to 500 years (Figure 4-2).

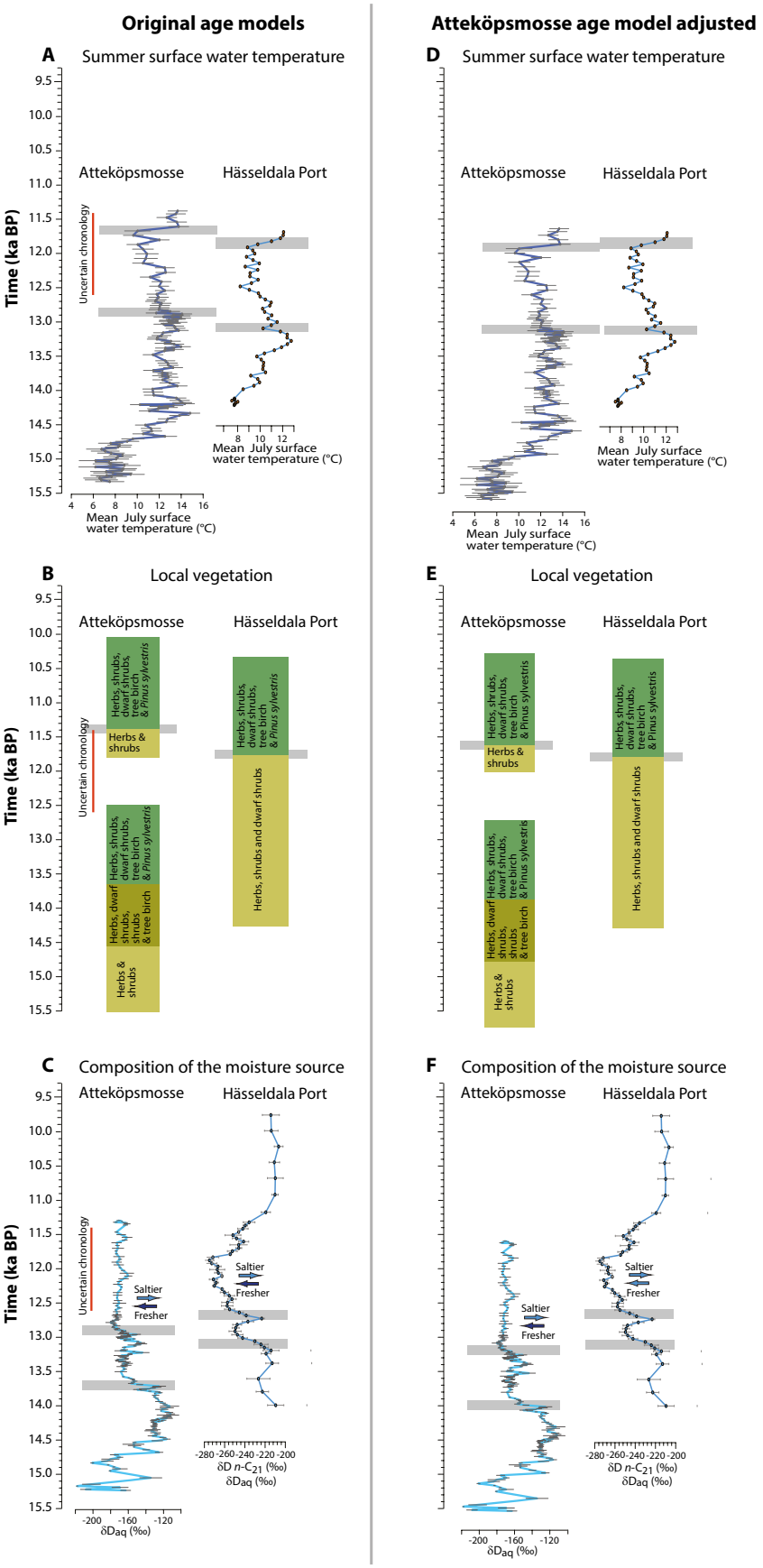

Figure 4-1. *Temporal comparison of selected proxies for Atteköpsmosse and Hässeldala Port. A) Summer surface lake water temperature, b) local vegetation changes and c) moisture source composition on the time scale of each respective site. D) Summer surface lake water temperature, e) local vegetation changes and f) changes in moisture source composition on the adjusted timescale for Atteköpsmosse (see text for a detailed explanation).*

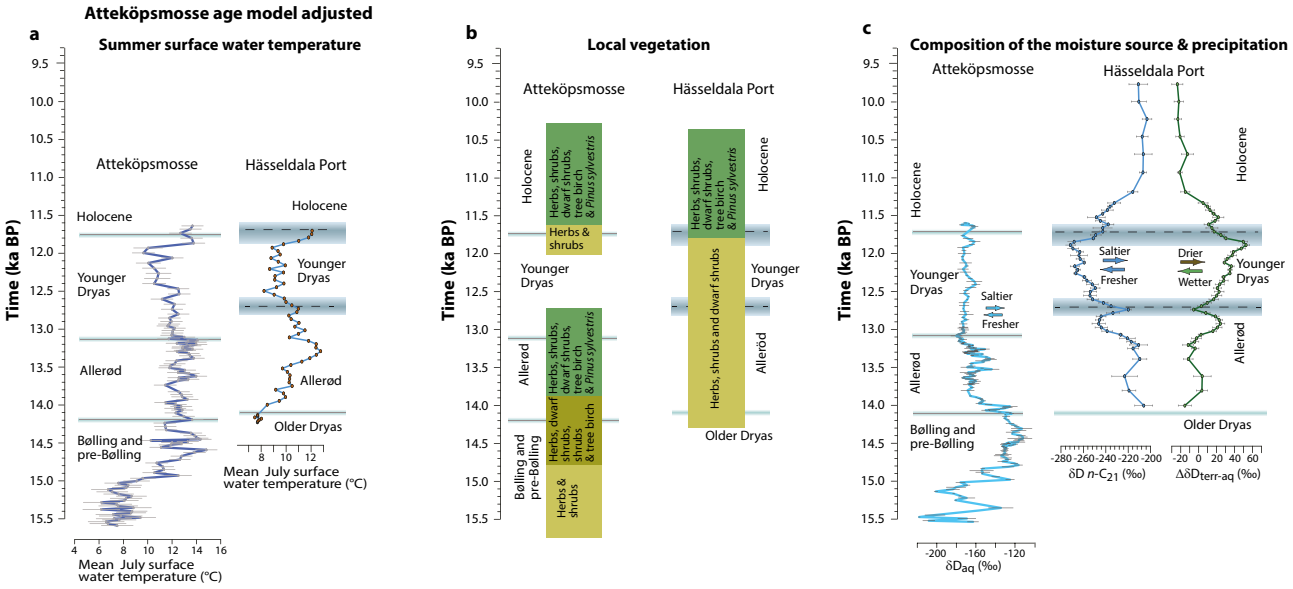

Figure 4-2. *Comparison of selected proxies for Atteköpsmosse and Hässeldala Port on the adjusted time-scale for Atteköpsmosse (see Figure 4-1) in relation to the regional pollen zones. A) Summer surface lake water temperature; b) local vegetation; c) composition of the moisture source and inferred precipitation.*

Given the arguments outlined above, we conclude that the age-depth model for Atteköpsmosse has limitations, especially between 12.6 and 11.3 ka BP, and that the age assignment of the pollen zone boundaries, notably across the Allerød-Younger Dryas pollen zone transition has a high degree of uncertainty. For the temporal and spatial comparison between the two sites, we therefore present the multi-proxy data set of Atteköpsmosse on an adjusted time scale (Figure 4-3).

The comparison between the western (Atteköpsmosse) and the eastern site (Hässeldala Port) shows that the southwestern part of Sweden became free of active and stagnant ice much earlier than the southeastern part (Figure 4-3). Sedimentation in the ancient basin at Atteköpsmosse started around, or possibly before, 15.5 ka BP, i.e. several thousand years earlier than at Hässeldala Port. This makes Atteköpsmosse the oldest studied multi-proxy site in Sweden and allows reconstructing environmental and climatic changes during the pre-Bølling and Bølling pollen zones. During this early part of Atteköpsmosse's history, lake surface water summer temperatures rose from around 6–8 °C before 15 ka BP to 12–15 °C after 15 ka BP. The shift in local plant communities from herb and shrub dominated vegetation to including dwarf shrubs and tree birch seems, however, to have occurred a few hundred years later, at around 14.8 ka BP. Plant indicator species inferred minimum mean July temperatures for the time interval prior to 14.8 ka BP are around 16 °C and compare well to temperatures estimated based on the plant macrofossil record on Kullen Peninsula at Björkerödsmosse and Håkullsmosse (Liedberg Jönsson 1988). The composition of the moisture source for Atteköpsmosse, as evidenced by hydrogen isotopes, suggests initially marked shifts between fresher and more saline conditions, which are at 14.8 ka BP followed by overall saline conditions. Variable amounts of freshwater input from the melting Fennoscandian Ice Sheet into the Nordic Seas could account for these signals.

Between 14.8 and 13.9 ka BP (~Bølling interstadial), summer surface water temperatures in the lake at Atteköpsmosse fluctuated between 10 and 15 °C and were much warmer than in Hässeldala Port, which had become ice free around 14.2 ka BP (Figure 4-3). Colder summer surface lake water temperatures of around 8 °C at Hässeldala Port are likely a response to melting of stagnant ice around the lake. However, temperatures rise rapidly and attained 10 °C at 13.9 ka BP. While the vegetation around Atteköpsmosse was made up of herbs, grasses, dwarf shrubs, shrubs and tree birch, the local vegetation around Hässeldala Port seems to have been composed of herbs and shrubs only. Climate indicator plant species suggest minimum mean summer temperatures of around 12–13 °C for Atteköpsmosse during the Bølling interstadial, whereas those for the Kullen Peninsula sites range around 13–14 °C. These different values are likely due to the fact that the plant macrofossil record of the two Kullen Peninsula sites is much more diverse and much richer (Liedberg-Jönsson 1988) than at Atteköpsmosse. Lower inferred minimum mean summer temperatures at Atteköpsmosse could therefore just be an artefact of not having found these specific plant species in the analysed samples. The composition of the moisture source, as evidenced by hydrogen isotopes, suggests overall more saline conditions (Figure 4-3) at S-Swedish sites.

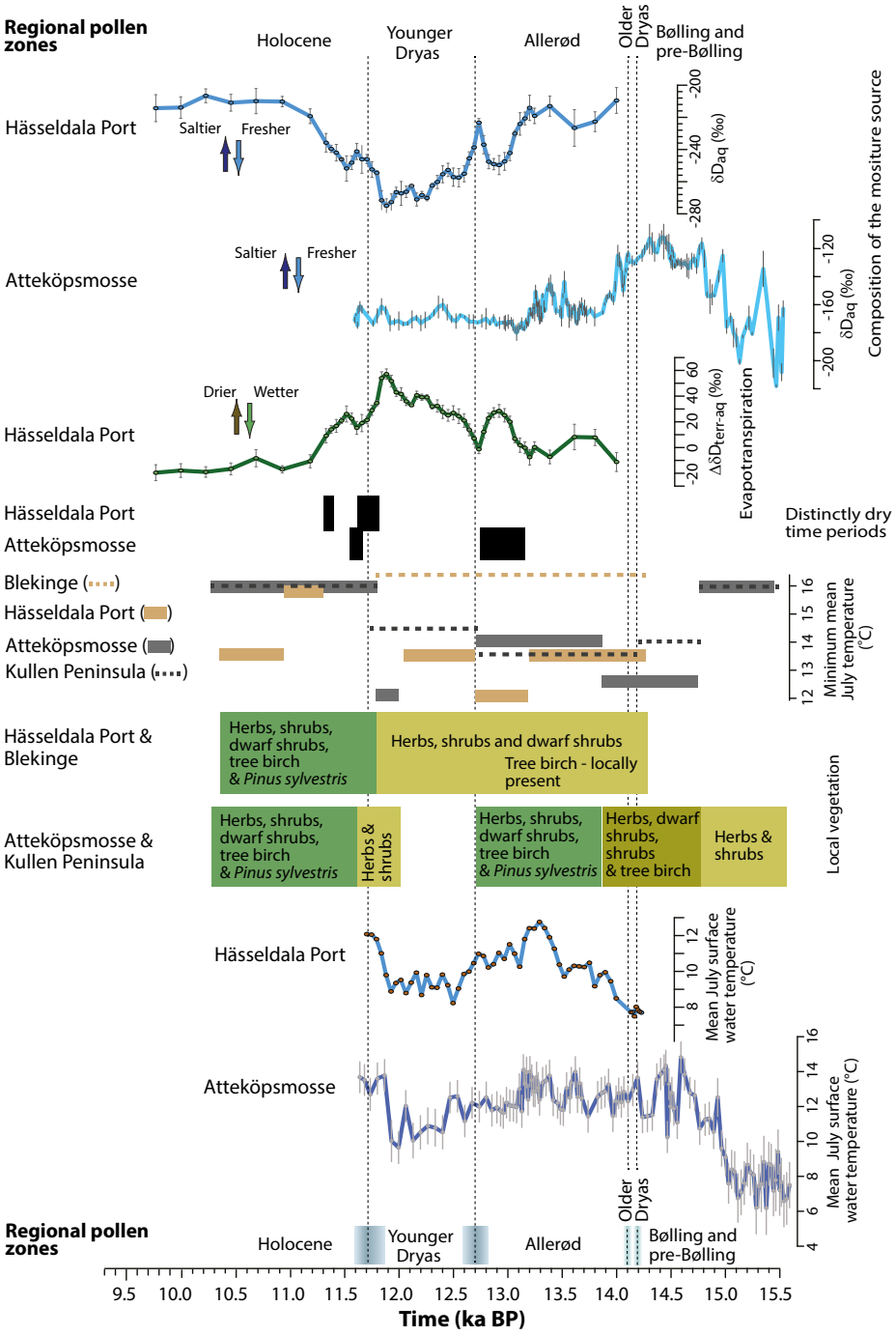

Figure 4-3. *Multi-proxy climate and environmental records for Atteköpsmosse and Hässeldala Port including chironomid-inferred mean July surface water temperatures, local vegetation as reconstructed based on plant macrofossil remains, plant-indicator species based minimum mean July temperatures, charcoal as an indicator for dryness and availability of fire-sensitive woody plants, and hydrogen isotopes as indicators of evaporation and of changes in moisture source composition. In addition, we show minimum mean July temperatures as reconstructed using the plant macrofossil records of Björkerödsmosse and Håkullsmosse on Kullen Peninsula (Liedberg Jönsson 1988) and the pollen and plant macrofossil records of Berglund (1966) for Blekinge. For Björkerödsmosse and Håkullsmosse we base our minimum mean July temperature estimates on the presence of Herniaria glabra during the pre-Bølling, of Callitriche hermaphroditica during the Bølling, of narrow-leaved Potamogeton (Potamogeton cf. vaginatus; P. cf. pusillus) during the Older Dryas and the Allerød, of Dianthus deltoides during the Younger Dryas and of Lycopus europaeus during the Preboreal regional pollen zones (Table 4-1) (Wohlfarth et al. 2018). For Blekinge, we use Typha latifolia and Jasione montana, which occur as pollen grains during the Allerød (Berglund 1966) and Myriophyllum spicatum, M. verticillatum and Jasione montana, which occur as pollen grains during the Younger Dryas (Berglund 1966, Wohlfarth et al. 2017) (Table 4-1). These latter indicator species suggest that minimum mean summer temperatures could locally have reached ≥16.5 °C both during Allerød and during Younger Dryas.*

Between 13.9 and 13.1 ka BP (~Allerød interstadial) summer lake water surface temperatures for Atteköpsmosse were around 12–14 °C, while those for Hässeldala Port continuously increased and attained similar values only between 13.4–13.1 ka BP. The local vegetation around Atteköpsmosse also included *Pinus sylvestris* at this time, whereas herbs, shrubs and dwarf shrubs dominated around Hässeldala Port. Tree birch may, however, have been locally present, as suggested by macroscopic finds (Berglund 1966) (Figure 4-3). Inferred minimum mean July temperatures at Atteköpsmosse and on Kullen Peninsula were around 13–14 °C and compare well with each other and also with those estimated for Hässeldala Port. In contrast, inferred minimum mean July temperatures based on the data set of Berglund (1966) are considerably higher, at around 16 °C. Both hydrogen isotope curves, for Atteköpsmosse and Hässeldala Port, suggest relative changes in moisture source composition around 14.0–13.9 ka BP, although the hydrogen isotope values are not comparable with each other. This is likely a result of fraction effects, since Atteköpsmosse is located much closer to its moisture source as compared to Hässeldala Port. Moreover, the latter site could be influenced by its location close to the Baltic Ice Lake. The relative change from a saltier to a fresher moisture source composition around 14.0–13.9 ka BP was followed by a more saline signal between 13.6 and ~13.1 ka BP seen at both sites (Figure 4-3).

Table 4-1. Plant indicator species used for assessing minimum mean July temperatures using the fossil plant assemblages of Björkerödsmosse and Håkullsmosse on Kullen Peninsula (Liedberg Jönsson 1988) and the pollen and plant macrofossil records of (Berglund 1966) for Blekinge. The temperature assignment follows (Väliranta et al. 2015).

Plant taxa	Minimum mean July temperature (°C)
Callitriche hermaphroditica	14
Dianthus deltoides	14.4
Herniaria glabra	16.0
Jasione montana	16.5
Lycopus europaeus	15.9
Myriophyllum spicatum group	12.2
Myriophyllum verticillatum	13.8
Potamogeton cf. vaginatus	13.6
Potamogeton cf. pusillus	13.6
Typha latifolia	15.7

Lake surface water summer temperatures at both sites started to decline after 13.1 ka BP and reached the lowest Younger Dryas values between 12.4–12.0 ka BP (Atteköpsmosse) and 12.5–12.0 ka BP (Hässeldala Port), respectively. The local terrestrial vegetation around Atteköpsmosse does not reflect this temperature change since herbs, shrubs, dwarf shrubs, tree birch and *Pinus sylvestris* seem to persist until at least 12.7 ka BP. The same holds true for Hässeldala Port, where herbs, shrub and dwarf shrub vegetation continued to persist. Coincident with the YD decline in summer surface water temperature at both sites, we note a decline in inferred minimum mean summer temperatures for Hässeldala Port, while minimum mean summer temperatures for Atteköpsmosse and Kullen Peninsula remained similar as during the previous time interval. Given that inferred minimum mean July temperatures for Blekinge (Berglund 1966) are still around 16 °C, lower temperatures at Hässeldala Port are likely due to the 'absence' of a specific climate indicator species in the analysed samples. This does however not necessarily mean that the plant was not present around Hässeldala Port. It only means that we did not recover the full spectrum of plants, which had originally been present around the site. High amounts of charcoal in Atteköpsmosse between 13.1–12.7 ka BP suggest higher fire intensities and as such drier climate early YD conditions. This is corroborated by the hydrogen isotope record of Hässeldala Port, which can be interpreted as reflecting progressively drier conditions. The hydrogen isotope values for both sites now also point to overall fresher moisture source conditions after 13.1 ka BP.

The marked rise in lake water surface summer temperatures seen for both sites between 11.9–11.8 ka BP (10 to 14 °C in Atteköpsmosse and 9 to 13 °C in Hässeldala Port) leads the change in vegetation at Atteköpsmosse with a few hundred years, but coincides with a change in vegetation at Hässeldala

Port seen as a replacement of the herb, shrub, dwarf shrub vegetation with open birch and pine forests. Climate indicator plant species for Atteköpsmosse indicate minimum mean July temperatures of around 12 °C for 12 ka BP, while those for the Kullen Peninsula sites suggest values of around 14 °C between 12.7 and 11.8 ka BP (YD), which is closer to those inferred from Hässedala Port, but far below those for Blekinge in general (Figure 4-3). Around 11.7 ka BP climate indicator species inferred minimum mean summer temperatures rise to 15–16 °C (Atteköpsmosse, Kullen Peninsula) and attain similar values at Hässeldala Port by 11.3 ka BP. This temperature increase marks the end of the YD. High amounts of charcoal present at both sites between 11.7 and 11.3 ka BP compare to persistent dry conditions inferred from hydrogen isotopes (Figure 4-3). Proxies for moisture source composition display no significant changes at Atteköpsmosse, while those at Hässeldala Port indicate a marked shift from fresher to more saline conditions, coincident with the rise in summer surface lake water temperatures. Warmer minimum mean July temperatures, wetter conditions and a saltier moisture source thus characterise the start of the Holocene.

4.2 Climate simulations and proxy-data comparison for the last deglaciation

In this section, we first discuss our new simulation results in the context of previous simulations that have been made with a focus on the last deglaciation and the Younger Dryas. Then we discuss the importance of atmospheric blocking, which was simulated by our high-resolution experiments for the local to regional climate during the last deglaciation (see Section 3.5.1), the importance to account for changes in seasonality (see Section 3.5.3), and the potential impact of strong changes in precipitation (see Section 3.5.4) as an additional key factor to understand cold/stadial climate conditions.

4.2.1 Comparison with previous simulations of the last deglaciation

Previous simulations of the last deglaciation and of the rapid transition from BA to YD had a strong focus on the role of the paleo-ocean and specifically on changes in the strength of the AMOC (e.g. Stocker and Wright 1991, Rahmstorf 1995, Stouffer et al. 2006, Menviel et al. 2011, He 2011, Liu et al. 2012). From a modelling point of view, the strong rapid cooling as that of the YD can technically only be obtained by imposing large fresh water fluxes on the ocean model and hence to enforce a significant weakening of the AMOC. The ~1 100-year long cold period of the YD and other stadials are therefore explained by a shift to a weaker AMOC state (Stocker and Wright 1991, Björck et al. 1996, Broecker 1998, McManus et al. 2004) in combination with atmosphere-ocean-sea-ice feedbacks (e.g. Rach et al. 2014, Muschitiello et al. 2015b).

The concept that a shift in the strength of the AMOC is the main driver behind cold/warm/cold transitions is widely accepted and consistent with geological evidence for AMOC changes (McManus et al. 2004). Coupled atmosphere-ocean models generally reproduce the winter dominated annual cooling signal in Greenland ice cores (Steffensen et al. 2008, Buizert et al. 2014) by enforcing a strong AMOC reduction, but these simulations are not able to reproduce the chironomid-inferred European summer cooling during the YD without additional changes in e.g. solar forcing (Renssen et al. 2000, 2015) with the exception of CCSM3 (He 2011, Liu et al. 2012). Because of this discrepancy between chironomid-based July temperatures and model simulations, additional forcing mechanisms for a YD cooling have been suggested (Renssen et al. 2000, 2015, Wunsch 2006, Zhang et al. 2014, Zhu et al. 2014) (including e.g. a reduction in solar activity) in combination with an AMOC slowdown (Renssen et al. 2000, 2015). While low solar activity may have contributed to the onset of the YD (Renssen et al. 2000), proxy evidence for a long-term millennial-scale negative radiative forcing is lacking. In addition, low solar activity would be overcompensated within few centuries owing to the high and rapidly increasing orbital summer forcing during YD. Lower solar activity in combination with increased dust and vegetation changes during the YD may provide some negative forcing not accounted for in our simulation. However, the negative forcing is much smaller than the strong increase in orbital summer insolation and cannot explain the strong cooling as e.g. reflected by chironomid-inferred July temperatures. Overall, the reason for these model-proxy mismatches, and hence the answer to the question whether the AMOC slowdown and related feedbacks were the only drivers behind the YD cold period, were thus open questions at the start of the present study.

For our simulations, we a-priori accepted the concept of a strong reduction of the AMOC as a key driver behind the YD by prescribing the horizontal boundary conditions for CESM1 based on the SST's and the sea-ice fraction from CCSM3 (He 2011, Liu et al. 2012). Although this approach does not include transient changes in paleo-ocean temperature between the selected very warm (AL) and extreme cold state (YD) in the CCSM3 simulation, the selected time periods for our CESM1 simulations are designed to provide the outer limits of a plausible envelope of paleo-ocean state changes for the BA-YD transition. The climatic analysis and comparison of our CESM1 simulations for BA and YD may hence be based on the rather most extreme possible changes in the paleo-ocean state for which CESM1 is used to simulate the related atmosphere-land-ice impacts at high spatial resolution.

The results from our CESM1 simulation confirm previous YD simulations (Isarin et al. 1998, Renssen et al. 2000, 2015), which were unable to simulate a summer cooling over Europe in response to an ocean state with a strong AMOC slowdown. The only way to simulate cold European summers with an AMOC-only scenario so far stems from the TraCe-21ka simulation with CCSM3 as shown in Figure 3-11. As briefly discussed in Section 3.3.2 (Figure 3-12), cold European summers during the YD can be simulated by maintaining a strong westerly flow across Europe also during the summer period. As clearly evident from the wind field comparison between the very coarse model resolution of CCSM3 and the high resolution of our CESM1 simulations (Figure 3-12), such a strong westerly flow pattern during summer appears very unlikely from a fluid-dynamical perspective in the presence of a still massive Fennoscandian Ice Sheet.

It would of course be important to run the same experiments with different models and different atmospheric resolutions for the YD, e.g. with different ice sheet configurations. However, the proxy-based evidence for warm YD summers (using plant indicator species) clearly argues against cold summers and against a strong westerly flow during summer. The atmospheric blocking of a westerly flow over Europe during summer seems to have been a dominant mechanism during the last deglaciation and underlines the importance to run high resolution climate simulations in order to capture the regional to large-scale impact of ice sheets on atmospheric circulation.

4.2.2 The role of atmospheric blocking for the climate during the last deglaciation

The proxy-based evidence for stable and warm summer conditions during the YD, based on climate indicator plant species across Europe, confirms the warm YD summers simulated by CESM1. The comparison of our simulated summer temperature response and mean wind patterns with those simulated by CCSM3 suggests that atmospheric blocking over the Fennoscandian Ice Sheet was the main driver to maintain warm YD summers, independent from the dramatic oceanic cooling and southward extension of sea-ice. The summer cooling due to a strong westerly flow that was simulated by CCSM3 for Europe and Eurasia is only simulated until May in CESM1 (Figure 3-16a). Atmospheric blocking of westerly flow did therefore most likely only occur during two to three YD summer months (June, July and August). The collapse of the blocking effect outside of the summer season explains why an extreme change in seasonality with very cold conditions lasting from September to May can co-occur with very short warm June to August summers. These findings confirm an earlier hypothesis that changes in seasonality may be the dominant aspect behind abrupt climate shifts, such as the start of the YD (Denton et al. 2005) or Dansgaard-Oeschger interstadial/stadial changes (Flückiger et al. 2008). It is thus not surprising that certain proxies, like chironomids or terrestrial pollen, which incorporate a much longer climatic signal, may not capture such a short warm episode given the dominance of very strong cooling during the rest of the year.

Our CESM1 simulation for BA versus YD captures only the two most extreme changes in terms of the paleo-ocean state in CCSM3. It is hence difficult to assess whether the simulated statistically significant ($p < 0.05$) warming of 0.5 to 1.5 K over central and eastern Europe did occur during the mid-YD (clim12k). Such a warming would have notable implications for the melting of the Fennoscandian Ice Sheet and also for the fresh water flux to the Baltic Ice Lake and/or the Nordic Seas (Muschitiello et al. 2015b).

In our sensitivity experiment, which simulated the YD as a cold-ocean-only event with unchanged radiative forcing relative to BA (clim13kYD), enhanced atmospheric blocking and warming over central Europe occur as a direct thermodynamic response to the strong ocean cooling. Such

a “cold-ocean-warm-summer” mechanism is consistent with climatological analyses of recent summer heat waves (Duchez et al. 2016, Ionita et al. 2017). As shown for the change of the summer SLP-pattern over the Northern Hemisphere, a cold ocean alone leads to a significant strengthening of atmospheric blocking over the British Isles and the Norwegian coastline (Figure 3-14d). A less cold North Atlantic and/or less sea-ice during the YD would thus imply less strengthening of the atmospheric blocking and less or no warming over Europe during summer. Although it appears counter-intuitive, a less cold North Atlantic can lead to a cooler European summer climate and vice versa.

Given that CESM1 simulates warmer summers than CCSM3 during the YD, a fully coupled CESM1 simulation with an actively run ocean may yield considerably less sea-ice during summer than prescribed in our simulation based on CCSM3. While warm YD summers due to atmospheric blocking are faithfully simulated by our model, uncertainties remain regarding the magnitude of the potential warming or regional cooling over Europe because of the uncertain representation of the paleo-ocean state. This uncertainty is currently difficult to quantify because i) climate indicator plant species only provide information on minimum mean July temperatures; ii) a sample does not capture all plants that grew at the respective location and time; iii) the Finnish data set used to reconstruct minimum mean July temperatures does not include summer temperatures ≥17 °C (Section 2.2.2, Table 2-1, Väliranta et al. 2015). We can therefore not rule out that summers were even warmer than suggested based on the available proxy evidence.

Atmospheric blocking as a key mechanism to explain late glacial European summer climate has been demonstrated here for the first time, although the existence of a thermodynamic induced tendency to such a blocking can also be seen in the coarse resolution CCSM3 simulation. Muschitiello et al. (2015b) for example show that CCSM3 simulates a comparable, although spatially less constrained, change in the summer SLP-pattern in response to a strong oceanic cooling over the North Atlantic. However, in the coarse resolution CCSM3 simulation, the SLP increase over Europe does not lead to blocking, while the higher model resolution in the CESM1 simulation clearly shows increased atmospheric blocking. Although the increase in summer SLP can thus be regarded as a robust thermodynamic response to strong ocean cooling in both models, it is the high-resolution atmospheric model only that is capable of actually simulating the atmospheric blocking.

4.2.3 Seasonality changes as a key feature of rapid climate shifts

The observations of time-transgressive regional differences in the timing and impact of the rapid cooling/warming at the onset and end of the YD have highlighted the importance of changes in westerly winds in response to a south-/northward shift of the sea-ice extent over the North Atlantic (Brauer et al. 2008, Lane et al. 2013, Rach et al. 2014) or the Nordic Seas (Muschitiello and Wohlfarth 2015, Muschitiello et al. 2015b). Based on the high spatial detail of our CESM1 simulations and the spatially extended plant climate indicator data set, we can now show that these changes are related to marked seasonality changes, which occurred outside of the summer months (autumn until late spring). The simulation is supported by multi-proxy evidence from western Germany, which explains the YD climate by shifts in the westerlies during the autumn, winter and spring season (Brauer et al. 2008).

Interestingly, and based on the analysis of the simulated wind flow over the Euro-Atlantic region in CESM1, it appears that it is not the change in westerly winds itself, but rather the fact that these winds had to cross much colder and/or largely ice-covered areas. This observation might explain the strong signal seen in YD isotopic proxy records (e.g. Lane et al. 2013, Rach et al. 2014, Muschitiello et al. 2015b). Combined with the plant indicator species approach and the CESM1 simulation employed here, we suggest that the isotope proxies indeed reflect a strong shift to a generally colder (and drier) YD climate, except for the peak summer months.

The presence of atmospheric blocking and hence the observed extreme changes in seasonality make it crucial to carefully evaluate the sensitivity of various proxies to changes in seasonality. As shown in Figure 3-16, the presence (e.g. July) or collapse (starting in September and lasting until May) of atmospheric blocking strongly influence the impact due to changes advected from the North Atlantic.

Strong seasonality changes rather than summer temperature changes have been discussed as an important factor during glacial periods with rapid climate shifts and presence of large ice sheets (Denton et al. 2005, Flückiger et al. 2008). To which extent thermodynamically induced atmospheric blocking in response to cold North Atlantic SST's may also persist without the presence of orographic blocking by an ice sheet, needs to be evaluated in the future. While observational evidence for such a link exists (Duchez et al. 2016, Ionita et al. 2017), state-of-the-art climate models generally tend to significantly underestimate the atmospheric blocking frequency even at high atmospheric resolutions (e.g. Scaife et al. 2010).

4.2.4 Potential implications of simulated changes in precipitation

Several paleoclimatic and paleoenvironmental studies mention a shift to drier conditions during YD (e.g. Lowe et al. 1994, Björck 2007, Rach et al. 2014, Muschitiello et al. 2015b, Wohlfarth et al. 2017) in addition to changes in temperature. A change towards drier conditions and lower humidity, already before the start of the YD, is also indicated by hydrogen isotope analyses of Swedish lake sediment records (Section 3.1.2, Figure 3-7 and Section 4.1 and Figure 4-3) (Muschitiello et al. 2015b, Wohlfarth et al. 2017, 2018) and other European sites (Rach et al. 2014). The disadvantage of any hydroclimate proxy is that they often only provide qualitative information about precipitation changes. It is therefore often difficult to distinguish the influence of precipitation from changes in evaporation and other factors, or to estimate the season during which these changes have taken place. The difference in mean hydrogen isotopes (δD_{aq}) values between BA and YD in our investigated Swedish lake sediments (Section 4.1, Figure 4-3) amounts for example to around −50 ‰ and implies a strong YD depletion of 20–30 % relative to the BA interval.

In the case of our CESM1 simulation, the strong oceanic cooling in combination with the southward extension of sea ice leads to strong reductions in seasonal precipitation (Section 3.5.4, Figure 3-17). Since most ecosystems are influenced by climatic changes taking place during late spring and summer, the significant reduction in precipitation by 10–20 % over central Europe and southern Sweden will have an impact on such ecosystems. The significantly reduced simulated precipitation (snow) during winter and spring may additionally impact these lateglacial ecosystems as it leads to less snow melt and hence increasingly drier soil conditions and less runoff to the lakes during the summer period. While some fraction of the strong reduction in precipitation may be compensated by less evaporation and/or longer snow cover until May (Figure 3-16d), the warm and dry conditions during summer will accumulate over time.

From a synoptic-scale meteorological perspective, the above described conditions are today known to be a key driver behind heat waves and droughts. As observed for the major European heat waves since the 1980's (Duchez et al. 2016) and described in more detail for the European drought of 2015 (Ionita et al. 2017), a lack of precipitation starting in spring leads to increasingly drier soil conditions during the summer season. The lack of soil moisture causes a positive warming feedback where less soil moisture leads to less evaporative cooling of near-surface temperatures. The lack of near-surface cooling leads to further warming and further enhances evaporation and decreases soil moisture. As a result of this positive feedback, which started with reduced moisture availability already in spring, followed by less precipitation in summer, mid- to late-summer conditions will be very warm and dry and may lead to heat waves and droughts. This would also explain why the slight additional warming during the YD mainly occurs during July and August and over very continental regions. Hence, warm and dry conditions maintained by atmospheric blocking in response to cold North Atlantic SST's become additionally amplified by a lack of precipitation/soil moisture.

Combining all the mechanisms that are involved in a strong ocean cooling as during the YD, but also as during modern-day heat waves (Figure 4-4), a warm and dry summer climate appears to be a robust implication where the cold ocean causes two major feedbacks: a strong reduction of moisture transport from the ocean to the continent and a strengthening of atmospheric blocking of westerly flow during summer; this creates and maintains warm and dry conditions until the westerly flow overturns the blocking in September. While unusually cold North Atlantic SST's today only cause hot and dry European summers during some years, the additional orographic blocking effect for westerly flow enforced by the Fennoscandian Ice Sheet (Figure 3-16b) explains why the mean state, as represented by the mean SLP pattern for July (Figure 3-14a), rather than exceptional years, like in the modern climate, dominated during the last deglaciation.

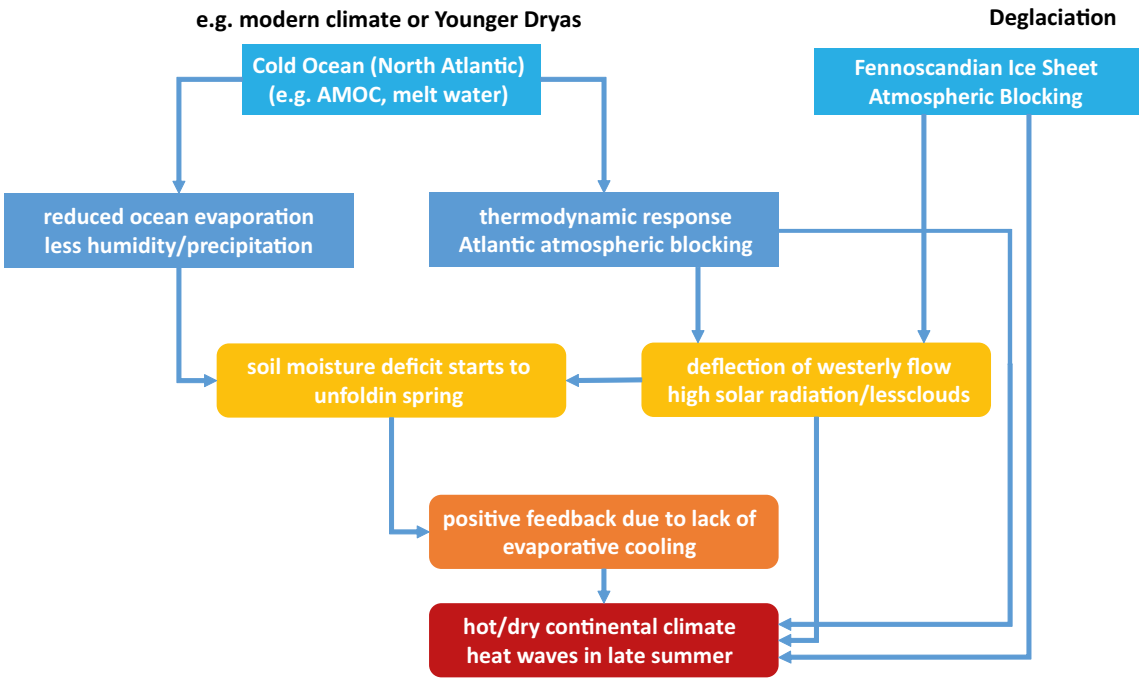

Figure 4-4. *Schematic synthesis of key processes which lead to dry and warm European summer conditions in response to strong oceanic cooling over the central North Atlantic.*

Wetter periods during warm ocean states like that of the BA, or later the early Holocene, can be explained by two effects: a weakening of the atmospheric blocking by warmer SST's and higher moisture availability, which results from warmer SST's. The strong agreement between proxy-evidence for warm/wet and cold/dry periods with the results of our CESM1 simulations strongly suggests that these rapid and strong climate transitions are mainly caused by the process where changes in North Atlantic SST's leads to atmospheric blocking, which in turn becomes amplified by positive soil moisture feedback in summer.

5 Synthesis and Conclusion

This project aimed at enhancing knowledge on climate evolution and variability in Scandinavia and Europe during the transition from a glacial into an interglacial climate state. We specifically focussed the study on the climate transitions of the last deglaciation and on the climate state and driving mechanisms that characterised the warm Bølling-Allerød (BA) interstadial and the cold Younger Dryas (YD) stadial. To achieve the overall aim of the study, the work was organised in two sub-projects:

(A) Compilation and analysis of multi-proxy records: To study the deglacial evolution of climatic and environmental changes over southern Sweden, we compiled and analysed qualitative as well as quantitative multi-proxy data based on transient lake sediment records from Atteköpsmosse and Hässeldala Port. In addition, we compiled and quantified published pollen and plant macrofossil datasets to gain a detailed spatiotemporal reconstruction of European summer temperatures for the BA and YD periods.

(B) Climate modelling and comparison with multi-proxy data: We developed a new paleoclimate model setup for the Earth System Model CESM1 which takes the presence of continental ice sheets and sea-level changes into account. We then used the paleo-version of CESM1 to perform and analyse a set of new high-resolution global climate model simulations for the BA and YD. The model results were compared to our newly-quantified European July temperature proxy compilation and key drivers behind regional to large-scale climatic drivers were identified.

5.1 Synthesis of proxy- and modelling results

Climate evolution over southern Sweden ~15 500 to ~9000 years BP

The comprehensive multi-proxy analysis of lake records from southern Sweden allowed us to gain a detailed reconstruction of transient changes of the local environment and climate during the last deglaciation. The sediment record retrieved from the ancient basin of Atteköpsmosse provides the oldest multi-proxy site for Sweden where sedimentation started already ~15.5 ka BP. This allows us to study the climate evolution of southern Sweden starting right after the northward retreat of the Fennoscandian Ice Sheet over the area. The proxy records cover the period from the pre-Bølling and Bølling pollen zones until the early Holocene.

Key results from the study of transient changes for southern Sweden are:

- Based on the high-resolution δD_{aq} records, we can identify distinct shifts in the moisture source composition related to fresher/saltier conditions in the North Atlantic and the Nordic Seas. Very salty oceanic conditions during the Bølling (~14.5 ka BP) found in Atteköpsmosse are consistent with proxy evidence for a very strong AMOC (McManus et al. 2004). Such a strong AMOC was also simulated by CCSM3 (He 2011) and has been explained as AMOC-overshoot in response to the recovery from the Oldest Dryas (Heinrich 1 event). Atteköpsmosse shows a tendency towards less salty conditions starting already around the Older Dryas (~14 ka BP) with no return to salty conditions during the late AL.
- Hässeldala Port suggests a later onset of a fresher moisture source during the AL (~13 ka BP) than Atteköpsmosse, with a timing more in line with a similar early depletion of $\delta^{18}O$ in Greenland ice cores. With the onset of the YD, a final sudden shift takes place to a fresh oceanic moisture source along with a similar shift to drier conditions. The YD terminates with a sudden shift back to saltier conditions consistent with the recovery of the AMOC at the onset of the Holocene.
- The initial early pre-YD depletion of $\delta^{18}O$ in Greenland ice cores as well as δD_{aq} in both Swedish lake records clearly suggests that a substantial increase in North Atlantic fresh water precedes and hence forces the AMOC response which then triggered the final abrupt onset of the YD. The consistent finding of a pre-YD depletion of $\delta^{18}O$ and δD_{aq} is important to note as it appears inconsistent with the idea of one single catastrophic drainage event as explanation for

the YD. More likely are contributions from both the Fennoscandian (Muschitiello et al. 2015b, Muschitiello 2016) and Laurentide Ice Sheets and/or a delayed response of the AMOC to the increase of North Atlantic freshwater.

- Changes in hydroclimate, estimated from reconstructed evapotransipiration of $\Delta\delta D_{terr\text{-}aq}$ of Hässeldala Port co-vary with the changes of a fresh/salty moisture source. This is consistent with other European sites (e.g. Lowe et al. 1994, Björck 2007, Rach et al. 2014, Muschitiello 2016) and confirms the general finding that cold stadial conditions are drier and warm interstadial conditions wetter. Our CESM1 simulation confirms the proxy evidence and suggests that the shift to drier conditions during the YD might have been quite extreme relative to the preceding AL (Figure 3-17). Although δD_{aq} of Atteköpsmosse shows a considerably earlier shift to a fresher moisture source and drier conditions than the early pre-YD shift during the AL at Hässeldala Port, a high amount of charcoal in the Atteköpsmosse record confirms that the shift to dry conditions happened during the late AL with increased biomass burning already before the YD. This might be an indication that dryness before the AL-YD transition led to widespread burning and disappearance of forests rather than a shift to a cold climate which seems to have taken place afterwards. This would further support the hypothesis that other reasons than summer temperatures led to the disappearance of European forests as the summer temperatures during the YD stayed warm (this study; Birks and Birks 2014, Schenk et al. 2018).
- Marked differences exist in local vegetation and in the immigration of trees at different sites in southern Sweden. An immigration of birch and pine into southwest Sweden takes place already during the Bølling and Allerød interstadial, respectively. The local presence of trees co-varies rather with changes in wetness/dryness than with summer temperatures.
- We find clear evidence that traditionally used reconstructions of deglacial July temperatures based on chironomids are generally up to several degrees colder than our reconstruction of minimum mean July temperatures based on climate indicator plant species following the extended quantification of Väliranta et al. (2015) used in this study (Schenk et al. 2018). To account for this difference, chironomid-based July temperatures were considered to reflect lake water temperatures while plant indicators reflect ambient air temperature (Wohlfarth et al. 2018). It should be noted though that modern observations generally show a high agreement between air and water temperatures for July (or the warmest month).
- A first test with a paleo-lake model simulation forced by model output from our CESM1 model suggests that a stationary relation exists between air and water July temperature even under extreme conditions of the YD (Ahmed et al. 2018). We therefore speculate that chironomids reflect a cold bias in July temperatures possibly in response to a significantly colder winter-spring season (Figure 3-16; Schenk et al. 2018) and hence a shorter open-ice season (Ahmed et al. 2018) during the YD.
- New evidence for chironomid-based July reconstructions for the Eemian at Sokli, northern Finland (Plikk 2018) suggests that July temperatures may be up to three degrees warmer if a continental training dataset is used rather than an oceanic training set. As there is generally consensus that the YD is dominated by a shift to a more continental climate (Denton et al. 2005, Schenk et al. 2018), a re-calculation of chironomid-based July temperatures with a more appropriate continental dataset might significantly reduce the gap to warmer July estimates from plant macrofossils and the climate simulation with CESM1 (Schenk et al. 2018).
- Consistent with the pre-YD shift to drier conditions with a fresher moisture source seen in δD_{aq}, chironomid-based lake water surface temperatures start to decline already before the start of the YD. Another shift to colder conditions takes place with the final onset of the YD and a rapid warming marks the onset of the Holocene.
- Based on climate indicator plant species, we find high minimum mean July air temperatures of ≥16 °C already during the pre-Bølling (~ 15.5 ka BP, Atteköpsmosse, Kullen Pensinula) which continue throughout the deglaciation (Blekinge) and early Holocene. With exception for Blekinge, southern Swedish records indicate somewhat lower minimum mean July temperatures of ≥13–14 °C during Bølling, Allerød and Younger Dryas. Because indicator plant species require higher July temperatures under continental conditions (e.g. on the Russian plain) compared to the same species in semi-oceanic conditions (e.g. Finland) (Väliranta et al. 2015), late-glacial temperatures were possibly higher than reconstructed here. Hence, the already quite high July

temperatures of ≥16 °C are a rather conservative estimate and even warmer conditions cannot be ruled out. Such high summer temperatures are consistent with high orbital summer insolation during the late deglaciation in combination with atmospheric blocking over Fennoscandia as simulated by CESM1 (Schenk et al. 2018).

New high-resolution climate model simulations with CESM1

As part of this study, we conducted the first high-resolution full-complexity climate model simulations for two specific periods of the late deglaciation with the Community Earth System Model (CESM1). The time periods for the high-resolution simulations were defined in such a way that we could compare the climate states with the warmest interglacial conditions of the late Allerød (13 ka BP) with the coldest stadial conditions of the mid-YD (12.170 ka BP). The warmest and coldest periods of the BA-YD transition were defined in terms of simulated transient surface temperatures over the region of Denmark and southern Sweden based on a previous coarse-resolution but fully coupled atmosphere-ocean-model with CCSM3 (He 2011).

An important part of setting up a high-resolution paleo-version of CESM1 was to include a new state-of-the-art ice sheet reconstruction of GLAC-1b. The Bayesian method used to reconstruct ice sheets combines physical-dynamical consistent ice sheet modelling with several thousands of geological evidences on local to regional ice sheet extent over time. For CESM1, the ice sheet reconstructions were interpolated on a global paleo-topography which takes the glacio-isostatic land adjustment and low sea-levels into account. Most important topographic changes for the BA-YD simulations over the Euro-Atlantic region compared to previous model simulations are a realistic representation of the North Sea as mainly land area and the Baltic Sea is represented as small ice lake south of the Fennoscandian Ice Sheet. In addition, a large part of today's shallow Arctic-Siberian shelf sea is simulated as land area consistent with low sea-levels of the late deglaciation.

Key improvements from using a high-resolution model simulation for the late-gacial climate

- With a horizontal model resolution of ~ 100 km (0.9° × 1.25°), our new CESM1 simulations provide the so far highest model resolution applied to dynamically reconstruct late-glacial climate conditions. In comparison to previous model simulations, an at least four times higher resolution leads to a much more realistic representation of fluid dynamics in response to the presence of large continental ice sheets.
- Our evaluation of the near-surface wind pattern around continental ice sheets confirms the evaluation of previous climate model simulations for the LGM over North America (Oster et al. 2015) which also demonstrated that a higher model resolution is important to adequately reproduce flow over continental ice sheets. Similar to our study, they found a considerably better agreement with regional climate reconstructions for a higher model resolution in which a stronger high pressure system dominates atmospheric circulation over the ice sheet.
- A key difference of our CESM1 simulation relative to previous coarse resolution simulation with CCSM3 is achieved for the European summer climate. Although CESM1 uses identical SST's and the same orbital as well as greenhouse gas forcing as CCSM3 for BA and YD, the high-resolution simulation suggests warm summers also during the YD owing to a blocking of westerly flow from the cold North Atlantic during the summer period. The blocking of westerly flow by the Fennoscandian Ice Sheet is not simulated by CCSM3 where the low-resolution leads to strong zonal flow across the ice sheet and cold European summers during YD (Schenk et al. 2018). Our compilation of plant-based European July temperatures confirms that the simulation of warm summers during the YD are realistic and that such warm summer conditions can only be explained by atmospheric blocking of westerly flow by the Fennoscandian Ice Sheet.
- Despite using the same SST's and sea-ice fraction, CESM1 suggests that winter temperatures during the YD are considerably colder over the Euro-Atlantic region than simulated by CCSM3. Although winter temperatures were not the focus of this study owing to a lack of available winter proxy data, the much stronger winter cooling over the central North Atlantic brings CESM1 considerably closer to $\delta^{18}O$-based estimates from the Greenland ice cores.

- A previous comparison of CCSM3 with $\delta^{18}O$ from Greenland ice cores has shown that the simulated winter cooling for the YD is considerably less than suggested by ice core signals (Buizert et al. 2014). Because the depletion of $\delta^{18}O$ during the YD was even higher than for the Oldest Dryas – although the AMOC was still considerably stronger during the YD than during the OD (McManus et al. 2014) and the YD received higher radiative forcing owing to higher GHG and orbital forcing – it has been argued that the depleted isotope signal in Greenland $\delta^{18}O$ might reflect too cold temperatures rather than that the simulation with CCSM3 would produce too warm temperatures for the YD. As a result, Buizert et al. (2014) argued that temperature-inference from $\delta^{18}O$ may not provide reliable information by itself. However, the severe winter cooling predicted by our CESM1 simulation rather supports the cold ice core signal than the warmer CCSM3 simulation suggesting a comparably severe winter cooling.
- Based on the considerably improved agreement between the severe winter cooling simulated by CESM1 and $\delta^{18}O$-inferred severe cooling registered in Greenland ice cores for the YD, it is plausible to assume a severe winter cooling over Europe (Figure 3-16f) which was more extreme over north-western NW-Europe (up to −18 K colder) than eastern Europe (on average around −5 K but with large spatial differences).

Seasonality changes rather than summer temperatures dominate stadial changes

Both, the compilation of plant-based July temperatures for Europe as well as our new CESM1 simulation do not support the summer cooling signal reflected by other proxies for the YD (from e.g. chironomids, Schenk et al. 2018). While plant indicator species do not suggest any change in July temperatures for BA relative to YD (median $\Delta T = 0$ for all regions), CESM1 suggests a slight but statistically significant warming of 0.5 to 1.5 K over continental regions of eastern Europe. Owing to the potential cold bias of the plant-indicator species approach under continental conditions (Väliranta et al. 2015), it can be argued that the simulated warming over eastern Europe is well in the range of the uncertainty of plant-indicators with a known continentality bias of ~1.3 K as e.g. Typha *latifolia* in Fennoscandia follows the +15.7 °C July temperature isoline in Finland while it corresponds to the +17 °C July isoline in continental Russia.

Overall, the simulated severe winter cooling in combination with a warm short and dry summer according to CESM1 is consistent with the previous hypothesis suggesting that abrupt climate change during the YD is dominated by a shift to continental conditions (Denton et al. 2005). The shift to continental conditions is clearly visible as a change in seasonality in CESM1 (Figure 3-16) explained by strong and cold westerly flow during autumn, winter and spring but atmospheric blocking during summer maintaining warm conditions independent from the severe ocean cooling of the YD.

The coarse resolution simulation of CCSM3 is in contrast not able to simulate increased continentally owing to its too strong zonal flow which leads to too warm winters and too cool summers and hence an unrealistically flat seasonal cycle. The finding of increased continentality for the YD and most likely other stadial climates is crucial because this has to be taken into account in future proxy-studies where a falsely used oceanic or sub-continental calibration dataset can lead to a strong cold bias for derived summer temperatures (Plikk 2018). The presence of thermophillous plant species requiring ≥16 °C in southern Sweden from ~15.5 ka BP until the Holocene is a clear indication that significant changes in seasonality/continentality dominate the shifts between stadials and interstadials while summer temperatures remain fairly high also during stadial conditions. CESM1 suggests that such high stable summer temperature in Europe can only be explained by atmospheric blocking over Fennoscandia as otherwise summer temperatures during the stadial would be cold as simulated by CCSM3 – which is clearly inconsistent with proxy evidence from southern Sweden and Europe.

New evolving evidence further supporting the presence of warm summers during the YD comes from revised datings of ice sheet retreat of Scotland's Ice Fields (Bromley et al. 2014, 2018). New ^{14}C-estimates suggest that the ice sheets retreated rapidly during full stadial conditions during the YD and that the last pulse of glaciation took place during the late AL or earlierst part of the YD. Consistent with proxy- and simulation results from this study, they conclude that enhanced summertime melting and hence warm summers characterise stadial conditions despite the severe winter cooling of the YD.

Precipitation / hydroclimate

In terms of hydroclimatic changes, proxies from southern Sweden (Section 3.1.3, Muschitiello et al. 2015b, Muschitiello 2016, Wohlfarth et al. 2017, 2018) as well as from other parts of Europe (e.g. Lowe et al. 1994, Björck 2007, Rach et al. 2014, 2017, Muschitiello 2016) provide clear evidence for considerably drier conditions during the YD relative to the preceding interstadial of BA or the onset of the Holocene. Simulated changes in seasonal precipitation from CESM1 confirm the shift to significantly drier conditions during the YD relative to BA across the entire Euro-Atlantic region. The spatial pattern and seasonal distribution of reductions in precipitation (Figure 3-17) are clearly linked to the strong southward extension of sea-ice and/or the very cold SST's during summer. Although hydroclimate proxies only allow qualitative estimates for relative changes towards drier or wetter conditions, the proxy-inferred changes in hydroclimate clearly support the significant reduction in precipitation simulated by CESM1 in response to a strong oceanic cooling and southward extension of sea-ice during the YD.

The very high-resolution transient hydroclimate record of Meerfelder Maar in Germany (Rach et al. 2014, 2017) further supports the interpretation that the southward shift of the sea-ice front at the onset of the YD is responsible for the shift to drier conditions. While the time-slice simulations cannot be used to study the transient shift from BA to YD, the hydroclimate record of Meerfelder Maar suggests that the shift do drier conditions followed the cooling with a lag of ~ 170 years (Rach et al. 2014). Records from southern Sweden suggest an earlier change to drier conditions than central Germany and point towards spatiotemporal differences in the onset of the YD consistent with time-transgressive shifts found for other locations across Europe and the British Isles (Lane et al. 2013, Muschitiello and Wohlfarth 2015).

The evolution of hydrogen records from southern Sweden generally suggest distinct shifts in moisture source composition related to fresher/saltier conditions in the North Atlantic and the Nordic Seas (Figure 3-7 and 4-3). Specifically, the study of the Hässeldata site suggests that the YD continued to become drier towards the end of the stadial, with a similar trend to a fresher moisture source. The YD in southern Sweden terminates with a sudden shift to wetter conditions which coincide with a saltier moisture source at the onset of the Holocene (Figure 4-3). The cold-ocean-only sensitivity study with CESM1 suggests that the cold ocean alone leads to intensified atmospheric blocking. CESM1 provides a consistent explanation for the proxy-evidence from southern Sweden that the driest conditions in the mid-YD with the highest freshwater moisture source corresponds to the period of maximal sea-ice extent with the most intense atmospheric blocking leading to the driest conditions during the mid-YD.

In summary, the proxy evidence from central Germany and southern Sweden is consistent with the simulated changes in precipitation and confirms that the southward extension of sea-ice during the YD is a key driver of hydroclimate changes during the YD. Although the intensification of atmospheric blocking during summer additionally decreases precipitation during the summer season of the YD, the major reduction in precipitation can be attributed to spring and the southern position of the sea-ice front. Overall, the severe cooling lasting until May, combined with short warm and dry summers, renders the stadial climate of the YD quite harsh in terms of growing conditions for terrestrial vegetation. The detailed analysis of the multi-proxy indicators from southern Sweden indicates that the shift to drier conditions might be more significant than summer temperature changes – consistent with the simulated extreme changes in precipitation by CESM1.

Governing mechanisms behind the climate of the Younger Dryas stadial

The high resolution of our CESM1 simulations, with realistic boundary conditions with respect to continental ice sheets and adjusted paleo-topography, provided an optimal base to study atmospheric circulation during the BA and YD in unprecedented detail. A key result of this study is the realistic simulation of fluid dynamical constraints leading to orographic blocking of atmospheric flow over the Fennoscandian Ice Sheet during summer. The blocking of flow over the ice sheet leads to an overall large-scale atmospheric blocking of westerly flow over Europe and represents the mean state of deglacial summer conditions over Europe. The mean state blocking pattern is clearly visible as a high pressure ridge connecting the Azores High with the high pressure conditions over FIS. This

blocking pattern prevents the westerly flow from advecting changes in North Atlantic SST's towards Europe during summer and explains why proxy evidence from Atteköpsmosse suggest ≥16 °C throughout the deglaciation from 15.5 ka BP until the Holocene independent from stadial climate cooling of the pre-Bølling, OD or YD.

For the comparison of BA with YD, CESM1 suggests that atmospheric blocking during the YD further intensifies and spatially expands over the British Isles and Norwegian Sea in response to the strong oceanic cooling as consequence of the AMOC slowdown. While the presence of atmospheric blocking is largely linked to the presence of the FIS, the YD-simulation as well as the cold-ocean-only sensitivity simulation also demonstrate the importance of cold North Atlantic SST's as a stabilizing factor of atmospheric blocking over Northern Europe. This thermodynamic response of the simulated blocking to cold SST's is consistent with very recent observations where record-breaking cold SST's over the central North Atlantic coincide with intense atmospheric blocking events over Europe and severe heat waves and droughts since the 1980's (Duchez et al. 2016, Ionita et al. 2017). Like in our simulation for the YD, the record-breaking cold SST's in recent years are clearly linked to a slowdown of the AMOC (e.g. Ceasar et al. 2018) since around 1950 and confirm a physically plausible thermodynamic link between cold North Atlantic SST's, AMOC-slowdown and warm/dry European summers for both, the YD and possibly other stadials as well as the modern climate.

In addition to the atmospheric blocking as mean state linked to the presence of the Fennoscandian Ice Sheet and the intensified blocking in response to cold North Atlantic SST's, a third mechanism supporting warm European summers during the YD results from large-scale teleconnections with sea-level pressure changes over the Greenland and the Arctic. Relative to BA, the climate simulations suggest a significantly lower pressure over the Arctic and hence an increase in the zonal pressure gradient over the North Atlantic in response to the AMOC-slowdown/oceanic cooling of the YD. This change in the pressure gradient implies a shift to a positive state of the Arctic Oscillation (AO+) which shows a high significant positive correlation with warmer summer temperatures over Europe.

The presence of persistent atmospheric blocking supported by FIS, the cold North Atlantic SST's and the AO+ teleconnection amplify the rapidly increasing orbital summer insolation which is a fourth forcing mechanism behind warm summers during the deglaciation including the YD. The cold-ocean-only experiment with CESM1 suggests that cold SST's intensify atmospheric blocking while the increase in orbital summer insolation tends to weaken the blocking. Although no transient high-resolution simulations could be performed for this project with CESM1, the sensitivity experiment suggests that the cold SST's and resulting intensified blocking are a more dominant forcing of warm European summers during the early YD (and early deglaciation) while high orbital summer insolation becomes more important during the late YD (and late deglaciation) where the blocking becomes weaker. Because atmospheric blocking has a large impact also on precipitation advected from the North Atlantic, this interpretation is consistent with the proxy-evidence that stadials with a cold ocean and strong blocking of precipitation are drier and interstadials with warmer SST's and weaker blocking are wetter. The dependency of the hydroclimate shift on atmospheric blocking adds to the general tendency following the Clausius-Clapeyron equation that colder conditions lead to lower water vapour pressure in the air. The combination of both effects explains why the simulated reduction in precipitation is quite extreme during the YD further supporting the hypothesis that shifts to drier conditions rather than cold summers dominate stadial-interstadial changes including the disappearance of European forests during the YD.

5.2 Conclusion

Based on the reconstruction and analysis of our multi-proxy climate reconstruction for southern Sweden and Europe, we find clear evidence for remarkably high summer temperatures throughout the deglaciation. Based on the longest geological records of Sweden, July temperatures over southern Sweden were at least around +16 °C from the beginning of the record at the pre-Bølling (~15.5 ka BP) until the early Holocene (~10 ka BP). Our new high-resolution climate model simulations for the late BA and mid-YD with CESM1 confirm the presence of warm European summers as reconstructed from lake records of southern Sweden and quantified July temperatures based on climate indicator

plant species from over 120 lakes across Europe. The clear proxy evidence for both remarkably high July temperatures as well as the transient stability of a warm summer climate throughout the deglaciation including the YD stadial can only be explained by the simulated atmospheric blocking of westerly flow over the FIS during summer.

The distinct shifts between stadial and interstadial climate states, which are clearly visible in summer lake water temperatures (chironomids) as well as hydroclimate proxies ($\Delta\delta D_{aq}$, $\Delta\delta D_{terr\text{-}aq}$), appear to be driven by changes in seasonality/continentality in response to changes in North Atlantic SST's. South Swedish lake water temperatures co-vary with shifts in moisture source and dryness and appear to represent extreme changes dominating until late spring (May) which are linked to variations in the position of the southern sea-ice front and AMOC strength.

Our CESM1 simulation generally confirms the proxy-evidence for drier conditions during the YD stadial and indicates that the reduction in precipitation might have been rather extreme. Because there is a clear signal for a first early pre-YD shift towards colder/drier condition during the AL in southern Swedish chironomid- and $\Delta\delta D_{aq}$-records, as well as in $\Delta\delta^{18}O$ records from Greenland ice cores, it appears likely that increased meltwater inflow to the North Atlantic Ocean during the AL caused already cooler and drier conditions and the abrupt onset of the YD represents only the final step with the final AMOC slowdown. The pre-YD cooling and drying seen in proxy records suggests that the YD was not caused by a single catastrophic event but rather a gradual increase of meltwater and/or multiple drainage events from the Baltic Ice Lake and the FIS.

Overall, we conclude that the consistency of proxy- and modelling evidence for warm European summers also during the YD provides robust evidence for the presence of atmospheric blocking over FIS during the deglaciation. The abrupt shifts between stadial and interstadials are caused by shifts in seasonality/continentality and dryness and represent the climatic response to shifts in North Atlantic SST's, position of the sea-ice front and hence the strength of the AMOC.

References

SKB's (Svensk Kärnbränslehantering AB) publications can be found at www.skb.com/publications.

Aichner B, Herzschuh U, Wilkes H, Vieth A, Böhner J, 2010. δD values of *n*-alkanes in Tibetan lake sediments and aquatic macrophytes – a surface sediment study and application to a 16 ka record from Lake Koucha. Organic Geochemistry 41, 779–790.

Ahmed E, Parducchi L, Unneberg P, Ågren R, Schenk F, Rattray J E, Han L, Muschitiello F, Pedersen M W, Smittenberg R H, Yamoah K A, Slotte T, Wohlfarth B, 2018. Archaeal community successions in Late glacial lake sediments: evidence from ancient DNA. Quaternary Science Reviews 181, 19–29.

Ampel L, Kylander M E, Steinthorsdottir M, Wohlfarth B, 2014. Abrupt climate change and early lake development – the Lateglacial diatom flora at Hässeldala Port, southeastern Sweden. Boreas 44, 94–102.

Andersson M, 2004. Pollenstratigraphic response for tephra horizons during the last glacial–interglacial (LGIT) transition in southernmost Sweden. MSc thesis. Department of Physical Geography and Quaternary Geology, Stockholm University.

Atkinson T C, Briffa K R, Coope G R, Joachim M J, Perry D W, 1986. Climatic calibration of coleopteran data. In Berglund B E (ed). Handbook of holocene palaeoecology and palaeohydrology. Chichester: Wiley, 851–858.

Atkinson T C, Briffa K R, Coope G R, 1987. Seasonal temperatures in Britain during the past 22,000 years, reconstructed using beetle remains. Nature 325, 587–592.

Berglund B E, 1966. Late-quaternary vegetation in eastern Blekinge, south-eastern Sweden. Stockholm. (Opera botanica 12)

Berglund B E, Ralska-Jasiewiczowa M, 1986. Pollen analysis and pollen diagrams. In Berglund, B E (ed). In Berglund B E (ed). Handbook of holocene palaeoecology and palaeohydrology. Chichester: Wiley, 455–484.

Birks H H, Birks H J B, 1998. D.G. Frey and E.S. Deevey review 1: Numerical tools in palaeolimnology – Progress, potentialities, and problems. Journal of Paleolimnology 20, 307–332.

Birks H H, Birks H J B, 2014. To what extent did changes in July temperature influence late glacial vegetation patterns in NW-Europe? Quaternary Science Reviews 106, 262–277.

Birks H J B, Birks H H, 2000. Future uses of pollen analysis must include plant macrofossils. Journal of Biogeography 27, 31–35.

Björck S, 1981. A stratigraphic study of Late Weichselian deglaciation, shore displacement and vegetation history in south-eastern Sweden. Oslo: Universitetsforlaget. (Fossils and Strata 14)

Björck S, 1984. Bio- and chronostratigraphic significance of the Older Dryas Chronozone – on the basis of new radiocarbon dates. Geologiska Föreningen i Stockholm Förhandlingar 106, 81–91.

Björck S, 2007. Younger Dryas oscillation, global evidence. In Elias S A (ed). Encyclopedia of Quaternary science. Oxford: Elsevier, 1987–1994.

Björck S, Möller P, 1987. Late Weichselian environmental history in southeastern Sweden during the deglaciation of the Scandinavian ice sheet. Quaternary Research 28, 1–37.

Björck S, Kromer B, Johnsen S, Bennike O, Hammarlund D, Lemdahl G, Possnert G, Rasmussen T L, Wohlfarth B, Hammer C U, Spurk M, 1996. Synchronised terrestrial-atmospheric deglacial records around the North Atlantic. Science 274, 1155–1160.

Braconnot P, Harrison S P, Kageyama M, Bartlein P J, Masson-Delmotte V, Abe-Ouchi A, Otto-Bliesner B, Zhao Y, 2012. Evaluation of climate models using palaeoclimatic data. Nature Climate Change 2, 417–424.

Brauer A, Haug G H, Dulski P, Sigman D M, Negendank J F W, 2008. An abrupt wind shift in western Europe at the onset of the Younger Dryas cold period. Nature Geoscience 1, 520–523.

Briggs R D, Pollard D, Tarasov L, 2014. A data-constrained large ensemble analysis of Antarctic evolution since the Eemian. Quaternary Science Reviews 103, 91–115.

Broecker W S, 1998. Paleocean circulation during the last deglaciation. a bipolar seesaw? Paleoceanography 13, 119–121.

Bromley G R M, Putnam, A E, Rademaker K M, Lowell T V, Schaefer J M, Hall B, Winckler G, Birkel S D, Borns H W, 2014. Younger Dryas deglaciation of Scotland driven by warming summers. Proceedings of the National Academy of Sciences 111, 6215–6219.

Bromley G R M, Putnam A, Borns H, Lowell T, Sandford T, Barrell D, 2018. Interstadial rise and Younger Dryas demise of Scotland's last ice fields. Paleoceanography and Paleoclimatology, 33, 412–429.

Bronk Ramsey C, 2008. Deposition models for chronological records. Quaternary Science Reviews 27, 42–60.

Bronk Ramsey C, 2009. Bayesian analysis of radiocarbon dates. Radiocarbon 51, 337–360.

Bronk Ramsey C, 2010. OxCal Program, v417. Radiocarbon accelerator unit. University of Oxford, UK.

Brooks S J, Langdon P G, Heiri O, 2007. The identification and use of Palaearctic Chironomidae larvae in palaeoecology. London: Quaternary Research Association. (QRA Technical Guide 10.)

Buizert C, Gkinis V, Severinghaus J P, He F, Lecavalier B S, Kindler P, Leuenberger M, Carlson A E, Vinther B, Masson-Delmotte V, White J W C, Liu Z, Otto-Bliesner B, Brook E J, 2014. Greenland temperature response to climate forcing during the last deglaciation. Science 345, 1177–1180.

Carlson A E, Clark P U, 2012. Ice sheet sources of sea level rise and freshwater discharge during the last deglaciation. Review of Geophysics 50, RG4007. doi:10.1029/2011RG000371

Ceasar L, Rahmstorf S, Robinson A, Feulner G, Saba V, 2018. Observed fingerprint of a weakening Atlantic Ocean overturning circulation. Nature 556, 191–196.

Cheng J, Liu Z, He F, Otto-Bliesner B L, Colose C, 2011. Impact of North Atlantic – GIN Sea exchange on deglaciation evolution of the Atlantic Meridional Overturning Circulation. Climate of the Past 7, 935–940.

Clark P U, Shakun J D, Baker P, Bartlein P J, Brewer S, Brook E, Carlson A E, Cheng H, Kaufman D S, Liu Z, Marchitto T M, Mix A C, Morrill C, Otto-Bliesner B L, Pahnke K, Russell J M, Whitlock C, Adkins J F, Blois J L, Clark J, Colman S M, Curry W B, Flower B P, He F, Lynch-Stieglitz J, Markgraf V, McManus J F, Mitrovica J X, Moreno P I, Williams J W, 2012. Global climate evolution during the last deglaciation. Proceedings of the National Academy of Sciences 2012, E1134–E1142.

Colleoni F, Rosenbloom N, 2014. CESM 1.0.5 near past initial conditions user guide: prescribing ice sheets. CMCC Research Papers Issue RP0221. Available at: https://www.cmcc.it/wp-content/uploads/2014/05/CESM_IC_Colleoni.pdf

Colleoni F, Wekerle C, Masina S, 2014. Long-term safety of a planned geological repository for spent nuclear fuel in Forsmark – estimate of maximum ice sheet thicknesses. SKB TR-14-21, Svensk Kärnbränslehantering AB.

Coope G R 1986. Coleoptera analysis In Berglund B E (ed). Handbook of Holocene Palaeoecology and Palaeohydrology. Chichester: Wiley, 703–714.

Coope G R, Lemdahl G, Lowe J J, Walkling A, 1998. Temperature gradients in northern Europe during the last glacial–Holocene transition (14–9 ^{14}C kyr BP) interpreted from coleopteran assemblages. Journal of Quaternary Science 13, 419–433.

Davies S, Wastegård S, Wohlfarth B, 2003. Extending the limits of the Borrobol Tephra to Scandinavia and detection of new early Holocene tephras. Quaternary Research 59, 345–352.

Davies S M, Wohlfarth B, Wastegård S, Andersson M, Blockley S, Possnert G, 2004. Were there two Borrobol Tephras during the early Lateglacial period: implications for tephrochronology? Quaternary Science Reviews 23, 581–589.

Denton G H, Alley R B, Comer G C, Broecker W S, 2005. The role of seasonality in abrupt climate change. Quaternary Science Reviews 24, 1159–1182.

Denton G H, Anderson R F, Toggweiler J R, Edwards R L, Schaefer J M, Putnam A E, 2010. The last glacial termination. Science 328, 1652–1656.

Deschamps P, Durand N, Bard E, Hamelin B, Camoin G, Thomas A L, Henderson G M, Okuno J, Yokoyama Y, 2012. Ice-sheet collapse and sea level rise at the Bølling warming 14,600 years ago. Nature Communications 483, 559–564.

Duchez A, Frajka-Williams E, Josey S A, Evans D G, Grist J P, Marsh R, McCarthy G D, Sinha B, Berry D I, Hirschi J J-M, 2016. Drivers of exceptionally cold North Atlantic Ocean temperatures and their link to the 2015 European heat wave. Environmental Research Letters 11, 074004. doi:10.1088/1748-9326/11/7/074004

Eglinton G, Hamilton R J, 1967. Leaf epicuticular waxes. Science 156, 1322–1335.

Eglinton T I, Eglinton G, 2008. Molecular proxies for paleoclimatology. Earth and Planetary Science Letters 275, 1–16.

EPICA Community Members, 2006. One-to-one coupling of glacial climate variability in Greenland and Antarctica. Nature 444, 195–198.

Ficken K J, Li B, Swain D L, Eglington G, 2000. An *n*-alkane proxy for the sedimentary input of submerged/floating freshwater aquatic macrophytes. Organic Geochemistry 31, 745–749.

Flückiger J, Knutti R, White J W C, Renssen H, 2008. Modeled seasonality of glacial abrupt climate events. Climate Dynamics 31, 633–645.

Garcin Y, Melnick D, Strecker M R, Olago D, Tiercelin J-J, 2012. East African mid-Holocene wet–dry transition recorded in palaeo-shorelines of Lake Turkana, northern Kenya Rift. Earth and Planetary Science Letters 331–332, 322–334.

Gent P R, Danabasoglu G, Donner L J, Holland M M, Hunke E C, Jayne S R, Lawrence D M, Neale R B, Rasch P J, Vertenstein M, Worley P H, Yang Z-L, Zhang M, 2011. The Community Climate System Model Version 4. Journal of Climate 24, 4973–4991.

He F, 2011. Simulating transient climate evolution of the last deglaciation with CCSM3. PhD thesis. University of Wisconsin-Madison.

He F, Shakun J D, Clark P U, Carlson A E, Liu Z, Otto-Bliesner B L, Kutzbach J E, 2013. Northern Hemisphere forcing of Southern Hemisphere climate during the last deglaciation. Nature 494, 81–85.

Heiri O, Lotter A F, 2001. Effect of low count sums on quantitative environmental reconstructions. an example using subfossil chironomids. Journal of Paleolimnology 23, 343–350.

Heiri O, Brooks S J, Renssen H, Bedford A, Hazekamp M, Ilyashuk B, Jeffers E S, Lang B, Kirilova E, Kuiper S, Millet L, Samartin S, Toth M, Verbruggen F, Watson J E, van Asch N, Lammertsma E, Amon L, Birks H H, Birks H J B, Mortensen M F, Hoek W Z, Magyari E, Sobrino C M, Seppä H, Tinner W, Tonkov S, Veski S, Lotter A F, 2014. Validation of climate model-inferred regional temperature change for late-glacial Europe. Nature Communications 5, 4914. doi:10.1038/ncomms5914

Hoek W Z, Yu Z C, Lowe J J, 2008. INTegration of Ice-core, MArine, and TErrestrial records (INTIMATE): refining the record of the Last Glacial–Interglacial Transition. Quaternary Science Reviews 27, 1–5.

Huang Y, Shuman B, Wang Y, Webb T, 2004. Hydrogen isotope ratios of individual lipids in lake sediments as novel tracers of climatic and environmental change: a surface sediment test. Journal of Paleolimnology 31, 363–375.

Hughes A L C, Gyllencreutz R, Lohne S Ø, Mangerud J, Svendsen J I, 2016. The last Eurasian ice sheets – a chronological database and time-slice reconstruction, DATED-1. Boreas 45, 1–45.

Håkansson S, 1984. University of Lund Radiocarbon Dates XVII. Radiocarbon 26, 392–411.

Ionita M, Tallaksen L M, Kingston D G, Stagge J H, Laaha G, Van Lanen H A J, Scholz P, Chelcea S M, Haslinger K, 2017. The European 2015 drought from a climatological perspective. Hydrology and Earth System Sciences 21, 1397–1419.

Isarin R F B, Bohncke S J P, 1999. Mean July temperatures during the Younger Dryas in north-western and central Europe as inferred from climate indicator plant species. Quaternary Research 51, 158–173.

Ivanovic R F, Gregoire L J, Kageyama M, Roche D M, Valdes P J, Burke A, Drummond R, Peltier W R, Tarasov L, 2016. Transient climate simulations of the deglaciation 21–9 thousand years before present (version 1) – PMIP4 Core experiment design and boundary conditions. Geoscientific Model Development 9, 2563–2587.

Joos F, Spahni R, 2008. Rates of change in natural and anthropogenic radiative forcing over the past 20,000 years. Proceedings of the National Academy of Sciences 105, 1425–1430.

Juggins S, 2007. C2 Version 1.5: Software for ecological and palaeoecological data analysis and visualisation. Newcastle upon Tyne: University of Newcastle.

Juggins S, 2013. Quantitative reconstructions in palaeolimnology: new paradigm or sick science? Quaternary Science Reviews 64, 20–32.

Karlatou-Charalampopoulou A, 2016. Vegetation responses to Late Glacial climate shifts as reflected in a high-resolution pollen record from Blekinge, south-eastern Sweden, compared with responses of proxies. PhD thesis. Geological Institute, Lund University, Sweden.

Kylander M E, Klaminder J, Wohlfarth B, Löwemark L, 2013. Geochemical responses to paleoclimatic changes in southern Sweden since the late glacial: the Hässeldala Port lake sediment record. Journal of Paleolimnology 50, 57–70.

Lambert F, Kug J-S, Park R J, Mahowald N, Winckler G, Abe-Ouchi A, O'ishi R, Takemura T, Lee J-H, 2013. The role of mineral-dust aerosols in polar temperature amplification. Nature Climate Change 3, 487–491.

Lane C S, Brauer A, Blockley S P E, Dulski P, 2013. Volcanic ash reveals time-transgressive abrupt climate change during the Younger Dryas. Geology 41, 1251–1254.

Liedberg Jönsson B, 1988. The Late Weichselian macrofossil flora in western Skåne, southern Sweden. PhD thesis. Lund University, Sweden.

Liu Z, Otto-Bliesner B L, He F, Brady E C, Tomas R, Clark P U, Carlson A E, Lynch-Stieglitz J, Curry W, Brook E J, Erickson D, Jacob R, Kutzbach J, Cheng J, 2009. Transient simulation of last deglaciation with a new mechanism for Bølling–Allerød warming. Science 325, 310–314.

Liu Z, Carlson A E, He F, Brady E C, Otto-Bliesner B L, Briegleb B P, Wehrenberg M, Clark P U, Wu S, Cheng J, Zhang J, Noone D, Zhu J, 2012. Younger Dryas cooling and the Greenland climate response to CO_2. Proceedings of the National Academy of Sciences 109, 11101–11104.

Lowe J J, Ammann B, Birks H H, Björck S, Coope G R, Cwynar L, de Beaulieu J-L, Mott R J, Peteet D M, Walker M J C, 1994. Climatic changes in areas adjacent to the North Atlantic during the last glacial–interglacial transition (14–9 ka BP): a contribution to IGCP-253. Journal of Quaternary Science 9, 185–198.

Lowe J J, Rasmussen S O, Björck S, Hoek W Z, Steffensen J P, Walker M J C, Yu Z, the INTIMATE group, 2008. Synchronisation of palaeoenvironmental events in the North Atlantic region during the Last Termination: a revised protocol recommended by the INTIMATE group. Quaternary Science Reviews 27, 6–17.

Luoto T P, Nevalainen L, 2013. Long-term water temperature reconstructions from mountain lakes with different catchment and morphometric features. Scientific Reports 3, 2488. doi:10.1038/srep02488

Luoto T P, Rantala M V, Galkin A, Rautio M, Nevalainen L, 2016. Environmental determinants of chironomid communities in remote northern lakes across the treeline – Implications for climate change assessments. Ecological Indicators 61, 991–999.

Mangerud J, Andersen S T, Berglund B E, Donner J J, 1974. Quaternary stratigraphy of Norden, a proposal for terminology and classification. Boreas 3, 109–128.

McManus J F, Francois R, Gherardi J-M, Keigwin L D, Brown-Leger S, 2004. Collapse and rapid resumption of Atlantic meridional circulation linked to deglacial climate changes. Nature 428, 834–837.

Menviel L, Timmermann A, Elison Timm O, Mouchet A, 2011. Deconstructing the Last Glacial termination: the role of millennial and orbital-scale forcings. Quaternary Science Reviews 30, 1155–1172.

Moreno A, Svensson A, Brooks S J, Connor S, Engels S, Fletcher W J, Genty D, Heiri O, Labuhn I, Perşoiu A, Peyron O, Sadori L, Valero-Garcés B, Wulf S, Zanchetta G, data contributors, 2014. A compilation of Western European terrestrial records 6–8 ka BP: towards an understanding of latitudinal climatic gradients. Quaternary Science Reviews 106, 167–185.

Morill C, LeGrande A N, Renssen H, Bakker P, Otto-Bliesner B L, 2012. Model sensitivity to North Atlantic freshwater forcing at 8.2 ka. Climate of the Past 9, 955–968.

Muschitiello F, 2016. Deglacial impact of the Scandinavian Ice Sheet on the North Atlantic climate system. PhD thesis. Department of Geological Sciences, Stockholm University.

Muschitiello F, Wohlfarth B, 2015. Time-transgressive environmental shifts across Northern Europe at the onset of the Younger Dryas. Quaternary Science Reviews 109, 49–56.

Muschitiello F, Andersson A, Wohlfarth B, Smittenberg R H, 2015a. The C_{20} highly branched isoprenoid biomarker – A new diatom–sourced proxy for summer trophic conditions? Organic Geochemistry 81, 27–33.

Muschitiello F, Pausata F S R, Smittenberg R H, Salih A A M, Watson J E, Brooks S J, Whitehouse N J, Karlatou-Charalampopoulou A, Wohlfarth B, 2015b. Fennoscandian freshwater control on Greenland hydrological shifts at the onset of the Younger Dryas. Nature Communications 6, 8939. doi:10.1038/ncomms9939

Myhre G, Highwood E J, Shine K P, Stordal F, 1998. New estimates of radiative forcing due to well mixed greenhouse gases. Geophysical Research Letters 25, 2715–2718.

Oster J L, Ibarra D E, Winnick M J, Maher K, 2015. Steering of westerly storms over western North America at the Last Glacial Maximum. Nature Geoscience 8, 201–205.

Plikk A, 2018. The Eemian Interglacial at Sokli, northern Finland. PhD thesis. Department of Physical Geography, Stockholm University.

Rach O, Brauer A, Wilkes H, Sachse D, 2014. Delayed hydrological response to Greenland cooling at the onset of the Younger Dryas in western Europe. Nature Geoscience 7, 109–112.

Rach O, Kahmen A, Brauer A, Sachse D, 2017. A dual-biomarker approach for quantification of changes in relative humidity from sedimentary lipid *D/H* ratios. Climate of the Past 13, 741–757.

Rahmstorf S, 1995. Bifurcations of the Atlantic thermohaline circulation in response to changes in the hydrological cycle. Nature 378, 145–149.

Ramaswamy V, Boucher O, Haigh J, Hauglustaine D, Haywood J, Myhre G, Nakajima T, Shi G Y, Solomon S, 2001. Radiative forcing of climate change. In Houghton J T, Ding Y, Griggs D J, Noguer M, van der Linden P J, Dai X, Maskell K, Johnson C A (eds). Climate change 2001: the scientific basis: contribution of Working Group I to the third assessment report of the Intergovernmental Panel on Climate Change. New York: Cambridge University Press, 349–416.

Rasmussen S O, Bigler M, Blockley S P E, Blunier T, Buchardt S L, Clausen H B, Cvijanovic I, Dahl-Jensen D, Johnsen S J, Fischer H, Gkinis V, Guillevic M, Hoek W Z, Lowe J J, Pedro J, Popp T, Seierstad I K, Steffensen J P, Svensson A M, Vallelonga P, Vinther B M, Walker M J C, Wheatley J J, Winstrup M, 2014a. A stratigraphic framework for robust naming and correlation of abrupt climatic changes during the last glacial period based on three synchronized Greenland ice core records. Quaternary Science Reviews 106, 14–28.

Rasmussen S O, Birks H H, Blockley S P E, Brauer A, Hajdas I, Hoek W Z, Lowe J J, Moreno A, Renssen H, Roche D M, Svensson A M, Walker M J C, 2014b. Dating, synthesis, and interpretation of palaeoclimatic records of the Last Glacial cycle and model-data integration: advances by the INTIMATE (INTegration of Ice-core, MArine and TErrestrial records) COST Action ES0907. Quaternary Science Reviews 106, 1–13.

Reimer P J, Bard E, Bayliss A, Warren Beck J W, Blackwell P G, Bronk Ramsey C, Buck C E, Cheng H, Edwards R L, Friedrich M, Grootes P M, Haflidason H, Hajdas I, Hatté C, Heaton T J, Hoffmann D L, Hogg A G, Hughen K A, Kaiser K F, Kromer B, Manning S W, Niu M, Reimer R W, Richards D A, Scott E M, Southon J R, Staff R A, Turney C S M, van der Plicht J, 2013. IntCal13 and Marine13 radiocarbon age calibration curves 0–50,000 years cal BP. Radiocarbon 55, 1869–1887.

Renssen H, van Geel B, van der Plicht J, Magny M, 2000. Reduced solar activity as a trigger for the start of the Younger Dryas? Quaternary International 68–71, 373–383.

Renssen H, Mairesse A, Goosse H, Mathiot P, Heiri O, Roche D M, Nisancioglu K H, Valdes P, 2015. Multiple causes of the Younger Dryas cold period. Nature Geoscience 8, 946–949.

Sachse D, Radke J, Gleixner G, 2004. Hydrogen isotope ratios of recent lacustrine sedimentary *n*-alkanes record modern climate variability. Geochimica et Cosmochimica Acta 68, 4877–4889.

Sachse D, Radke J, Gleixner G, 2006. δD values of individual *n*-alkanes from terrestrial plants along a climatic gradient – Implications for the sedimentary biomarker record. Organic Geochemistry 37, 469–483.

Sachse D, Billault I, Bowen G J, Chikaraishi Y, Dawson T E, Feakins S J, Freeman K H, Magill C R, McInerney F, van der Meer M T J, Polissar P, Robins R J, Sachs J P, Schmidt H-L, Sessions A L, White J W C, West J B, Kahmen A, 2012. Molecular paleohydrology: interpreting the hydrogen-isotopic composition of lipid biomarkers from photosynthesizing organisms. Annual Review of Earth and Planetary Sciences 40, 221–249.

Sandgren P, Snowball I, 2001. The Late Weichselian sea level history of the Kullen Peninsula in northwest Skåne, southern Sweden. Boreas 30, 115–130.

Scaife A A, Woollings T, Knight J, Martin G, Hinton T, 2010. Atmospheric blocking and mean biases in climate models. Journal of Climate 23, 6143–6152.

Schenk F, Väliranta M, Muschitiello F, Tarasov L, Heikkilä M, Björck S, Brandefelt J, Johannson A, Näslund J-O, Wohlfarth B, 2018. Warm summers during the Younger Dryas cold reversal. Nature Communications 9, 1634. doi:10.1038/s41467-018-04071-5

Steffensen J P, Andersen K A, Bigler M, Clausen H B, Dahl-Jensen D, Fischer H, Goto-Azuma K, Hansson M, Johnsen S J, Jouzel J, Masson-Delmotte V, Popp T, Rasmussen S O, Röthlisberger R, Ruth U, Stauffer B, Siggaard-Andersen M L, Sveinbjörnsdóttir A E, Svensson A, White J W C, 2008. High-resolution Greenland ice core data show abrupt climate change happens in few years. Science 321, 680–684.

Steinthorsdottir M, Wohlfarth B, Kylander M, Blaauw M, Reimer P J, 2013. Stomatal proxy record of CO_2 concentrations from the last termination suggests an important role for CO_2 at climate change transitions. Quaternary Science Reviews 68, 43–58.

Steinthorsdottir M, de Boer A M, Oliver K I C, Muschitiello F, Blaauw M, Reimer P J, Wohlfarth B, 2014. Synchronous records of pCO_2 and $\Delta^{14}C$ suggest rapid, ocean-derived pCO_2 fluctuations at the onset of Younger Dryas. Quaternary Science Reviews 99, 84–96.

Stocker T F, Wright D G, 1991. Rapid transitions of the ocean's deep circulation induced by changes in surface water fluxes. Nature 351, 729–732.

Stouffer R J, Yin J, Gregory J M, Dixon K W, Spelman M J, Hurlin W, Weaver A J, Eby M, Flato G M, Hasumi H, Hu A, Jungclaus J H, Kamenkovich I V, Levermann A, Montoya M, Murakami S, Nawrath S, Oka A, Peltier W R, Robitaille D Y, Sokolov A, Vettoretti G, Weber S L, 2006. Investigating the causes of the response of the thermohaline circulation to past and future climate changes. Journal of Climate 19, 1365–1387.

Tarasov L, Peltier R W, 2002. Greenland glacial history and local geodynamic consequences. Geophysical Journal International 150, 198–229.

Tarasov L, Dyke A S, Neal R M, Peltier W R, 2012. A data-calibrated distribution of deglacial chronologies for the North American ice complex from glaciological modelling. Earth and Planetary Science Letters 315–316, 30–40.

Theuerkauf M, Joosten H, 2012. Younger Dryas cold stage vegetation patterns of central Europe – climate, soil and relief controls. Boreas 41, 391–407.

Veres D-S, 2001. A comparative study between loss on ignition and total carbon analysis on Late Glacial sediments from Atteköps mosse, southwestern Sweden, and their tentative correlation with the GRIP event stratigraphy. MSc thesis. Department of Geology, Lund University, Sweden.

Veski S, Seppä H, Stančikaite M, Zernitskaya V, Reitalu T, Gryguc G, Heinsalu A, Stivrins N, Amon L, Vassiljev J, Heiri O, 2015. Quantitative summer and winter temperature reconstructions from pollen and chironomid data between 15 and 8 ka BP in the Baltic–Belarus area. Quaternary International 388, 4–11.

Väliranta M, Salonen J S, Heikkilä M, Amon L, Helmens K F, Klimaschewski A, Kuhry P, Kultti S, Poska A, Shala S, Veski S, Birks H H, 2015. Plant macrofossil evidence for an early onset of the Holocene summer thermal maximum in northern Europe. Nature Communications 6, 6809. doi:10.1038/ncomms7809

Wary M, Eynaud F, Swingedouw D, Masson-Delmotte V, Matthiessen J, Kissel C, Zumaque J, Rossignol L, Jouzel J, 2017. Regional seesaw between the North Atlantic and Nordic Seas during the last glacial abrupt climate events. Climate of the Past 13, 729–739.

Watson J, 2008. Quantifying Late Glacial climate change in Northwestern Europe using two insect proxies. PhD thesis. School of Geography, Archaeology and Palaeoecology, The Queen's University of Belfast.

Weaver A J, Saenko O A, Clark P U, Mitrovica J X, 2003. Meltwater pulse 1A from Antarctica as a trigger of the Bølling–Allerød warm interval. Science 299, 1709–1713.

Wohlfarth B, 1996. The chronology of the Last Termination: a review of high-resolution terrestrial stratigraphies. Quaternary Science Reviews 15, 267–284.

Wohlfarth B, Björck S, Lemdahl G, Ising J, 1994. Ice recession and depositional environment in the Blekinge archipelago of the Baltic Ice Lake. GFF 116, 3–12.

Wohlfarth B, Blaauw M, Davies S M, Andersson M, Wastegård S, Hormes A, Possnert G, 2006. Constraining the age of Lateglacial and early Holocene pollen zones and tephra horizons in southern Sweden with Bayesian probability methods. Journal of Quaternary Science 21, 321–334.

Wohlfarth B, Muschitiello F, Greenwood S L, Andersson A, Kylander M, Smittenberg R H, Steinthorsdottir M, Watson J, Whitehouse N J, 2017. Hässeldala – a key site for Last Termination climate events in northern Europe. Boreas 46, 143–161.

Wohlfarth B, Luoto T, Muschitiello F, Väliranta M, Björck S, Davies S M, Kylander M, Ljung K, Reimer P J, Smittenberg R H, 2018. Climate and environment in southwest Sweden 15.5–11.3 cal. ka BP. Boreas 47, 687–710.

Wunsch C, 2006. Abrupt climate change: an alternate view. Quaternary Research 65, 191–203.

Zhang X, Lohmann G, Knorr G, Purcell C, 2014. Abrupt glacial climate shifts controlled by ice sheet changes. Nature 512, 290–294.

Zhu J, Liu Z, Zhang X, Eisenman I, Liu W, 2014. Linear weakening of the AMOC in response to receding glacial ice sheets in CCSM3. Geophysical Research Letters 41, 6252–6258.

Appendix 1

A1.1 Geographical site description and temperatures for BA, YD and ΔT

Coordinates are given as decimals of °N (Lat,) and °E (Lon.); altitude in [m] above modern sea-level. Proxy group 1 consists of type F (flies = chironomids), WF (water flees, cladocera), and B (beetles, coleoptera). Group 2 includes type M (plant macrofossils) and P (aquatic pollen). The classification for BA and YD distinguishes a = aquatic, e = emergent and t = terrestrial. Temperatures are given in °C rounded to the first decimal. The temperature difference ΔT = YD minus BA. See A1.2 for the plant indicator species used. References for each site are given in A1.3 and the full reference list is given in A1.4. The data compilation has been published as supplementary data of Schenk et al. (2018).

Site name	Country	LAT	LON	ALT	type	class	T BA	T YD	ΔT
Abernethy Forest	UK	57.14	−3.72	221	F	a; a	12.1	8.3	−3.8
Cunswick Tarn	UK	54.20	−2.47	135	F	a; a	12.6	8.3	−4.3
Ech paleolake	France	43.04	−0.05	710	F	a; a	16.4	15.4	−0.9
Egelsee	Switzerland	47.11	8.35	770	F	a; a	14.7	13.8	−0.9
Fiddaun Lough	Ireland	53.02	−8.87	30	F	a; a	13.4	9.7	−3.8
Foppe	Switzerland	46.27	8.47	1470	F	a; a	12.0	12.5	0.5
Gerzensee	Switzerland	46.50	7.33	603	WF	a; a	11.9	9.7	−2.2
Gransmoor	UK	54.05	−0.18	8	F	a; a	13.7	10.3	−3.4
Hässeldala Port	Sweden	56.16	15.03	60	F	a; a	10.7	9.8	−0.9
Hawes Water	UK	54.11	−2.48	8	F	a; a	12.0	9.3	−2.7
Jansvatnet	Norway	70.65	23.67	53	F	a; a	5.8	5.8	0.0
Krakenes	Norway	62.02	5.00	38	F	a; a	9.3	7.9	−1.4
Kurjanovas	Latvia	56.52	27.98	111	F	a; a	13.1	11.3	−1.8
Lago di Lavarone	Italy	45.56	11.15	1100	F	a; a	14.2	13.8	−0.4
Lago Piccolo di Avigliana	Italy	45.03	7.23	365	F	a; a	17.9	16.6	−1.4
Laguna de la Roya	Spain	42.13	−6.79	1608	F	a; a	11.8	10.7	−1.1
Lake Brazi	Romania	45.23	22.54	1740	F	a; a	8.1	8.3	0.2
Lake Hijkermeer	Netherlands	52.53	6.29	14	F	a; a	16.0	13.8	−2.2
Lake Lautrey	France	46.35	5.51	788	F	a; a	16.6	14.8	−1.8
Lake Madjärn	Sweden	58.35	12.10	135	B	t; t	9.3	7.8	−1.5
Lake Mjällsjön	Sweden	57.00	12.35	72	B	t; t		9.8	
Lake Myklevatnet	Norway	61.55	5.13	123	F	a; a	10.3	9.0	−1.3
Lake Torreberga	Sweden	55.37	13.14	7	B	t; t		10.5	
Little Hawes Water	UK	54.11	−2.47	9	F	a; a	11.8	9.6	−2.2
Llanilid	UK	51.52	−3.45	60	B	t; t	15.0	12.0	−3.0
Loch Ashik	UK	57.23	−5.82	50	F	a; a	10.8	6.9	−3.9
Lough Nadourcan	Ireland	55.30	−7.54	70	F	a; a	12.0	9.2	−2.8
Lusvatnet	Norway	69.07	15.57	30	F	a; a	7.4	8.0	0.6
Maloja Riegel	Switzerland	46.24	9.41	1865	F	a; a	9.5	9.5	0.0
Nakri	Estonia	57.90	26.27	49	F	a; a	12.5	11.0	−1.5
Sunbiggin Tarn	UK	54.27	−2.30	250	F	a; a	11.7	8.4	−3.3
Urswick Tarn	UK	54.09	−3.07	33	F	a; a	12.7	8.8	−3.9
Usselo	Netherlands	52.12	6.49	29	B	t; t	16.1		
Whitrig Bog	UK	55.36	−2.36	125	F	a; a	10.7	8.5	−2.2
Abernethy Forest	UK	57.14	−3.72	221	M	t; t	10.0	10.0	0.0
Alinlampi	Finland	64.40	34.37	104	M	−; a		16.5	
Balupiany	Poland	54.32	22.22	153	M	−; t		14.5	
Bevardis	Lithuania	55.18	25.73	167	P	−; a		13.1	
Bled	Slovenia	46.37	14.10	475	M	a; −	11.9		
Bleekemeer	Netherlands	52.23	5.75	20	M	t; −	10.0		
Borchert	Netherlands	52.37	7.00	65	M	−; e		15.7	
Brackloon Lough	Ireland	53.76	−9.57	100	P	−; a		16.1	
Brekka	Norway	61.97	6.00	410	M	−; a		11.4	
Černé Lake	Czech Republic	49.18	13.18	1028	P	a/e	10.0	10.0	0.0
Charco da Candieira	Portugal	40.34	−7.58	1409	P	a; a	11.7	11.7	0.0
Creno Lake	France	42.20	8.95	1310	P	a; a	16.1	16.1	0.0

Site name	Country	LAT	LON	ALT	type	class	T BA	T YD	ΔT
Drymen	UK	57.48	−6.32	220	M	a; −	13.5		
Ezero	Bulgaria	42.72	26.93	120	M	e; −	15.7		
Gammelmose	Denmark	56.15	9.88	30	M	−; e		8.0	
Gerzensee	Switzerland	46.50	7.33	603	M	e; t	14.3	12.2	−2.1
Gutaiului Mountains	Romania	47.82	23.53	730	M	t; t	13.5	15.7	2.2
Haljala	Estonia	59.42	26.28	67	P	a; −	13.1		
Jansvatnet	Norway	70.65	23.67	53	M	−; e		8.0	
Juodonys	Lithuania	55.74	25.44	92	M	−; t		12.5	
Kasuciai	Lithuania	55.99	21.31	35	P	−; e		15.7	
Kojle−Perty	Poland	54.27	22.88	150	M	a; a	13.5	15.2	1.8
Körlättamossen	Sweden	56.10	13.07	118	M	a; e	14.0	14.3	0.3
Krakenes	Norway	62.02	5.00	38	P	a; a	11.7	11.7	0.0
Kupena	Bulgaria	41.98	24.33	1300	P	−; a		13.8	
Kurjanovas	Latvia	56.52	27.98	111	P	a; e	12.1	15.7	3.6
Lago de Ajo	Spain	43.05	−6.15	1570	P	−; a		16.1	
Lago Grande di Monticchio	Italy	40.94	15.61	656	M	t; −	16.0		
Lagoa de Lucenza	Spain	43.58	−7.12	1375	P	e; e	14.3	14.3	0.0
Laguna de La Roya	Spain	42.13	−6.79	1608	P	e; e	14.3	14.3	0.0
Lake Estanya	Spain	42.03	−0.53	670	P	a; e	11.7	15.7	4.0
Lake Fehér	Hungary	46.33	20.10	87	P	a; −	11.7		
Lake Fiddau	Ireland	53.02	−8.87	30	P	a; −	13.8		
Lake Łukie	Poland	51.40	23.08	163	P	a; a	13.5	12.2	−1.3
Lake St Anne	Romania	46.13	25.89	946	P	e; −	15.7		
Lake Švarcenberk	Czech Republic	49.15	14.71	412	M	e; e	15.7	15.7	0.0
Lerstadvatn	Norway	62.47	6.30	44	M	−; a		11.7	
Liastemmen	Norway	59.10	5.14	72	P	a; a	16.0	16.1	0.1
Lielais Svetinu	Latvia	56.76	27.13	96	M	t; t	12.2	12.2	0.0
Lielais Svetinu	Latvia	56.75	27.13	96	M	t; t	12.2	13.5	1.3
Lielais Svetinu	Latvia	56.75	27.13	96	M	a; t	14.4	13.5	−0.9
Llanilid	UK	51.52	−3.45	60	M	a; a	13.5	13.5	0.0
Llet−ti	Russia	66.52	59.30	50	M	−; e		15.7	
Loch Kinord	UK	57.18	−2.30	175	M	a; −	16.8		
Lusvatnet	Norway	69.07	15.57	30	M	−; t		10.0	
Madtjärn	Sweden	58.63	12.33	135	M	a; a	13.5	13.5	0.0
Mark Valley	Netherlands	51.53	4.78	15	M	e; e	15.7	15.7	0.0
Meerfelder Maar	Germany	50.10	6.88	337	P	e; e	15.7	15.7	0.0
Mekelermeer	Netherlands	52.23	5.75	20	M	a; −	15.7		
Milheeze	Netherlands	51.50	5.77	27	M	e; −	15.7		
Mjällsjön	Sweden	57.01	12.59	72	M	−; a		12.2	
N Wetterau	Germany	50.27	8.73	500	P	−; e		15.7	
Nakri	Estonia	57.90	26.27	49	M	−; a		11.7	
Navarrés 3	Spain	39.10	−0.68	225	P	e; e	15.7	15.7	0.0
Nero	Russia	57.17	39.42	93	M	a; −	14.0		
Palughetto	Italy	46.10	12.37	200	P	e; e	15.7	15.7	0.0
Pamerkiai	Lithuania	54.31	24.73	114	M	e; e	15.7	15.7	0.0
Pesce Luna	Italy	41.78	12.23	1	M	−; e		15.7	
Petrasiunai	Lithuania	55.85	25.70	107	P	−; e		15.7	
Pichozero	Russia	61.78	37.42	118	M	−; t		10.0	
Polabi	Czech Republic	50.25	14.58	300	P	−; e		15.7	
Popradské Lake	Slovakia	49.08	20.07	1513	P	a; a	11.7	11.7	0.0
Pozo do Carballal	Spain	42.71	−7.11	1330	P	e; a	14.3	11.7	−2.6
Pudozh	Russia	61.80	36.47	40	M	−; t		10.0	
Rieme 126	Belgium	51.17	3.78	15	M	e; −	15.7		
Rieme 143	Belgium	51.17	3.78	15	P	e; −	15.7		
Saham Mere	UK	52.58	0.81	38	P	a; a	13.5	11.7	−1.8
Sanbaria March	Spain	42.10	−6.73	1050	M	−; a		12.9	
Sea Mere	UK	52.57	1.00	38	P	a; a	12.2	13.5	1.3
Siles lake	Spain	38.40	−2.50	1320	P	a; a	11.7	11.7	0.0

Site name	Country	LAT	LON	ALT	type	class	T BA	T YD	ΔT
Site I	Poland	54.27	22.89	200	M	a; a	13.5	11.7	−1.8
Site II	Poland	54.22	22.84	200	M	a; a	13.5	11.7	−1.8
Slotseng	Denmark	55.32	9.27	40	P	a; a	13.8	13.8	0.0
Sluggan bog	UK	54.10	−6.30	40	M	t; −	10.0		
St. Ursin	France	48.52	0.25	280	P	e; −	15.7		
Steregoiu	Romania	47.81	23.54	790	P	a; a	13.5	11.7	−1.8
Straldzha mire	Bulgaria	42.63	26.77	137	P	e; e	15.7	15.7	0.0
Svartevatnet	Norway	62.40	5.93	370	M	−; a		11.4	
Tambichozero	Russia	61.93	37.90	122	M	t; e	10.0	8.0	−2.0
Tarnogrod plateau	Poland	50.00	23.12	215	M	a; a	14.1	14.1	0.0
Timan ridge	Russia	67.40	48.43	170	P	−; e		15.7	
Torreberga I	Sweden	55.62	13.24	100	P	−; a		13.9	
Turbuta	Romania	47.37	23.50	275	P	−; a		13.6	
Uddelermeer	Netherlands	52.23	5.75	20	M	a; a	14.2	14.2	0.0
Udriku	Estonia	59.37	25.93	95	M	a; −	13.5		
Valle di Castiglione	Italy	41.89	12.76	44	P	e; e	15.7	15.7	0.0
Villarquemado	Spain	40.50	−1.30	1 000	P	a; a	11.7	11.7	0.0
Wolin Island	Poland	54.00	14.63	4	P	e; e	15.7	15.7	0.0

A1.2 Plant taxon or species used for local temperature estimates

See A1.3 for references of the used data sources.

Site name	Taxon or species for BA	Taxon or species for YD
Abernethy Forest	Birch	Birch seed
Alinlampi		Najas flexilis
Balupiany		Alnus glutinosa seed
Bevardis		Nuphar
Bled	Callitriche sp.	
Bleekemeer	Birch	
Borchert		Typha
Brackloon Lough		Littorella
Brekka		Subularia aquatica
Černé Lake	Sparganium/Typha angustifolium	Sparganium/Typha angustifolium
Charco da Candieira	Potmogeton sp.	Potamogeton sp.
Creno Lake	Littorella	Littorella
Drymen	Nymphaea sp.	
Ezero	Typha	
Gammelmose		Menyanthes trifoliata
Gerzensee	Lythrum salicaria	Pinus sylvestris seed
Gutaiului Mountains	Picea	Campanula latifolia
Haljala	Nuphar	
Jansvatnet		Comarum palustre
Juodonys		Trifolium repens
Kasuciai		Typha
Kojle-Perty	Potmogeton filiformis	Najas marina
Körlättamossen	Potamogeton praelongus	Alisma plantago-aquatica
Krakenes	Potamogeton sp.	Potamogeton sp.
Kupena		Lemna
Kurjanovas	Myriophyllum spicatum	Typha
Lago de Ajo		Littorella
Lago Grande di Monticchio	Tilia	
Lagoa de Lucenza	Alisma plantago-aquatica	Alisma plantago-aquatica
Laguna de La Roya	Alisma plantago-aquatica	Alisma plantago-aquatica
Lake Estanya	Potamogeton sp.	Typha
Lake Fehér	Potamogeton sp.	

Site name	Taxon or species for BA	Taxon or species for YD
Lake Fiddau	Myriophyllum verticillatum	
Lake Łukie	Nymphaea	Myriophyllum spicatum
Lake St Anne	Typha	
Lake Švarcenberk	Typha	Typha
Lerstadvatn		Potamogeton sp.
Liastemmen	Cladium mariscus	Littorella
Lielais Svetinu	Pinus sylvestris	Pinus sylvestris needle
Lielais Svetinu	Pinus sylvestris	Picea abies needle
Lielais Svetinu	Zannichellia palustris	Picea abies needle
Llanilid	Nymphaea alba	Nymphaea alba
Llet-ti		Typha
Loch Kinord	Najas flexilis	
Lusvatnet		Tree birch seed
Madtjärn	Potamogeton filiformis	Potamogeton filiformis
Mark Valley	Typha	Typha
Meerfelder Maar	Typha	Typha
Mekelermeer	Elatine hexandra	
Milheeze	Typha	
Mjällsjön		Potamogeton pusillus (berchtoldii)
N Wetterau		Typha latifolia
Nakri		Potamogeton sp.
Navarrés 3	Typha	Typha
Nero	Callitriche hermaphroditica	
Palughetto	Typha	Typha
Pamerkiai	Typha	Typha
Pesce Luna		Typha
Petrasiunai		Typha
Pichozero		Cristatella
Polabi		Typha
Popradské Lake (Pleso)	Potamogeton sp.	Potamogeton sp.
Pozo do Carballal	Alisma plantago-aquatica	Potamogeton sp.
Pudozh		Alnus incana seed
Rieme 126	Typha	
Rieme 143	Typha	
Saham Mere	Nymphaea	Potamogeton sp.
Sanbaria March		Potamogeton natans
Sea Mere	Myriophyllum spicatum	Nymphaea
Siles lake	Potamogeton sp.	Potamogeton sp.
Site I	Potamogeton filiformis	Potamogeton sp.
Site II	Potamogeton filiformis	Potamogeton sp.
Slotseng	Myriophyllum verticillatum	Myriophyllum verticillatum
Sluggan bog	Birch	
St. Ursin	Typha	
Steregoiu	Nymphaea	Potamogeton sp.
Straldzha mire	Typha latifolia type	Typha latifolia type
Svartevatnet		Subullaria aquatica
Tambichozero	Birch	Menyanthes trifoliata
Tarnogrod plateau	Ceratophyllum	Ceratophyllum
Timan ridge		Typha
Torreberga I		Myriophyllum verticillatum
Turbuta		Lemna
Uddelermeer	Elatine hexandra	Elatine hexandra
Udriku	Potamogeton filiformis	
Valle di Castiglione	Typha	Typha
Villarquemado	Potamogeton sp.	Potamogeton sp.
Wolin Island	Typha	Typha

A1.3 References to the original data sources

The full references are listed at the end as appendix data references.

Site name	Group	References
Abernethy Forest	Group 1	Matthews et al. 2011, Brooks et al. 2012
Cunswick Tarn	Group 1	Lang et al. 2010
Ech paleolake	Group 1	Millet et al. 2012
Egelsee	Group 1	Wehrli et al. 2007, Laroque-Tobler et al. 2010
Fiddaun Lough	Group 1	van Ash and Hoek 2012
Foppe	Group 1	Samartin et al. 2012
Gerzensee	Group 1	Lotter et al. 2000, 2012
Gransmoor	Group 1	Walker et al. 1993, Lowe et al. 1995
Hässeldala Port	Group 1	Muschitiello and Wohlfarth 2015
Hawes Water	Group 1	Jones et al. 2002, Bedford et al. 2004, Lang et al. 2010
Jansvatnet	Group 1	Birks et al. 2012
Krakenes	Group 1	Birks et al. 1996
Kurjanovas	Group 1	Veski et al. 2015
Lago di Lavarone	Group 1	Filippi et al. 2007, Heiri et al. 2007
Lago Piccolo di Avigliana	Group 1	Finsinger and Tinner 2006, Laroque and Finsinger 2008
Laguna de la Roya	Group 1	Allen et al. 1996, Muñoz Sobrino et al. 2013
Lake Brazi	Group 1	Tóth et al. 2012
Lake Hijkermeer	Group 1	Heiri et al. 2007
Lake Lautrey	Group 1	Heiri and Millet 2005, Peyron et al. 2005, Magny et al. 2006
Lake Madjärn	Group 1	Björck et al. 1996
Lake Mjällsjön	Group 1	Björck et al. 1996
Lake Myklevatnet	Group 1	Nesje et al. 2014
Lake Torreberga	Group 1	Björck et al. 1996
Little Hawes Water	Group 1	Lang et al. 2010
Llanilid	Group 1	Walker and Harkness 1990, Turney 1999, Walker et al. 2003
Loch Ashik	Group 1	Walker and Lowe 1990, Lowe and Walker 1991, Brooks et al. 2012
Lough Nadourcan	Group 1	Turney et al. 2006, Watson et al. 2010
Lusvatnet	Group 1	Aarnes et al. 2012, Birks et al. 2014
Maloja Riegel	Group 1	Ilyashuk et al. 2009
Nakri	Group 1	Veski et al. 2015
Sunbiggin Tarn	Group 1	Lang et al. 2010
Urswick Tarn	Group 1	Lang et al. 2010
Usselo	Group 1	Van Geel et al. 1989
Whitrig Bog	Group 1	Mayle et al. 1997, 1999, Brooks and Birks 2000
Abernethy Forest	Group 2	Birks 2003
Alinlampi	Group 2	Vasari et al. 2007
Balupiany	Group 2	Karpińska-Kołaczek et al. 2013
Bevardis	Group 2	Gaidamavičius et al. 2011
Bled	Group 2	Andrič et al. 2009
Bleekemeer	Group 2	Bohncke and Wijmstra 1988
Borchert	Group 2	Van Geel et al. 1980
Brackloon Lough	Group 2	von Engelbrechten et al. 2000
Brekka	Group 2	Birks and Van Dinter 2010
Černé Lake	Group 2	Vočadlová et al. 2015
Charco da Candieira	Group 2	van der Knaap and van Leeuwen 1997
Creno Lake	Group 2	Reille et al. 1997
Drymen	Group 2	Vasari and Vasari 1968
Ezero	Group 2	Magyari et al. 2013
Gammelmose	Group 2	Andresen et al. 2000
Gerzensee	Group 2	Tobolski and Ammann 2000
Gutaiului Mountains	Group 2	Feurdean and Bennike 2004, Feurdean et al. 2007
Haljala	Group 2	Saarse et al. 2009
Jansvatnet	Group 2	Birks et al. 2012
Juodonys	Group 2	Stančikaitė et al. 2009

Site name	Group	References
Kasuciai	Group 2	Seiriene et al. 2006
Kojle-Perty	Group 2	Gałka et al. 2014
Körlättamossen	Group 2	Hammarlund and Lemdahl 1994
Krakenes	Group 2	Birks 2000, Birks and Birks 2013, Väliranta et al. 2015
Kupena	Group 2	Huttunen et al. 1992
Kurjanovas	Group 2	Heikkilä et al. 2009
Lago de Ajo	Group 2	McKeever 1984, Allen et al. 1996
Lago Grande di Monticchio	Group 2	Huntley et al. 1999
Lagoa de Lucenza	Group 2	Muñoz Sobrino et al. 2001
Laguna de La Roya	Group 2	Muñoz Sobrino et al. 2013
Lake Estanya	Group 2	Vegas-Vilarrúbia et al. 2013
Lake Fehér	Group 2	Sümegi et al. 2013
Lake Fiddau	Group 2	van Asch and Hoek 2012
Lake Łukie	Group 2	Zawiska et al. 2015
Lake St Anne	Group 2	Magyari et al. 2014
Lake Švarcenberk	Group 2	Hošek et al. 2014
Lerstadvatn	Group 2	Birks and van Dinter 2010
Liastemmen	Group 2	Paus 1989
Lielais Svetinu	Group 2	Amon et al. 2014
Lielais Svetinu	Group 2	Amon et al. 2014
Lielais Svetinu	Group 2	Veski et al. 2012
Llanilid	Group 2	Walker et al. 2003
Llet-ti	Group 2	Väliranta et al. 2006
Loch Kinord	Group 2	Vasari and Vasari 1968
Lusvatnet	Group 2	Birks 2015
Madtjärn	Group 2	Björck et al. 1996
Mark Valley	Group 2	Vandenberghe and Bohncke 1985, Bohncke et al. 1987
Meerfelder Maar	Group 2	Engels et al. 2015
Mekelermeer	Group 2	Bohncke and Wijmstra 1988
Milheeze	Group 2	Bos et al. 2006
Mjällsjön	Group 2	Björck et al. 1996
N Wetterau	Group 2	Andresen et al. 2000
Nakri	Group 2	Amon et al. 2012
Navarrés 3	Group 2	Carrión and Van Geel 1999
Nero	Group 2	Wohlfarth et al. 2006
Palughetto	Group 2	Vescovi et al. 2007
Pamerkiai	Group 2	Stančikaitė et al. 2009
Pesce Luna	Group 2	Di Rita et al. 2013
Petrasiunai	Group 2	Stančikaitė et al. 2009
Pichozero	Group 2	Wohlfarth et al. 1999, 2002, 2004, 2007
Polabi	Group 2	Petr et al. 2014
Popradské Lake (Pleso)	Group 2	Rybníčková and Rybníček 2006
Pozo do Carballal	Group 2	Muñoz Sobrino et al. 1997
Pudozh	Group 2	Wohlfarth et al. 1999, 2002, 2004, 2007
Rieme 126	Group 2	Bos et al. 2013
Rieme 143	Group 2	Bos et al. 2013
Saham Mere	Group 2	Bennett 1988
Sanbaria March	Group 2	Turner and Hannon 1988
Sea Mere	Group 2	Hunt and Birks 1982
Siles lake	Group 2	Carrión 2002
Site I	Group 2	Gałka and Sznel 2013, Gałka et al. 2014
Site II	Group 2	Gałka and Sznel 2013, Gałka et al. 2014
Slotseng	Group 2	Mortensen et al. 2011
Sluggan bog	Group 2	Walker et al. 2012
St. Ursin	Group 2	Barbier and Visset 2003
Steregoiu	Group 2	Björkman et al. 2003
Straldzha mire	Group 2	Connor et al. 2013
Svartevatnet	Group 2	Birks and van Dinter 2010

Site name	Group	References
Tambichozero	Group 2	Wohlfarth et al. 1999, 2002, 2004, 2007
Tarnogrod plateau	Group 2	Kołaczek et al. 2015
Timan ridge	Group 2	Paus et al. 2003
Torreberga I	Group 2	Berglund and Digerfeldt 1970
Turbuta	Group 2	Feurdean et al. 2007
Uddelermeer	Group 2	Bohncke and Wijmstra 1988
Udriku	Group 2	Amon and Saarse 2010
Valle di Castiglione	Group 2	Di Rita et al. 2013
Villarquemado	Group 2	Aranbarri et al. 2014
Wolin Island	Group 2	Latałowa and Borówka 2006

A1.4 Full reference list to the original data sources

Aarnes I, Bjune A E, Birks H H, Balascio N L, Bakke J, Blaauw M, 2012. Vegetation responses to rapid climatic changes during the last deglaciation 13,500–8,000 years ago on southwest Andøya, arctic Norway. Vegetation History and Archaeobotany 21, 17–35.

Allen J R M, Huntley B, Watts W A, 1996. The vegetation and climate of northwest Iberia over the last 14,000 years. Journal of Quaternary Science 11, 125–147.

Amon L, Saarse L, 2010. Postglacial palaeoenvironmental changes in the area surrounding Lake Udriku in North Estonia. Geological Quarterly 51, 85–94.

Amon L, Veski S, Heinsalu A, Saarse L, 2012. Timing of Lateglacial vegetation dynamics and respective palaeoenvironmental conditions in southern Estonia: evidence from the sediment record of Lake Nakri. Journal of Quaternary Science 27, 169–180.

Amon L, Veski S, Vassiljev J, 2014. Tree taxa immigration to the eastern Baltic region, south-eastern sector of Scandinavian glaciation during the Late–glacial period (14,500–11,700 cal. B.P.). Vegetation History and Archaeobotany 23, 207–216.

Andresen C S, Björck S, Bennike O, Heinemeier J, Kromer B, 2000. What do $\Delta^{14}C$ changes across the Gerzensee oscillation/GI-1b event imply for deglacial oscillations? Journal of Quaternary Science 15, 203–214.

Andrič M, Massaferro J, Eicher U, Ammann B, Leuenberger M, Martinčič A, Marinova E, Brancelj A, 2009. A multi-proxy Late-glacial palaeoenvironmental record from Lake Bled, Slovenia. In Buczkó K, Korponai J, Padisák J, Starratt S (eds). Palaeolimnological proxies as tools of environmental reconstruction in fresh water. Dordrecht: Springer, 121–141.

Aranbarri J, González-Sampériz P, Valero-Garcés B, Moreno A, Gil-Romera G, Sevilla-Callejo M, García-Prieto E, Di Rita F, Mata M P, Morellón M, Magri D, Rodríguez-Lázaro J, Carrión J S, 2014. Rapid climatic changes and resilient vegetation during the Lateglacial and Holocene in a continental region of south-western Europe. Global and Planetary Change 114, 50–65.

Barbier D, Visset L, 2003. Pollen analysis of the Saint-Ursin peat bog (Mayenne, Massif armoricain, Northwest France): detection of late glacial and Holocene sequences. Revue d'Archéométrie 27, 55–66.

Bedford A, Jones R T, Lang B, Brooks S, Marshall J D, 2004. A Late-glacial chironomid record from Hawes Water, northwest England. Journal of Quaternary Science 19, 281–290.

Bennett K D, 1988. Holocene pollen stratigraphy of central East Anglia, England, and comparison of pollen zones across the British Isles. New Phytologist 109, 237–253.

Berglund B E, Digerfeldt G, 1970. A palaeoecological study of the late-glacial lake at Torreberga, Scania, South Sweden. Oikos 21, 98–128.

Birks H H, 2000. Aquatic macrophyte vegetation development in Kråkenes Lake, western Norway, during the late-glacial and early-Holocene. Journal of Paleolimnology 23, 7–19.

Birks H H, 2003. The importance of plant macrofossils in the reconstruction of Lateglacial vegetation and climate: examples from Scotland, western Norway, and Minnesota, USA. Quaternary Science Reviews 22, 453–473.

Birks H H, 2015. South to north: contrasting late-glacial and early-Holocene climate changes and vegetation responses between south and north Norway. The Holocene 25, 37–52.

Birks H H, Van Dinter M, 2010. Lateglacial and early Holocene vegetation and climate gradients in the Nordfjord–Ålesund area, western Norway. Boreas 39, 783–798.

Birks H H, Birks H J B, 2013. Vegetation responses to late-glacial climate changes in western Norway. Preslia 85, 215–237.

Birks H H, Battarbee R W, Beerling D J, Birks H J B, Brooks S J, Duigan C A, Gulliksen S, Haflidason H, Hauge F, Jones V J, Jonsgard B, Kårevik M, Larsen E, Lemdahl G, Løvlie R, Mangerud J, Peglar S M, Possnert G, Smol J P, Solem J O, Solhøy I, Solhøy T, Sønstegaard E, Wright H E, 1996. The Kråkenes late-glacial palaeoenvironmental project. Journal of Paleolimnology 15, 281–286.

Birks H H, Jones V J, Brooks S J, Birks H J B, Telford R J, Juggins S, Peglar S M, 2012. From cold to cool in northernmost Norway: Lateglacial and early Holocene multi-proxy environmental and climate reconstructions from Jansvatnet, Hammerfest. Quaternary Science Reviews 33, 100–120.

Birks H H, Aarnes I, Bjune A E, Brooks S J, Bakke J, Kühl N, Birks H J B, 2014. Lateglacial and early-Holocene climate variability reconstructed from multi-proxy records on Andøya, northern Norway. Quaternary Science Reviews 89, 108–122.

Björck S, Kromer B, Johnsen S, Bennike O, Hammarlund D, Lemdahl G, Possnert G, Rasmussen T L, Wohlfarth B, Hammer C U, Spurk M, 1996. Synchronized terrestrial atmospheric deglacial records around the North Atlantic. Science 274, 1155–1160.

Björkman L, Feurdean A, Wohlfarth B, 2003. Late-Glacial and Holocene forest dynamics at Steregoiu in the Gutaiului Mountains, Northwest Romania. Review of Palaeobotany and Palynology 124, 79–111.

Bohncke S, Wijmstra L E X, 1988. Reconstruction of Late-Glacial lake-level fluctuations in The Netherlands based on palaeobotanical analyses, geochemical results and pollen-density data. Boreas 17, 403–425.

Bohncke S, Vandenberghe J E F, Coope R, Reiling R, 1987. Geomorphology and palaeoecology of the Mark valley (southern Netherlands): palaeoecology, palaeohydrology and climate during the Weichselian Late Glacial. Boreas 16, 69–85.

Bos J A A, Bohncke S, Janssen C R, 2006. Lake-level fluctuation and small-scale vegetation-patterns during the late-glacial in the Netherlands. Journal of Paleolimnology 35, 211–238.

Bos J A A, Verbruggen F, Engels S, Crombé P, 2013. The influence of environmental changes on local and regional vegetation patterns at Rieme (NW Belgium): implications for Final Palaeolithic habitation. Vegetation History and Archaeobotany 22, 17–38.

Brooks S J, Birks H J B, 2000. Chironomid-inferred late-glacial air temperatures at Whitrig Bog, southeast Scotland. Journal of Quaternary Science 15, 759–764.

Brooks S J, Matthews I P, Birks H H, Birks H J B, 2012. High resolution Lateglacial and early-Holocene summer air temperature records from Scotland inferred from chironomid assemblages. Quaternary Science Reviews 41, 67–82.

Carrión J S, 2002. Patterns and processes of Late Quaternary environmental change in a montane region of southwestern Europe. Quaternary Science Reviews 21, 2047–2066.

Carrión J, Van Geel B, 1999. Fine-resolution Upper Weichselian and Holocene palynological record from Navarrés (Valencia, Spain) and a discussion about factors of Mediterranean forest succession. Review of Palaeobotany and Palynology 106, 209–236.

Connor S E, Ross S A, Sobotkova A, Herries AIR, Mooney S D, Longford C, Iliev I, 2013. Environmental conditions in the SE Balkans since the Last Glacial Maximum and their influence on the spread of agriculture into Europe. Quaternary Science Reviews 68, 200–215.

Di Rita F, Anzidei A P, Magri D, 2013. A Lateglacial and early Holocene pollen record from Valle di Castiglione (Rome): Vegetation dynamics and climate implications. Quaternary International 288, 73–80.

Engels S, Van Geel B, Buddelmeijer N, Brauer A, 2015. High-resolution palynological evidence for vegetation response to the Laacher See eruption from the varved record of Meerfelder Maar (Germany) and other central European records. Review of Palaeobotany and Palynology 221, 160–170.

Feurdean A, Bennike O, 2004. Late Quaternary palaeoecological and palaeoclimatological reconstruction in the Gutaiului Mountains, northwest Romania. Journal of Quaternary Science 19, 809–827.

Feurdean A, Mosbrugger V, Onac B, Polyak V, Veres D, 2007. Younger Dryas to mid-Holocene environmental history of the lowlands of NW Transylvania, Romania. Quaternary Research 68, 364–378.

Filippi M L, Heiri O, Arpenti E, Angeli N, Bortolotti M, Lotter A F, van der Borg K, 2007. Evoluzione paleoambientale dal Tardoglaciale a oggi ricostruita attraverso lo studio dei sedimenti del Lago di Lavarone (Altopiano di Folgaria e Lavarone, Trentino). Studi Trentini di Scienze Naturali – Acta Geologica 82, 279–298. (In Italian.)

Finsinger W, Tinner W, 2006. Holocene vegetation and land-use changes in response to climatic changes in the forelands of the southwestern Alps, Italy. Journal of Quaternary Science 21, 243–258.

Gaidamavičius A, Stančikaitė M, Kisielienė D, Mažeika J, Gryguc G, 2011. Post-glacial vegetation and environment of the Labanoras Region, East Lithuania: implications for regional history. Geological Quarterly 55, 269–284.

Gałka M, Sznel M, 2013. Late Glacial and Early Holocene development of lakes in northeastern Poland in view of plant macrofossil analyses. Quaternary International 292, 124–135.

Gałka M, Tobolski K, Bubak I, 2014. Late Glacial and Early Holocene lake level fluctuations in NE Poland tracked by macro-fossil, pollen and diatom records. Quaternary International 388, 23–38.

Hammarlund D, Lemdahl G, 1994. A Late Weichselian stable isotope stratigraphy compared with biostratigraphical data: a case study from southern Sweden. Journal of Quaternary Science 9, 13–31.

Heikkilä M, Fontana S, Seppä H, 2009. Rapid lateglacial tree population dynamics and ecosystem change in the eastern Baltic region. Journal of Quaternary Science 24, 802–815.

Heiri O, Millet L, 2005. Reconstruction of Late Glacial summer temperatures from chironomid assemblages in Lac Lautrey (Jura, France). Journal of Quaternary Science 20, 33–44.

Heiri O, Cremer H, Engels S, Hoek W Z, Peeters W, Lotter A F, 2007. Lateglacial summer temperatures in the Northwest European lowlands: a chironomid record from Hijkermeer, the Netherlands. Quaternary Science Reviews 26, 2420–2437.

Hošek J, Pokorný P, Kubovčík V, Horáček I, Žáčková P, Kadlec J, Rojik F, Lisá L, Bučkuliaková S, 2014. Late glacial climatic and environmental changes in eastern-central Europe: Correlation of multiple biotic and abiotic proxies from the Lake Švarcenberk, Czech Republic. Palaeogeography, Palaeoclimatology, Palaeoecology 396, 155–172.

Hunt T G, Birks H J B, 1982. Devensian Late-Glacial vegetational history at Sea Mere, Norfolk. Journal of Biogeography 9, 517–538.

Huntley B, Watts W A, Allen J R M, Zolitschka B, 1999. Palaeoclimate, chronology and vegetation history of the Weichselian Lateglacial: comparative analysis of data from three cores at Lago Grande di Monticchio, southern Italy. Quaternary Science Reviews 18, 945–960.

Huttunen A, Huttunen R L, Vasari Y, Panovska H I P, Bozilova E D B, 1992. Late Glacial and Holocene history of flora and vegetation in the Western Rhodopes Mountains Bulgaria. Acta Botanica Fennica 144, 63–80.

Ilyashuk B, Gobet E, Heiri O, Lotter A F, van Leeuwen J F N, van der Knaap W O, Ilyashuk E, Oberli F, Ammann B, 2009. Lateglacial environmental and climatic changes at the Maloja Pass, Central Swiss Alps, as recorded by chironomids and pollen. Quaternary Science Reviews 28, 1340–1353.

Jones R T, Marshall J D, Crowley S F, Bedford A, Richardson N, Bloemendal J, Oldfield F, 2002. A high resolution, multiproxy Late-glacial record of climate change and intrasystem responses in northwest England. Journal of Quaternary Science 17, 329–340.

Karpińska-Kołaczek M, Kołaczek P, Stachiwicz-Rybla R, Obidowicz, 2013. Palaeobotanical studies on Late Glacial and Holocene vegetation development and transformations of the 'Wielkie Błoto' mire near Gołdap (north-eastern Poland). Acta Palaeobotanica 53, 53–67.

Kołaczek P, Gałka M, Karpińska-Kołaczek M, 2015. Succession of arboreal taxa during the Late Glacial in south-eastern Poland: climatic implications. Palaeogeography, Palaeoclimatology, Palaeoecology 421, 1–14.

Lang B, Brooks S J, Bedford A, Jones R T, Birks H J B, Marshall J D, 2010. Regional consistency in Lateglacial chironomid-inferred temperatures from five sites in north-west England. Quaternary Science Reviews 29, 1528–1538.

Larocque I, Finsinger W, 2008. Late-glacial chironomid-based temperature reconstructions for Lago Piccolo di Avigliana in the southwestern Alps (Italy). Palaeogeography, Palaeoclimatology, Palaeoecology 257, 207–223.

Laroque-Tobler I, Heiri O, Wehrli M, 2010. Late Glacial and Holocene temperature changes at Egelsee, Switzerland, reconstructed using subfossil chironomids. Journal of Paleolimnology 43, 649–666.

Latałowa M, Borówka R, 2006. The Allerød/Younger Dryas transition in Wolin Island, northwest Poland, as reflected by pollen, macrofossils, and chemical content of an organic layer separating two aeolian series. Vegetation History and Archaeobotany 15, 321–331.

Lotter A F, Birks H J B, Eicher U, Hofmann W, Schwander J, Wick L, 2000. Younger Dryas and Allerod summer temperatures at Gerzensee (Switzerland) inferred from fossil pollen and cladoceran assemblages. Palaeogeography, Palaeoclimatology, Palaeoecology 159, 349–361.

Lotter A F, Heiri O, Brooks S, van Leeuwen J F N, Eicher U, Ammann B, 2012. Rapid summer temperature changes during Termination 1a: high-resolution multi-proxy climate reconstructions from Gerzensee (Switzerland). Quaternary Science Reviews 36, 103–113.

Lowe J J Walker, M J C, 1991. Vegetational history of the Isle of Skye: 2. The Flandrian. In Ballantyne C K , Benn D I , Lowe J J, Walker M J C (editors) The Quaternary of the Isle of Skye: field guide, Cambridge: Quaternary Research Association , 119–142.

Lowe J J, Walker M J C, Coope G R, Sheldrik C, Harkness D D, 1995. Direct comparison of UK temperatures and Greenland snow accumulation rates, 15 000–12 000 yr ago. Journal of Quaternary Science 10, 175–180.

Magny M, Aalbersberg G, Bégeot C, Benoit-Ruffaldi P, Bossuet G, Disnar J-R, Heiri O, Laggoun-Defarge F, Millet L, Peyron O, Vannière B, Walter-Simonnet A-V, 2006. Environmental and climatic changes in the Jura mountains (eastern France) during the Last Glacial–Interglacial transition: a multi-proxy record from Lake Lautrey. Quaternary Science Reviews 25, 414–445.

Magyari E K, Gaydarska B, Pettitt P, Chapman J, 2013. Palaeo-environments of the Balkan Lateglacial and their potential – were humans absent from the Garden of Eden? Bulgarian e-Journal of Archaeology 3, 1–30.

Magyari E K, Veres D, Wennrich V, Wagner B, Braun M, Jakab G, Karátson D, Pál Z, Ferenczy G, St-Onge G, Rethemeyer J, Francois J P, von Reumont F, Schäbitz F, 2014. Vegetation and environmental responses to climate forcing during the Last Glacial Maximum and deglaciation in the East Carpathians: attenuated response to maximum cooling and increased biomass burning. Quaternary Science Reviews 106, 278–298.

Matthews I P, Birks H H, Bourne A J, Brooks S J, Lowe J J, Macleod A, Pyne-O'Donnell S D F, 2011. New age estimates and climatostratigraphic correlations for the borrobol and penifiler tephras: Evidence from Abernethy Forest, Scotland. Journal of Quaternary Science 26, 247–252.

Mayle F E, Lowe J J, Sheldrick C, 1997. The late devensian lateglacial palaeoenvironmental record from Whitrig Bog, SE Scotland. 1. Lithostratigraphy, Geochemistry and Palaeobotany. Boreas 26, 279–295.

Mayle F E, Bell M, Birks H H, Brooks S J, Coope G R, Lowe J J, Sheldrick C, Shijie L, Turney C S M, Walker M J C, 1999. Climate variations in Britain during the Last Glacial–Holocene transition (15.0–11.5 cal ka BP): comparison with the GRIP ice-core record. Journal of the Geological Society 156, 411–423.

McKeever M H, 1984. Comparative palynological studies of two lake sites in western Ireland and northwestern Spain. PhD thesis. Trinity College, Dublin, Ireland.

Millet L, Rius D, Galop D, Heiri O, Brooks S J, 2012. Chironomid-based reconstruction of Lateglacial summer temperatures from the Ech palaeolake record (French western Pyrenees). Palaeogeography, Palaeoclimatology, Palaeoecology 315–316, 86–99.

Mortensen M F, Birks H H, Christensen C, Holm J, Noe-Nygaard N, Odgaard B V, Olsen J, Rasmussen K L, 2011. Lateglacial vegetation development in Denmark – New evidence based on macrofossils and pollen from Slotseng, a small-scale site in southern Jutland. Quaternary Science Reviews 30, 2534–2550.

Muñoz Sobrino C, Ramil-Rego P, Rodríguez Guitián M A, 1997. Upland vegetation in the northwest Iberian peninsula after the last glaciation: forest history and deforestation dynamics. Vegetation History and Archaeobotany 6, 215–233.

Muñoz Sobrino C, Ramil-Rego P, Rodríguez Guitían M A, 2001. Vegetation in the mountains of northwest Iberia during the last glacial-interglacial transition. Veget Hist Archaeobot 10, 7–21.

Muñoz Sobrino C, Heiri O, Hazekamp M, van der Velden D, Kirilova E P, García-Moreiras I, Lotter A F, 2013. New data on the Lateglacial period of SW Europe: a high resolution multiproxy record from Laguna de la Roya (NW Iberia). Quaternary Science Reviews 80, 58–77.

Muschitiello F, Wohlfarth B, 2015. Time-transgressive environmental shifts across Northern Europe at the onset of the Younger Dryas. Quaternary Science Reviews 109, 49–56.

Nesje A, Bakke J, Brooks S J, Kaufman D S, Kihlberg E, Trachsel M, D'Andrea W J, Matthews J A, 2014. Late glacial and Holocene environmental changes inferred from sediments in Lake Myklevatnet, Nordfjord, western Norway. Vegetation History and Archaeobotany 23, 229–248.

Paus A, 1989. Late Weichselian vegetation, climate, and floral migration at Liastemmen, North Rogaland, south-western Norway. Journal of Quaternary Science 4, 223–242.

Paus A, Svendsen J I, Matiouchkov A, 2003. Late Weichselian (Valdaian) and Holocene vegetation and environmental history of nothern Timan Ridge European Arctic Russia. Quaternary Science Reviews 22, 2285–2302.

Petr L, Sádlo J, Žáčková P, Lisá L, Novák J, Rohovec J, Pokorný P, 2014. Late-Glacial and Holocene environmental history of an Oxbow Wetland in the Polabí Lowland (River Elbe, Czech Republic); a context-dependent interpretation of a multi-proxy analysis. Folia Geobotanica 49, 137–162.

Peyron O, Bégeot C, Brewer S, Heiri O, Magny M, Millet L, Ruffaldi P, Van Campo E, Yu G, 2005. Late-Glacial climatic changes in Eastern France (Lake Lautrey) from pollen, lake-levels, and chironomids. Quaternary Research 64, 197–211.

Reille M, Gamisans J, de Beaulieu J-L, Andrieu V, 1997. The late-glacial at Lac de Creno (Corsica, France): a key site in the western Mediterranean basin. New Phytologist 135, 547–559.

Rybníčková E, Rybníček K, 2006. Pollen and macroscopic analyses of sediments from two lakes in the High Tatra mountains, Slovakia. Vegetation History and Archaeobotany 15, 345–356.

Saarse L, Niinemets E, Amon L, Heinsalu A, Veski S, Sohar K, 2009. Development of the late glacial Baltic basin and the succession of vegetation cover as revealed at Palaeolake Haljala, northern Estonia. Estonian Journal of Earth Sciences 58, 317–333.

Samartin S, Heiri O, Vescovi E, Brooks S J, Tinner W, 2012. Lateglacial and early Holocene summer temperatures in the southern Swiss Alps reconstructed using fossil chironomids. Journal of Quaternary Science 27, 279–289.

Seiriene V, Stancikaite M, Kisieline D, Sinkunas P, 2006. Lateglacial environment inferred from palaeobotanical and 14C data of sediment sequence from Lake Kasuciai, West Lithuania. Baltica 19, 80–90.

Stančikaitė M, Kisielienė D, Moe D, Vaikutienė G, 2009. Lateglacial and early Holocene environmental changes in northeastern Lithuania. Quaternary International 207, 80–92.

Sümegi P, Magyari E, Dániel P, Molnár M, Törőcsik T, 2013. Responses of terrestrial ecosystems to Dansgaard–Oeshger cycles and Heinrich-events: a 28,000-year record of environmental changes from SE Hungary. Quaternary International 293, 34–50.

Tobolski K, Ammann B, 2000. Macrofossils as records of plant responses to rapid Late Glacial climatic changes at the three sites in the Swiss Alps. Palaeogeography, Palaeoclimatology, Palaeoecology 159, 251–259.

Tóth M, Magyari E K, Brooks S J, Braun M, Buczkó K, Báint M, Heiri O, 2012. A chironomid-based reconstruction of late glacial summer temperatures in the southern Carpathians (Romania). Quaternary Research 77, 122–131.

Turner C, Hannon G E, 1988. Vegetational evidence for Late Quaternary climatic changes in Southwest Europe in relation to the influence of the North Atlantic Ocean. Philosophical Transactions of the Royal Society of London B: Biological Sciences, The Royal Society, 318, 451–485.

Turney C S M, 1999. Lacustrine bulk organic $\delta^{13}C$ in the British Isles during the Last Glacial-Holocene Transition (14–9 ka ^{14}C BP). Arctic, Antarctic and Alpine Research 31, 71–81.

Turney C S M, van den Burg K, Wastegård S, Davies S M, Whitehouse N J, Pilcher J R, Callaghan C, 2006. North European last glacial-interglacial transition (LGIT; 15–9 ka) tephrochronology: extended limits and new events. Journal of Quaternary Science 21, 335–345.

van Asch N, Hoek W Z, 2012. The impact of summer temperature changes on vegetation development in Ireland during the Weichselian Lateglacial interstadial. Journal of Quaternary Science 27, 441–450.

van der Knaap W O, van Leeuwen J F N, 1997. Late Glacial and early Holocene vegetation succession, altitudinal vegetation zonation, and climatic change in the Serra da Estrela, Portugal. Review of Palaeobotany and Palynology 97, 239–285.

Van Geel B, Bohncke S J P, Dee H, 1980. A palaeoecological study of an upper late glacial and Holocene sequence from “de Borchert”, the Netherlands. Review of Palaeobotany and Palynology 31, 367–392.

Van Geel B, Coope G R, Van Der Hammen T, 1989. Palaeoecology and stratigraphy of the lateglacial type section at Usselo (the Netherlands). Review of Palaeobotany and Palynology 60.

Vandenberghe J, Bohncke S, 1985. The Weichselian Late Glacial in a small lowland valley (Mark River, Belgium and the Netherlads). Bulletin de l’Association francaise pour l’étude du Quaternaire 2, 167–175.

Vasari Y, Vasari A, 1968. Late- and post-glacial macrophytic vegetation in the lochs of northern Scotland. Acta Botanica Fennica 80, 1–120.

Vasari Y, Kuznetsov O, L Lavrova, N B, Shelekova T S, Vasari A, 2007. Alinlampi, a Late-Glacial site in the northen Karelian Republic. Annales Botanici Fennici 44, 42–55.

Vegas-Vilarrúbia T, González-Sampériz P, Morellón M, Gil-Romera G, Pérez-Sanz A, Valero-Garcés B, 2013. Diatom and vegetation responses to Late Glacial and Early

Holocene climate changes at Lake Estanya (Southern Pyrenees, NE Spain). Palaeogeography, Palaeoclimatology, Palaeoecology 392, 335–349.

Vescovi E, Ravazzi C, Arpenti E, Finsinger W, Pini R, Valsecchi V, Wick L, Ammann B, Tinner W, 2007. Interactions between climate and vegetation during the Lateglacial period as recorded by lake and mire sediment archives in Northern Italy and Southern Switzerland. Quaternary Science Reviews 26, 1650–1669.

Veski S, Amon L, Heinsalu A, Reitalu T, Saarse L, Stivrins N, Vassiljev J, 2012. Lateglacial vegetation dynamics in the eastern Baltic region between 14,500 and 11,400 Cal yr BP: a complete record since the Bølling (GI-1e) to the Holocene. Quaternary Science Reviews 40, 39–53.

Veski S, Seppä H, Stančikaite M, Zernitskaya V, Reitalu T, Gryguc G, Heinsalu A, Stivrins N, Amon L, Vassiljev J, Heiri O, 2015. Quantitative summer and winter temperature reconstructions from pollen and chironomid data between 15 and 8 ka BP in the Baltic-Belarus area. Quaternary International 388, 4–11.

Vočadlová K, Petr L, Žáčková P, Křížek M, Křížová L, Hutchinson S H, Šobr M, 2015. The Lateglacial and Holocene in Central Europe: a multi-proxy environmental record from the Bohemian Forest, Czech Republic. Boreas 44, 769–784.

von Engelbrechten S, McGee E, Little D J, Mitchell F J G, 2000. A paleoecological study of Brackloon Wood, Co Mayo; Vegetation dynamics and human impact throughout the Holocene period (c.10,000 years BP – Present), Forest Ecosystem Research Group Report Department of Botany, Trinity College Dublin.

Väliranta M, Kultti S, Seppä H, 2006. Vegetation dynamics during the Younger Dryas-Holocene transition in the extreme northern taiga zone, northeastern European Russia. Boreas 35, 202–212.

Väliranta M, Salonen J S, Heikkilä M, Amon L, Helmens K, Klimaschewski A, Kuhry P, Kultti S, Poska A, Shala S, Veski S, Birks H H, 2015. Plant macrofossil evidence for an early onset of the Holocene summer thermal maximum in northern Europe. Nature Communications 6, 6809. doi:10.1038/ncomms7809

Walker M J C, Harkness D D, 1990. Radiocarbon dating the Devensian Lateglacial in Britain : new evidence from Llanilid, South Wales. Journal of Quaternary Science 5, 135–144.

Walker M J C, Lowe J J, 1990. Reconstructing the environmental history of the last glacial-interglacial transition: Evidence from the Isle of Skye, Inner Hebrides, Scotland. Quaternary Science Reviews 9, 15–49.

Walker M J C, Coope G R, Lowe J J, 1993. The Devensian (Weichselian) Lateglacial palaeoenvironmental record from Gransmoor, East Yorkshire, England. A contribution to the “North Atlantic seaboard programme” of IGCP-253, “Termination of the Pleistocene.” Quaternary Science Reviews 12, 659–680.

Walker M J C, Coope G R, Sheldrick C, Turney C S M, Lowe J J, Blockley S P E, Harkness D D, 2003. Devensian Lateglacial environmental changes in Britain: a multi-proxy environmental record from Llanilid, South Wales, UK, Quaternary Science Reviews 22, 475–520.

Walker M, Lowe J, Blockley S P E, Bryant C, Coombes P, Davies S, Hardiman M, Turney C S M, Watson J, 2012. Lateglacial and early Holocene palaeoenvironmental ‘events’ in Sluggan Bog, Northern Ireland: comparisons with the Greenland NGRIP GICC05 event stratigraphy. Quaternary Science Reviews 36, 124–138.

Watson J E, Brooks S J, Whitehouse N J, Reimer P J, Birks H J B, Turney C, 2010. Chironomid-inferred late-glacial summer air temperatures from Lough Nadourcan, Co. Donegal, Ireland. Journal of Quaternary Science 25, 1200–1210.

Wehrli M, Tinner W, Ammann B, 2007. 16 000 years of vegetation and settlement history from Egelsee (Menzingen, central Switzerland). The Holocene 17, 747–761.

Wohlfarth B, Bennike O, Brunnberg L, Demidov I, Possnert G, Vyahirev S, 1999. AMS ^{14}C measurements and macrofossil analyses of a varved sequence near Pudozh, eastern Karelia, NW Russia. Boreas 29, 575–586.

Wohlfarth B, Filimonova L, Bennike O, Björkman L, Brunnberg L, Lavrova N, Demidov I, Possnert G, 2002. Late-Glacial and Early Holocene environmental and climatic Changenat Lake Tambichozero, Southeastern Russian Karelia. Quaternary Research 58, 261–272.

Wohlfarth B, Schwark L, Bennike O, Filimonova L, Tarasov P, Björkman L, Brunnberg L, Demidov I, Possnert G, 2004. Unstable early-Holocene climatic and environmental conditions in northwestern Russia derived from a multidisciplinary study of a lake-sediment sequence from Pichozero, southeastern Russian Karelia. The Holocene 14, 732–746.

Wohlfarth B, Tarasov P, Bennike O, Lacourse T, Subetto D A, Torssander P, Romanenko F, 2006. Late glacial and Holocene palaeoenvironmental changes in the Rostov-Yaroslavl' area, West Central Russia. Journal of Paleolimnology 35, 543–569.

Wohlfarth B, Lacourse T, Bennike O, Subetto D A, Tarasov P, Demidov I, Filimonova L, Sapelko T V, 2007. Climatic and environmental changes in north-western Russia between 15,000 and 8000 cal yr BP: a review. Quaternary Science Reviews 26, 1871–1883.

Zawiska I, Słowiński M, Correa-Metrio A, Obremska M, Luoto T, Nevalainen L, Woszczyk M, Milecka K, 2015. The response of a shallow lake and its catchment to Late Glacial climate changes – A case study from eastern Poland. Catena 126, 1–10.

Arkitektkopia AB, Bromma, 2019

SKB is responsible for managing spent nuclear fuel and radioactive waste produced by the Swedish nuclear power plants such that man and the environment are protected in the near and distant future.

skb.se